2015-12-01

Evaluating Long-Term Land Cover Changes for Malheur Lake, Oregon Using ENVI and ArcGIS

Ryan Joseph Woods
Brigham Young University

Evaluating Long-Term Land Cover Changes for Malheur Lake, Oregon Using ENVI and ArcGIS

Ryan Joseph Woods

A thesis submitted to the faculty of
Brigham Young University
in partial fulfillment of the requirements for the degree of

Master of Science

Gustavious P. Williams, Chair
E. James Nelson
Daniel P. Ames

Department of Civil and Environmental Engineering

Brigham Young University

December 2015

ABSTRACT

Evaluating Long-Term Land Cover Changes for Malheur Lake, Oregon
Using ENVI and ArcGIS

Ryan Joseph Woods
Department of Civil and Environmental Engineering, BYU
Master of Science

Land cover change over time can be a useful indicator of variations in a watershed, such as the patterns of drought in an area. I present a case study using remotely sensed images from Landsat satellites for over a 30-year period to generate classifications representing land cover categories, which I use to quantify land cover change in the watershed areas that contribute to Malheur, Mud, and Harney Lakes. I selected images, about every 4 to 6 years from late June to late July, in an attempt to capture the peak vegetation growth and to avoid cloud cover. Complete coverage of the watershed required that I selected an image that included the lakes, an image to the North, and an image to the West of the lakes to capture the watershed areas for each chosen year. I used the watershed areas defined by the HUC-8 shapefiles. The relevant watersheds are called: Harney-Malheur Lakes, Donner und Blitzen, Silver, and Silvies watershed. To summarize the land cover classes that could be discriminated from the Landsat images in the area, I used an unsupervised classification algorithm called Iterative Self-Organizing Data Analysis Technique (ISODATA) to identify different classes from the pixels. I then used the ISODATA results and visual inspection of calibrated Landsat images and Google Earth imagery, to create Regions of Interest (ROI) with the following land cover classes: Water, Shallow Water, Vegetation, Dark Vegetation, Salty Area, and Bare Earth. The ROIs were used in the following supervised classification algorithms: maximum likelihood, minimum distance, and Mahalanobis distance, to classify land cover for the area. Using ArcGIS, I removed most of the misclassified area from the classified images by the use of the Landsat CDR, combined the main, north, and west images and then extracted the watersheds from the combined image. The area in acres for each land cover class and watershed was computed and stored in graphs and tables.

After comparing the three supervised classifications using the amount of area classified into each category, normalized area in each category, and the raster datasets, I determined that the minimum distance classification algorithm produced the most accurate land cover classification. I investigated the correlation of the land cover classes with the average precipitation, average discharge, average summer high temperature, and drought indicators. For the most part, the land cover changes correlate with the weather. However, land use changes, groundwater, and error in the land cover classes may have accounted for the instances of discrepancy. The correlation of land cover classes, except Dark Vegetation and Bare Earth, are statistically significant with weather data. This study shows that Landsat imagery has the necessary components to create and track land cover changes over time. These results can be useful in hydrological studies and can be applied to models.

Keywords: watershed, land cover, Landsat, remote sensing, GIS, ISODATA, maximum likelihood, minimum distance, Mahalanobis distance, Malheur Lake

ACKNOWLEDGEMENTS

I would like to express my sincere gratitude to my Heavenly Father who has always been there and has helped me through inspiration and guidance in getting my research done. I would also like to thank my family for their immense support, encouragement, and prayers in working on this research.

I would like to thank Dr. Gustavious Paul Williams for his advice, encouragement, expertise, and foresight in the things I needed to do to keep the research moving along. I would not have been able to figure out the direction the research needed to go without him. I would like to thank Dr. E. James Nelson and Dr. Daniel P. Ames for their excellent feedback, challenging questions, and support in doing this research and in obtaining this degree. I would also like to thank Dr. A. Wood Miller for his questions and genuine interest in all things research.

I would like to thank the Remote Sensing Group for their help and enthusiasm. I would especially like to thank Carly Hansen and Zola Adjei for pioneering through their research that enriched my research so well. I would like to thank the Malheur National Wildlife Refuge for funding this research and believing in Carly Hansen's research enough to fund remote sensing research at BYU. I would also like to thank Dr. Fernando S. Fonseca for help in funding my tuition that gave me the chance to work on this research.

Last but not least, I would like to thank my friends who have been there through the ups and downs of the Civil Engineering major and for your collaboration with me on so many assignments, projects, and test reviews. I am also grateful for your friendship and genuine interest in my research. Thank you!

TABLE OF CONTENTS

LIST OF TABLES

LIST OF FIGURES

1 INTRODUCTION

Land cover is described as the physical and biological cover of the earth, which includes vegetation, water, earth, rock, and man-made structures (Zhou, 2008). Land cover is affected by the environment, animals, and people. However, when people become involved with the landscape, then the term is usually changed to land use. Land use also deals with the reasons why the land is developed and maintained or reverted back to a natural state. As land cover is a description of the type of surface presented rather than the reasons why man changed the landscape, this study will focus on land cover.

Land cover influences how a watershed transports water, how the water infiltrates, evaporates or flows overland towards the outlet. Land cover maps for the conterminous United States have been created on a national scale and are coarser in the West because of the large counties (Brown, Johnson, Loveland, & Theobald, 2005). However, land cover map series have not been created for the watersheds that track changes over long periods of time. Watersheds play a huge role in the development and sustaining of natural lakes, water bodies, and groundwater. As such, tracking the change of the watersheds over time can be of supreme interest to those who manage the associated streams, lakes, and reservoirs.

Determining land cover can be done with remote sensing, field surveys, and statistical surveys (USGS, 2015a). Field and statistical surveys require samples, and can be time consuming and expensive. Satellite images provide complete coverage for a watershed, and

because of the extent of historical data, support the study of changes over time. Since the study site is distant and there is a requisite for land cover change over time, I used satellite remote sensing methods for this study. Land cover types can be estimated by using remote sensing techniques, as each type of land cover exhibits a specific spectral signature.

There are many different types of satellites used for earth studies. Landsat (Land Satellite), Satellite Pour l'Observation de la Terre which translates to Satellite for observation of the Earth (SPOT), and Moderate Resolution Imaging Spectroradiometer (MODIS) are all suitable for determining land cover changes over a long period of time. In the comparative study by Lu, SPOT provided the best accuracy for land cover classification with a 10 meter spatial resolution. However, no sensor data or image processing routine is best for all land cover types (Lu, 2005). For this study, SPOT was not chosen because of the high cost of the images and MODIS was not chosen because of the low spatial resolution. MODIS' best spatial resolution is 250 meters. The Landsat satellite offers a spatial resolution of 30 meters with repetitive and synoptic observations of earth that have been archived for decades making these images ideal for land cover studies (Adjei, 2015). This long term archive is an additional benefit from using Landsat data as there are data, along with other spatial resolutions, dating back over 40 years.

The first Landsat satellite was launched on July 23, 1972 from Vandenberg Air Force Base, CA. In early 1975, the second Landsat satellite was launched and since that time, there have been at least two satellites in orbit taking imagery. Although Landsat satellites have been orbiting the earth since 1972, it was not until Landsat 4 in 1982, when 30-meter resolution became available, that there were data with a consistent resolution. The data archive for a 30-meter resolution spans from that period, 1982, until today. Because of the difficulties with using different spatial resolutions in the same study, this study starts with Landsat 5 images and goes

through Landsat 8 images. These images have the advantage of newer technology with a 30-meter resolution. Landsat 5 data began in 1984 and provided a continuous record until 2013. Landsat 7 began in 1999 and Landsat 8 began in 2013, both of which provide continuous data until today. USGS plans on launching Landsat 9 in 2023, which should have better sensors that what we currently have today. Landsat 5, 7, and 8 satellites all collect data in different wavelengths bands ranging from 0.43 to 2.35 μm and from 10.60 to 12.51 μm. The visible spectrum which our eyes can see is between 0.38 and 0.70 μm. Landsat records data in a broader spectrum providing more available data to work with. The wavelengths and their typical applications are shown in Table 1-1 and Table 1-2.

Table: 1-1 Landsat 5 TM and 7 ETM Band Distribution and Applications (Adjei, 2015)

Band Number	Description	Wavelength (μm)	Example Use
Band 1	Blue	0.45-0.52	Bathymetry, soil/vegetation distinction
Band 2	Green	0.52-0.60	Peak vegetation, plant vigor
Band 3	Red	0.63-0.69	Discriminates vegetation slopes
Band 4	Near Infrared	0.77-0.90	Emphasizes biomass content, distinguishing shorelines
Band 5	Short-wave Infrared	1.55-1.75	Discriminates moisture content, penetrates thin clouds
Band 6	Thermal Infrared	10.40-12.50	Observation of the effects of temperature and soil moisture
Band 7	Short-wave Infrared	2.08-2.35	Hydrothermally altered rocks, mineral deposits
Band 8 (Landsat 7 only)	Panchromatic	0.52-0.90	15 meter resolution

Table 1-2: Landsat 8 OLI and TIRS Band Distribution and Applications

Band Number	Description	Wavelength (μm)	Example Use
Band 1	Coastal aerosol	0.43-0.45	Coastal and aerosol studies
Band 2	Blue	0.45-0.51	Bathymetry, soil/vegetation distinction
Band 3	Green	0.53-0.59	Peak vegetation, plant vigor
Band 4	Red	0.64-0.67	Discriminates vegetation slopes
Band 5	Near Infrared (NIR)	0.85-0.88	Emphasizes biomass content, distinguishing shorelines
Band 6	Short-wave Infrared 1	1.57-1.65	Discriminates moisture content, penetrates thin clouds
Band 7	Short-wave Infrared 2	2.11-2.29	Improved moisture content, penetrates thin clouds
Band 8	Panchromatic	0.50-0.68	15 meter resolution
Band 9	Cirrus	1.36-1.38	Cirrus cloud contamination detection
Band 10	Thermal Infrared (TIRS) 1	10.60-11.19	100 meter resolution, Observation of the effects of temperature and soil moisture
Band 11	Thermal Infrared (TIRS) 2	11.50-12.51	100 meter resolution, Improved observation of the effects of temperature and soil moisture

There are various methods to infer land cover type from remote sensing data. Most of these techniques use a form of image classification where areas with similar spectral characteristics are grouped together or "classified" into separate classes. Some of the image classification techniques currently used with satellite imagery include unsupervised classifications, supervised classifications, and decision trees. The resulting remote sensing imagery, which is separated into different classes, can be used with geographic information system (GIS) to more accurately and easily quantify and map land cover change (Treitz, Howarth, & Gong, 1992; Weng, 2002). In this approach, the remote sensing software works with the image data which is processed to identify the different classes and the GIS system is used to analyze these images.

In this study, I will first evaluate the remotely sensed images using an unsupervised classification to determine the number of land classes that can be effectively differentiated from an image and then use different supervised classification methods to assign physical meaning to these classes to determine the land cover over a 30-year period. I will then analyze the resulting classified images using watershed shapefiles to create land cover maps for each watershed that drains into Malheur Lake using GIS software. I detail the steps I used to implement the classification method and map creation process. The study site is Malheur Lake, Oregon. From this site, I produce land cover maps of the watersheds that feed into Malheur Lake and evaluate the changes over a 30-year period. I chose images from late June to late July when the peak vegetation growth occurs to facilitate better image classification.

1.1 Study Site

This study will focus on the four watersheds that feed into the Malheur, Mud, and Harney Lakes which are displayed in Figure 1-1. The Harney-Malheur Lakes, Donner und Blitzen, Silver, and Silvies watersheds comprise an area of 3,356,406 acres (5,244.4 sq. miles) with the primary inflow from the Donner und Blitzen River, the Silvies River, direct precipitation, and Sodhouse Spring. Malheur Lake is a fresh water marsh, one of the largest in the United States. When Malheur Lake is at its highest, the lake has an average surface area of 35,000 to 50,000 acres with an approximate volume of 85,000 acre-feet, an average depth of 2 feet, and a maximum of 6 feet (Hubbard, 1975; Johnson, 1985). Harney Lake has a surface area of 26,400 acres, is eutrophic, and has a very high salinity, but is historically dry. In geologic time when these lakes are high enough, they spill over to the Malheur River and eventually into the Pacific Ocean. However because of a geologically recent lava flow, the lakes no longer flow into Malheur River (Johnson, 1985) and act as terminal lakes.

The scientists at the Malheur Lake National Refuge have a primary mission to conserve the habitat for the birds and mammals. Understanding changes in the watershed, which can have an impact on the habitat for these species, is critical. The area undergoes periods of wet and dry years and because of these periods and other factors, the land cover changes. This study starts out in a very wet season and ends in a wet season, but includes three wet-dry cycles in the process of about 30 years.

Figure 1-1: The Harney-Malheur, Donner und Blitzen, Silver, and Silvies Watersheds that Flow into the Lakes of the Malheur Lake National Refuge in Harney County, Oregon (USDA, 2015)

1.2 Background

The objective of this study is to use 30-meter Landsat images from Landsat-5 Thematic Mapper (TM), Landsat-7 Enhanced Thematic Mapper (ETM), and Landsat 8 Operational Land Imager (OLI) to determine the land cover types over time of the watersheds that impact Malheur Lake, Mud Lake, and Harney Lake. I accomplished this by assuming that vegetation is at its peak during late June through late July and using images from this time period as input to classification algorithms.

1.2.1 Unsupervised Classification

To determine the number of land cover types that could be inferred from an image, I used an unsupervised classification method called Iterative Self-Organizing Data Analysis Technique (ISODATA) classification. The A in ISODATA was added for aesthetic reasons. ISODATA assigns each pixel in an image to different classes based on spectral features. The unsupervised ISODATA results indicate how many separate classes can be effectively differentiated from the data. I used these classes along with a visual analysis of the satellite images to choose the areas to assign as training data for the land cover classes in the supervised training algorithms (Mather & Koch, 2011) . The ISODATA classification algorithm assigns pixels in the image to different classes by calculating class means using spectral bands. The class means are moved into different classes by distributing the data evenly among the classes then iteratively clusters the remaining pixels into the selected classes using the minimum distance technique. The minimum distance technique takes the mean of the vectors for each endmember and calculates the Euclidean distance, a multi-dimensional straight line distance between two points, for each of the remaining or unknown pixels to the mean vector for each class in multi-dimensional space (the spectral bands for Landsat) (Excelis, 2015). The pixel is assigned to the class that is closest – e.g., one with the shortest distance.

Once the pixels are assigned to a class, the ISODATA algorithm checks the standard deviation. If the cluster has a large standard deviation, then the cluster is split in half along a line perpendicular to the feature axis. This is shown for cluster B in Figure 1-2 since the standard deviation, s_x, is larger than the specified value. If the clusters are closer together and have a small standard deviation, then the clusters are merged together. I selected this method to statistically determine the number of land cover types that could be differentiated using the spectral data in

the images. Since I do not have access to ground truth data to identify what the resulting land cover types are, and because ISODATA identifies spectral clusters which can represent land cover types (Mather & Koch, 2011), I used the resulting ISODATA categories along with visual analysis to determine regions in an image that could be used to train classifiers for supervised classification methods. This approach uses the ISODATA routine to determine areas in the image that are statistically similar, then I used visual analysis to determine a few areas where these categories seem to coincide with a known land cover type. Using the ISODATA classification, I created Regions of Interest (ROI) to map the different land cover classes. Based on the appearance of the remotely sensed images and the locations of the classifications from the ISODATA algorithm, I assigned the following land cover classes: Bare Earth, Water, Shallow Water, Vegetation, Dark Vegetation, and Salty Area. However, there are actually 13 land cover classes in this study area. I have matched my land cover classes with those from the National Land Cover Database (NLCD) as follows: Bare Earth corresponds with Shrub/scrub and Herbaceous land cover classes, Water corresponds with Open Water land cover class, Shallow Water corresponds with Emergent Herbaceous Wetlands land cover class, Vegetation corresponds with Cultivated Crops and Hay/Pasture land cover classes, Dark Vegetation corresponds with Evergreen Forest land cover class, and Salty Area corresponds with the land cover class, Barren Land. There were a few land cover classes, which I am not sure how they correlate. These are Developed (low intensity), Developed (medium intensity), Developed (high intensity), Developed (open space), and Woody Wetland land cover classes (USGS, 2011). These land cover classes were not meant to be exact, but to give a general indication of the land cover and how it has changed over time.

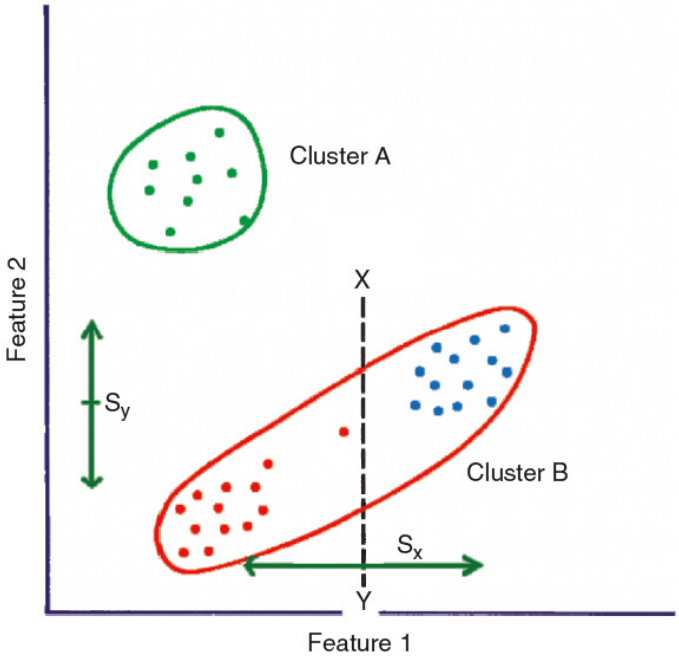

Figure 1-2: ISODATA Clustering (Mather & Koch, 2011)

1.2.2 Supervised Classification

Supervised classification algorithms are used when there is external knowledge of the area to select regions that are similar and can be classified together. This is usually based on ground truth or measurements in the field. Since I did not have any ground truth data or field measurements for the Malheur Lake watersheds, I used an unsupervised classification to determine the number of different land cover types that could be differentiated using Landsat imagery. Using the pseudo color images, colors that match what the eye sees, and the ISODATA classification, I defined classes with different names through the use of ROIs. These ROIs were used to train the supervised classification algorithms. I evaluated three different supervised classifications which I discuss below.

The maximum likelihood classification assumes that each class is normally distributed and determines the probability that a given pixel belongs to a specific class using the highest probability (Excelis, 2015; Mather & Koch, 2011). The maximum likelihood classification is calculated as follows:

$$g_i(x) = \ln[p(\omega_i)] - \tfrac{1}{2}\ln\left|\sum_i\right| - \tfrac{1}{2}(x - m_i)^T \sum_i^{-1}(x - m_i) \quad (1\text{-}1)$$

where *i* is class, *x* is the n-dimensional data where n is the number of bands, $p(\omega_i)$ is the probability that class ω_i occurs in the image and is assumed to be the same for all classes, $\left|\sum_i\right|$ is the determinant of the covariance matrix of the data in class ω_i, $\sum_i^{-1}$ is the inverse matrix, and m_i is the mean vector (Excelis, 2015).

The minimum distance classification is the same as the minimum distance technique, which takes the mean of the vectors for each endmember and calculates the Euclidean distance, straight line distance between two points in multidimensional space (the spectral bands for the Landsat data). The classification then assigns each of the remaining or unknown pixels to the closest mean vector for each class (Excelis, 2015).

The Mahalanobis distance classification is a direction-sensitive distance classifier that is similar to the maximum likelihood classification except it assumes all class covariances are equal (Excelis, 2015). The Mahalanobis distance squared is defined as:

$$D^2 = (x_m - \bar{x})' S^{-1}(x_m - \bar{x}) \quad (1\text{-}2)$$

where *m* is the index of the elements, x_m is the mth sample value (pixel vector), $\bar{x}$ is the mean vector, and *S* is the sample variance or covariance matrix. (Mather & Koch, 2011).

I selected these three supervised classification algorithms because of their ability to classify all areas of the imagery with the chosen classes from the ROIs. I did not choose a probability threshold for the supervised classifications such that all the pixels in the image would be classified through the selected ROIs allowing areas with larger uncertainty to be placed in a land cover class.

1.2.3 Extracting the Watershed from the Supervised Classifications

Researchers and scientists use land cover to characterize the overall watershed and determine how the surface will influence water flow. If the land cover changes significantly, the effect on the watershed can be considerable (Hernandez, 2000; Javed, Khanday, & Rais, 2011). For this study, I classified the images using the algorithms described above and used ArcGIS to analyze the change over time in each class in each watershed.

There have been similar studies on the topic. Javed et al (2011) categorized the Jaggar watershed in eastern Rajasthan for land cover using tone, texture, size, shape, pattern, association, and field knowledge. This was done for only the year 1998 (Javed et al., 2011). Huang (2012) categorized the land cover and land use for a subtropical coastal watershed in China to predict downstream water quality. This was done for an 11 year time period (Huang, 2012). In 2006, the United States Geological Survey (USGS) completed the first national land cover database using remote sensing data (Fry et al., 2011). The study by the USGS was for the entire conterminous United States for only the year 2006 without an emphasis on watersheds. My study is focused on the pixels and visual comparisons using visual remote sensing data on Google Earth to determine the land cover and then extract the data associated with each

watershed. My study is exclusive in that the study covers over a 30-year period and evaluates land cover change over an extended period of over time.

1.2.4 Problems

While there are 33 years of Landsat data with 30-meter pixels not all of these images are ideal for land cover studies because of the different issues that Landsat imagery has. Issues that can affect the images include cloud cover, atmospheric effects, scan lines (due to sensor hardware failures), mixed pixels, and satellite misreads. I minimized the effects of cloud cover by selecting images without clouds in the watershed areas to the extent possible. This is why the selected images are between the months of late June to late July and yearly spacing varies between 4 and 6 years instead of every 5 years. There is also some variability in the days because of when the Landsat satellite produced the images. Atmospheric effects were addressed through atmospheric calibration of the images using an ENVI function (Excelis, 2015). Scan lines started to become an issue for Landsat 7 after May 2003 due to a scan line correction failure, which is a mechanical failure on the satellite. To the extent possible, I removed scan lines failures by the use of the Landsat Climate Data Record (CDR) Surface Reflectance, but in most cases the area covered by the scan line failure was still lost because no data were available for those pixels. Mixed pixels are pixels that include land, water, and vegetation areas and can confuse classification algorithms. Mixed pixels were not directly addressed and I allowed the algorithms to classify any mixed pixels. This is valid because classifications that map one-pixel-to-one-class do not usually deal with mixed pixels (Mohd, 2012). Additionally, ground truth data were not available to help in addressing any mixed pixels that occurred. While most pixels are mixed to some extent, the mixed pixels that affect classification are minimal and generally occur at the

boundaries of the land cover types. Some of the satellite images have pixels that have visually anomalous values, colorful pixels, indicating noise in the collection. I did not try to perform any sort of noise reduction so these add to the error of the image processing but affect a very minimal number of pixels in the watersheds.

There are a number of practical issues with implementing the various classification schemes. For example, the ISODATA classification can spiral out of control when there are only three or fewer available classes leaving only one unclassified class. This is fixed by having more initial classes available. The maximum likelihood classification algorithm has an issue when an ROI, used to train the algorithm, only includes pixels that have the same value in one band. Essentially, this band has no variation and becomes an almost perfect linear combination of other bands thus creating a singularity (Excelis, 2015). To avoid this error, I selected a large number of pixels for training for each land cover class based off of the ISODATA classification and visual inspection. Another issue is with adding more area to the ROI files. By adding more area to a ROI, the output for the supervised classification will usually be slightly different than the previous supervised classification. In an attempt at the best possible classification, I compared the ISODATA classification and visual inspection of the imagery. Also, there had to be a certain number of land cover classes for the supervised classification algorithms to classify the areas correctly. For example, the Vegetation class alone did not pick up all of the vegetation in the area even with the ROIs in the same place. Another class called Dark Vegetation was needed to produce a more accurate land cover classification. Thus, the output split vegetation cover into two classes.

After classification, I imported the data into ArcGIS to clip the data in each watershed and run an analysis on the area of each watershed. When using ArcGIS to clip the watersheds

from the classified image, the number of pixels may be promoted (meaning more pixels are produced than are actually there) (Esri, 2015). This is true for both the *Extract by Mask* and *Clip (Data Management)* tool. From these tools, I observed that the edges of the watershed after clipping were jagged leaving small pieces of the watershed unclassified and other parts of the watershed overclassified. In other words, the watershed after clipping the 30-meter pixels, results in a stair-stepped boundary, thus promoting the number of pixels. This error would not occur if partial pixels were included after clipping. I evaluated a number of different methods for clipping the raster dataset (pixels) and used the method that created the least amount of pixels that crossed the boundary.

The watersheds that flow into Malheur Lake occupy an area larger than a single Landsat image and extend into two adjacent images, three images total. Therefore, I downloaded and classified these adjacent images and merged the resulting data into one image with the *Mosaic to New Raster* tool. This tool works great, except when the tool is run a second time. The raster dataset name needs to be changed each time the tool is run, in order to avoid error, and is advantageous to saving the data. The last problem deals with saving the raster datasets as layer files. Output raster datasets, when run from the tools in ArcGIS, are saved in a file geodatabase and are linked to the raster dataset. Choosing the same output name for each tool run results in the previous version being deleted, even though the user saves the raster dataset as a layer file. This can be avoided by having different output names from the tool and then saving the raster datasets as layer files.

2 METHODS

2.1 Remotely Sensed Data

I used images from the USGS Earth Explorer website from Landsat 5 TM, 7 ETM, and 8 OLI satellites from June 1984 to July 2014 in the form of GeoTIFF files. The Landsat images are from these areas of the Landsat satellite orbit: path 43 and row 30, path 43 and row 29, and path 44 and row 30. Path 43 and row 30 is the main image which includes Malheur Lake and surrounding areas. Path 43 and row 29 is for the image North of Malheur Lake and Path 44 and row 30 is for the image to the West of Malheur Lake. The two extra areas for images were needed to capture the areas of the watershed that were not included in the main image for Malheur Lake. Since three images were needed to determine the land cover of the watersheds, the dates of the images were between 0 and 25 days apart, but land cover change over this short interval should be minimal. This should not pose too much error since land cover does not change rapidly except with urbanization (Xiao et al., 2006). Despite the ability for land cover to change rapidly with urbanization, the changes would not be on the order of 25 days. Also, the study area is a national refuge and should have a slower rate of change compared to an urban area.

Images after May 2003 using Landsat 7 have scan line issues. Scan lines are usually black lines that show up in the image and are unusable pixels. Cloud coverage can also be an issue as the ground is hidden from view. This is a problem with getting good land cover data for

watersheds when there are scan lines throughout the image and possibly clouds. Landsat CDR Surface Reflectance provides Essential Climate Variables that can compensate for an image that has scan lines by removing them from the image (USGS, 2015c). Clouds were avoided mostly by obtaining images that did not have cloud cover. Unfortunately, this was not the case in all images and therefore, some of the images have clouds. Landsat CDR can compensate for clouds. However, there are a few areas that are classified as clouds that are not clouds thus taking away accuracy. Therefore, Landsat CDR was not used to remove cloud cover. In this way, scan lines will not be given a land classification and the clouds will not have much area to be given a land classification, thus increasing the accuracy of this study. However, this also means that there are areas of the images that are removed and not used due to these defects.

Landsat imagery has atmospheric effects or haze since the image is taken from far away distances. I corrected for these issues by calibrating the images using a standard routine in ENVI (Excelis, 2015). Sometimes, the images have pixels that have unusual coloration and are obviously discolored meaning that there is noise in the image. These pixels add to the error of the classifications for land cover, but have minimal effect due to their limited numbers. An example of discolored pixels is shown in Figure 2-1.

2.1.1 Calibration and Processing

I calibrated the Landsat images to remove atmospheric effects and to standardize the images using the same method used by Adjei to result in images representing the top of the atmosphere reflectance. The calibration requires satellite gains and offsets, solar irradiance, sun elevation, and time, which are found in the metadata for the images. However, dark subtraction

was not used (Adjei, 2015). Equation 2-1 was used to calibrate the Landsat images to a range of reflectance of 0-1:

$$\rho_\lambda = \frac{\pi L_\lambda d^2}{S_\lambda \sin\theta} \tag{2-1}$$

where ρ_λ is the reflectance, L_λ is the radiance in units of W / (m^2 * sr * μm), d is the distance from the earth to the sun, S_λ is the solar irradiance with units of W / (m^2 * μm), and θ is the elevation of the sun in degrees (Excelis, 2015).

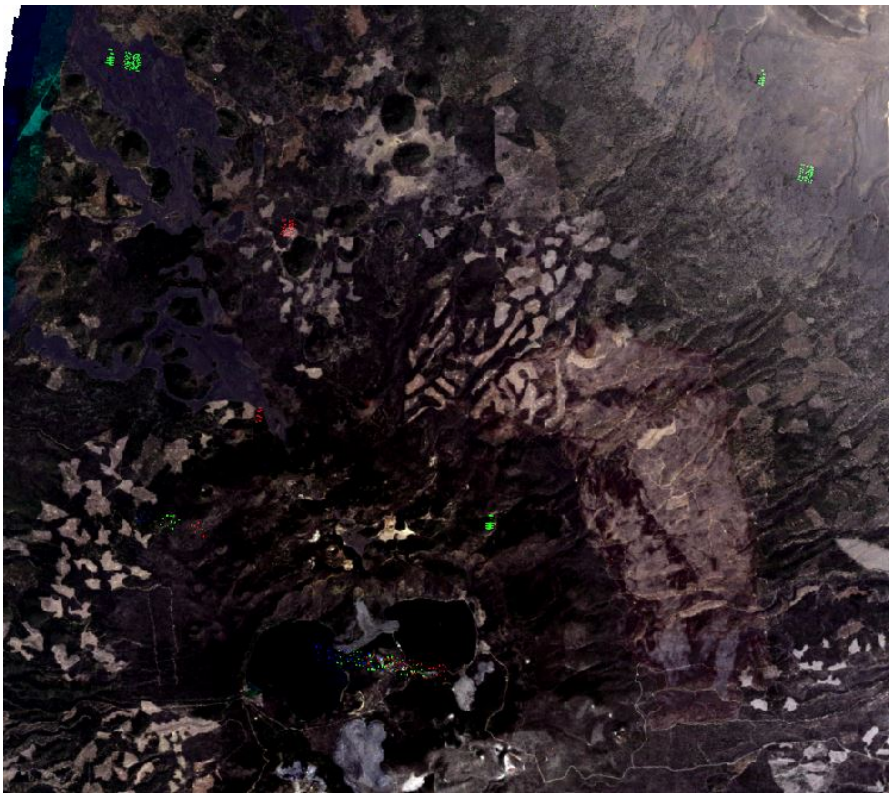

Figure 2-1: Calibrated Landsat Image West of Malheur Lake with Discolored Pixels for July 27, 1989

Another part of the classification is making sure that the bands match between the different satellites and the resolution is the same. Using the previous equation, Landsat 5 and 7 images are given a six band multispectral image. The bands are bands 1-5 and 7. Landsat 8 images are given a seven band multispectral image. Therefore, I selected bands 2-7 from the seven available bands because of their similarity to the bands from Landsat 5 and 7. Tables 1-1 and 1-2 have the specific wavelengths of the bands. Examples of calibrated Landsat images are shown in Figures 2-2 through 2-4.

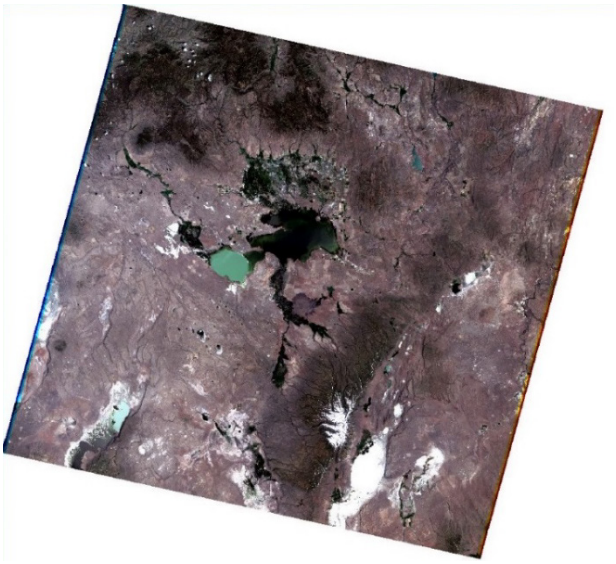

Figure 2-2: Calibrated Landsat Image of Malheur Lake and Surrounding Areas for June 28, 1984

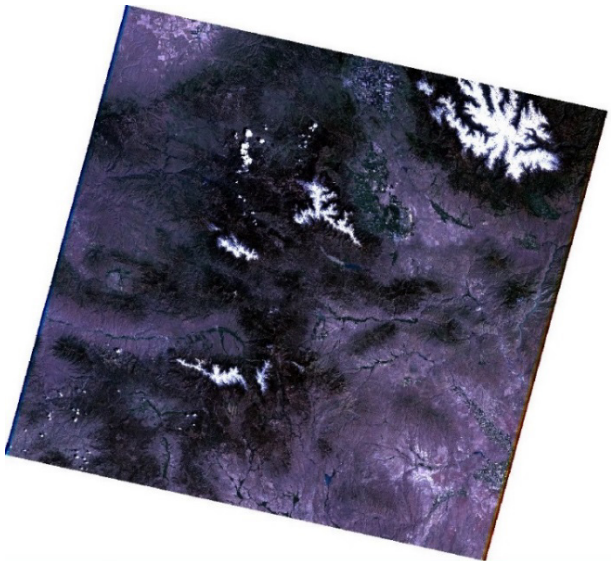

Figure 2-3: Calibrated Landsat Image North of Malheur Lake for June 28, 1984

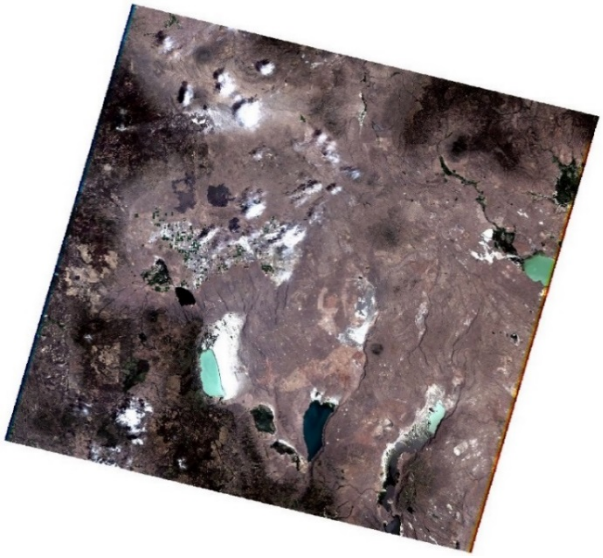

Figure 2-4: Calibrated Landsat Image West of Malheur Lake for July 5, 1984

2.2 Iterative Self-Organizing Data Analysis Technique (ISODATA) Unsupervised Classification

Initially, I classified the images using the ISODATA unsupervised classification. I parametrized the classification with the following values: the number of classes 10, maximum iterations 100, and minimum number of pixels in a class 1,000. The number of iterations were usually less than 10. All other parameters were standard. An ISODATA classified image is shown in Figure 2-5. When an image is classified with an unsupervised classification, the classes are not identified but pixels that have similar spectral features are grouped together. To identify land cover types, where areas existed that I could infer were a specific land cover type, I visually examined the calibrated Landsat images, along with Google Earth imagery and the ISODATA classifications to select ROIs to train the supervised classification methods.

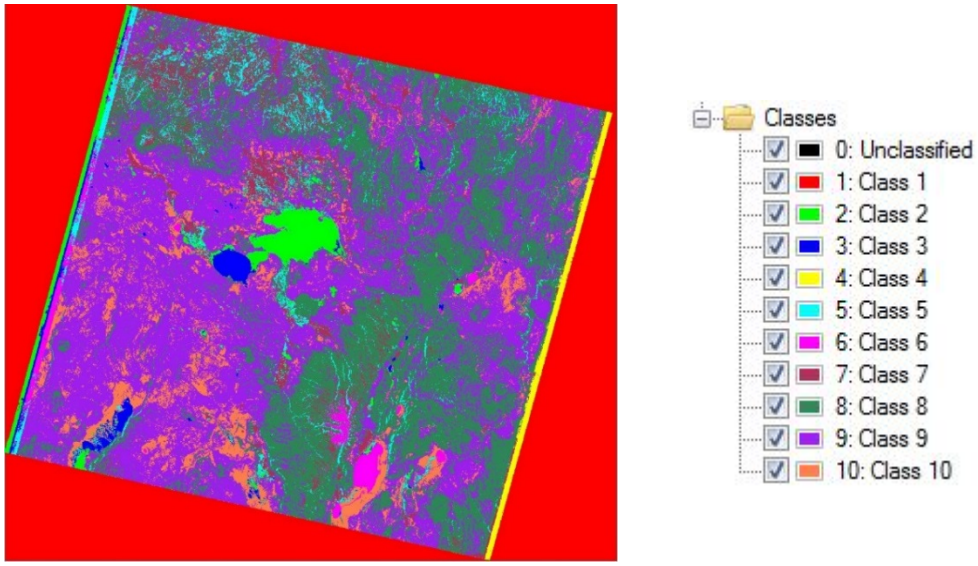

Figure 2-5: ISODATA Unsupervised Classification of Malheur Lake for June 28, 1984

I manually drew the ROIs on the calibrated Landsat image by comparing the ISODATA classification, the calibrated Landsat image, and Google Earth imagery. From these comparisons, I created ROIs for six identified classes: Water, Shallow Water, Vegetation, Dark Vegetation, Bare Earth, and Salty Area. More classes could be identified; however, this study was looking for the general land cover change that could affect the amount of water flowing into Malheur Lake, not how many classes can be identified. Also, these land cover classes were chosen to make sure that the areas that are vegetation are actually identified as vegetation. There is little value to divide the image into additional categories, which may be potentially less useful.

Land cover changes over time and there were noticeable differences among the images. This meant that the ROIs used for training in one image, may not include the same land cover in later images. This was especially true for areas that were classified as water, dark vegetation, and vegetation as the amount of precipitation in the watersheds fluctuated annually. This meant that for each year, I needed to identify ROIs for each class for each image and draw them on the image to select the pixels used to train the supervised classification algorithms. I did this by using the previous ROI file and making changes as needed by visually comparing the calibrated Landsat images, along with Google Earth imagery, and the ISODATA classification to accurately define any changes in the land cover area. Figure 2-6 shows a calibrated Landsat image with ROIs.

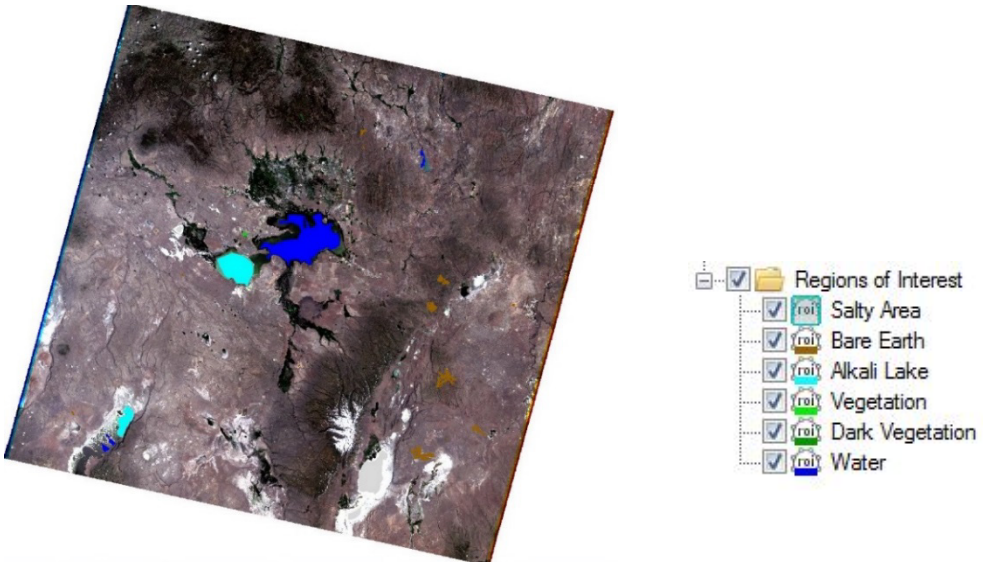

Figure 2-6: Calibrated Landsat Image of Malheur Lake with Regions of Interest (ROI) for June 28, 1984

2.3 Supervised Classification

Supervised classifications are similar to unsupervised classifications except they are based on training data selected by the user. The user identifies the training data using ROIs or ENVI Vector Files (EVF). EVF was not used because of the difficulty I had with getting the vector files to produce accurate results with the supervised classification algorithm. The software program ENVI has 12 supervised classifications available. Out of these classifications, three of them rely on other supervised classifications and therefore, I did not consider them for this study. Based on the initial runs, the binary encoding classification seemed to have great discrepancies with the ISODATA unsupervised classification and therefore, I did not use the classification. The parallelepiped, spectral angle mapper, and spectral information divergence classification did not classify some areas making the classification not viable for a land cover study. The neural net classification did not follow the ROI, making the area covered by the ROI a different

classification. The Support Vector Machine Classification was not used in this study because of complexity. After a preliminary evaluation, I selected three classification methods for this study which were based on their ability to classify all areas of the image, which was done by not having to select probability thresholds, and to closely honor the selected ROIs for training data. The supervised classifications I selected are maximum likelihood, minimum distance, and Mahalanobis distance classification.

2.3.1 Maximum Likelihood Classification

The maximum likelihood classification is based on the assumption that each class is normally distributed and determines the probability that a given pixel belongs to a specific class using the highest probability (Excelis, 2015; Mather & Koch, 2011). Figure 2-7 shows the maximum likelihood classification after it was trimmed in ArcGIS.

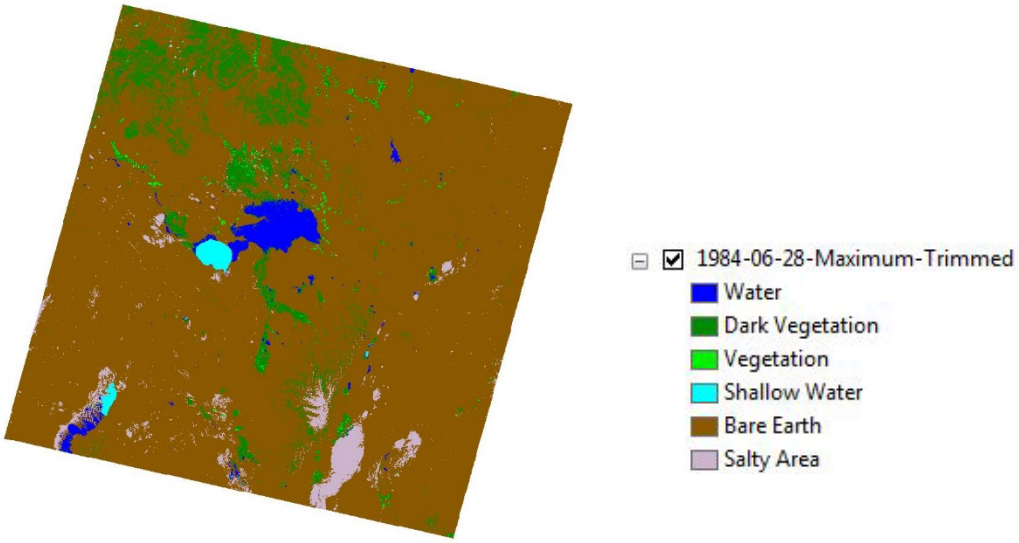

Figure 2-7: Maximum Likelihood Classification of Malheur Lake for June 28, 1984

2.3.2 Minimum Distance Classification

The minimum distance classification uses the mean of the vectors for each endmember and calculates the Euclidean distance, straight line distance between two points in multi-dimensional space, for each of the remaining or unknown pixels the distance to the mean vector for each class is computed, and assigned to the closest class (Excelis, 2015). Figure 2-8 shows the minimum distance classification after it was trimmed in ArcGIS.

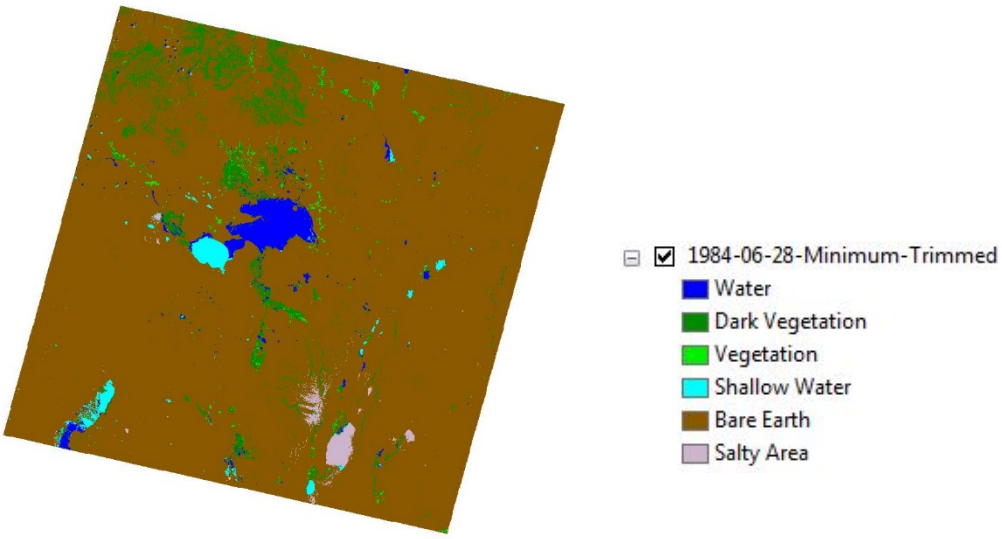

Figure 2-8: Minimum Distance Classification of Malheur Lake for June 28, 1984

2.3.3 Mahalanobis Distance Classification

The Mahalanobis distance classification is a direction-sensitive distance classifier that is similar to maximum likelihood classification except it assumes all class covariances are equal (Excelis, 2015). Figure 2-9 shows the Mahalanobis distance classification after it was trimmed in ArcGIS.

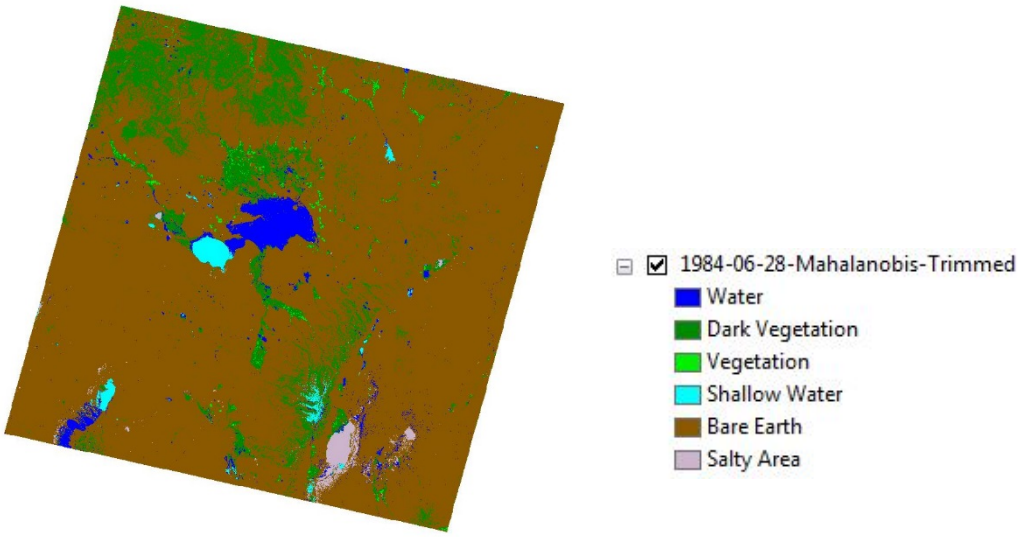

Figure 2-9: Mahalanobis Distance Classification of Malheur Lake for June 28, 1984

2.3.4 Extracting Watersheds with ArcGIS (Geographic Information System)

Once the images were classified, they were brought into ArcGIS through ENVI. To determine the best method for extracting the watersheds from the image, I used classifications from the main image with all of the watersheds that intersected that image. To define the watersheds, I used watershed shapefiles called HUC-8 (Hydrologic Unit Code) which were downloaded from the USDA website (USDA, 2015). I evaluated a number of different methods to extract the pixels in each watershed. These included the *Extract by Mask* tool, *Clip (Data Management)* tool using input features for clipping geometry and maintaining clipping extent with no data value, and *Clip (Data Management)* tool using input features for clipping geometry without a no data value. After reviewing each technique, I selected the *Clip (Data Management)* tool using input features for clipping geometry without a no data value since the tool created the least amount of pixels from the original image. However, the *Clip (Data Management)* tool using

input features for clipping geometry and maintaining clipping extent with no data value produced more accurate results than what I used for these watersheds only. Therefore, the tool used to extract the watersheds should be examined more closely with the watershed shapefiles. Table 2-1 shows the results of the extraction process. However, there should not be any extra pixels created or removed. This can be explained by the watershed boundaries and the pixels. Watershed boundaries generally curve to contour the earth's surface, but pixels are square meaning that the software has to choose whether the pixel that intersects a watershed boundary should be included in the extraction process or not.

Table 2-1: Comparison of Extraction Methods in ArcGIS

Method	Extra Pixels Created (All Watersheds)	Extra Pixels Created (Watersheds Only)
Extract by Mask	1,772	-1,409,058
Clip (Data Management) Input Features for Clipping Geometry; Maintain Clipping Extent; Without a NoData Value	10,145	-1,403,444
Clip (Data Management) Input Features for Clipping Geometry; Without a NoData Value	59	-1,408,774

I developed a model in ArcGIS using the classified images, Fill QA image, and watershed shapefiles, to quickly process the images. This model is displayed in Figures 2-10 and 2-11. Figure 2-10 represents the process for New Raster dataset's 1-3. A Fill QA image is an image provided in the Landsat CDR files that contains an area that surrounds the original image and removes areas on the sides of the image that are low in quality. The Fill QA image also

removes scan lines from an image. The Fill QA image pixels are marked as fill from the reflectance bands (USGS, 2015c).

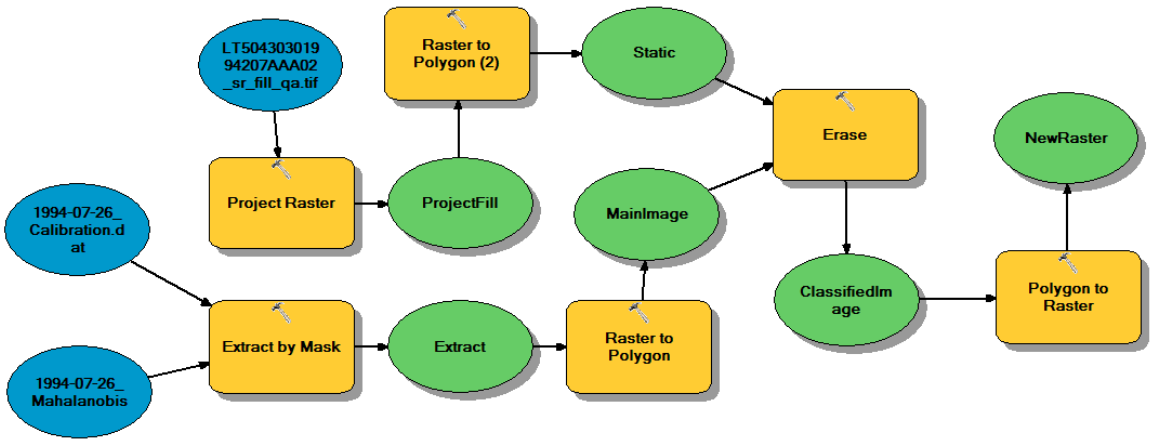

Figure 2-10: ArcGIS Model for Trimming the Classified Images

As can be seen in the model, there are a variety of tools. The *Project Raster* tool is used to change the current map projection of the Fill QA file to the same as the classified image. For the main image and the north image, this is UTM 11 (Universal Transverse Mercator), but for the west image, this is UTM 10. The *Raster to Polygon* tool is used to change a raster dataset to polygon features. This is useful as the *Erase* tool only uses features. The *Extract by Mask* tool extracts the cells of a raster dataset that match the area of the raster dataset mask. In this case, the calibrated Landsat image area is extracted from the classified image. This extraction process is needed because the *Raster to Polygon* tool will not recognize the classified image as a raster dataset until the raster dataset is extracted. The calibrated Landsat image does remove all of the excess from the classified image, but generally leaves a strip of misclassified area (Esri, 2015). This can be seen in Figure 2-12.

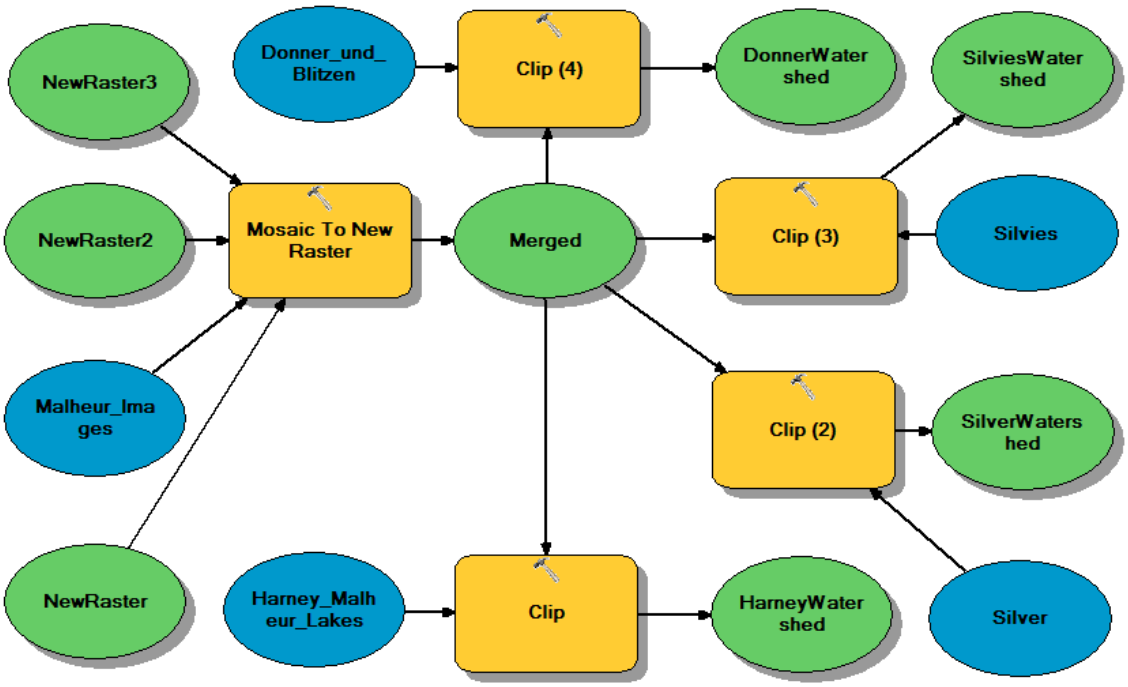

Figure 2-11: ArcGIS Model for Combining the Classified Images and Clipping Out the Watersheds

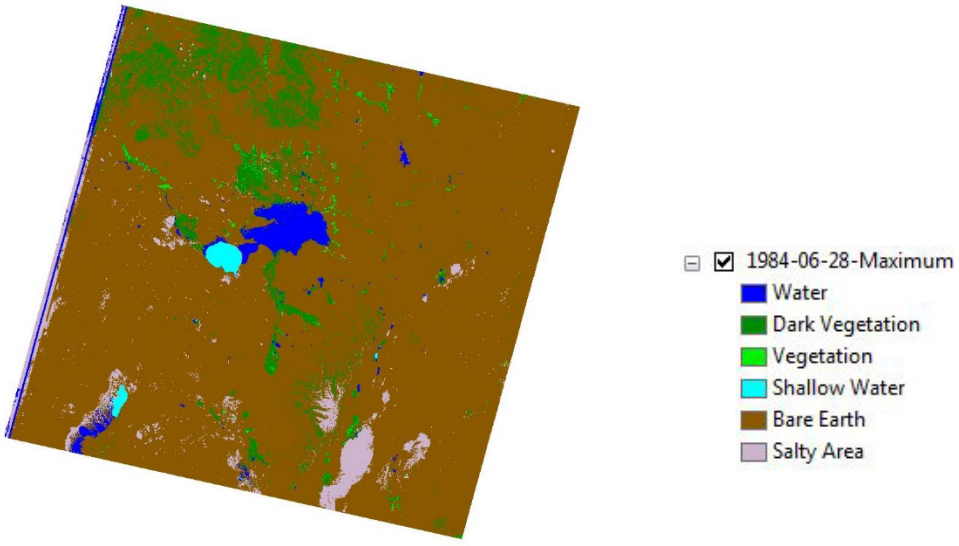

Figure 2-12: Maximum Likelihood Classification of Malheur Lake for June 28, 1984 After Extraction

The *Erase* tool removes a feature set area from the feature set. This is used to remove the strip of misclassified area along the edges of the images and scan lines, if the image has scan lines, using the Fill QA image. The *Polygon to Raster* tool is the same as the *Raster to Polygon* tool just in the opposite direction. Figures 2-7 through 2-9 show classified images after the *Raster to Polygon* tool has been run. The *Mosaic to New Raster* tool is used by taking multiple raster datasets and combining them into one raster dataset. The cell size and the number of bands were kept the same as the original classified images and the mosaic operator along with the mosaic color map were chosen as first to give precedence to the main image of Malheur Lake because of the overlap of the images. Figure 2-13 shows a combined image. Also, the *Mosaic to New Raster* tool creates a raster dataset and a folder with the same name as the raster dataset. When the model is run another time for other classifications, the model will stop at the *Mosaic to New Raster* tool. This is because the tool is trying to create a new folder for the new raster dataset, but the folder has the same name as the previous folder and raster dataset. To combat this issue, the user needs to change the raster dataset name in the model each time. The *Clip (Data Management)* tool extracts a portion of a raster dataset and has the option of using the input features of the watersheds as the clipping geometry thus extracting out the watersheds (Esri, 2015). Using the model gives the same results as using the *Clip (Data Management)* tool for the Donner und Blitzen and Harney-Malheur Lakes watersheds on the main image of Malheur Lake. On the other hand, the other two watersheds would have areas missing, thus making the full model necessary. Figure 2-14 shows the four watershed raster datasets. The watershed raster datasets for each classification over the 30-year study period are displayed in Appendix A.

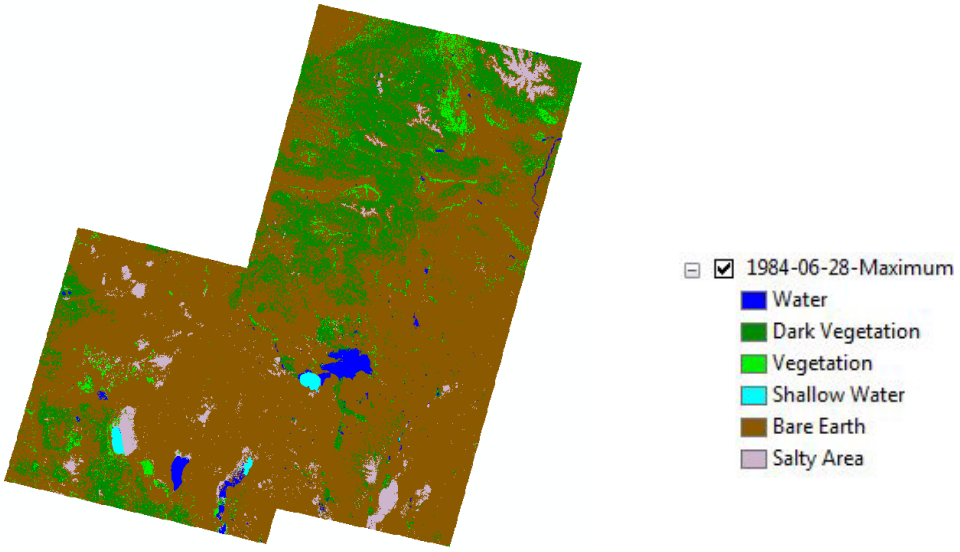

Figure 2-13: Maximum Likelihood Classification of Malheur Lake Combined Image for Midsummer 1984

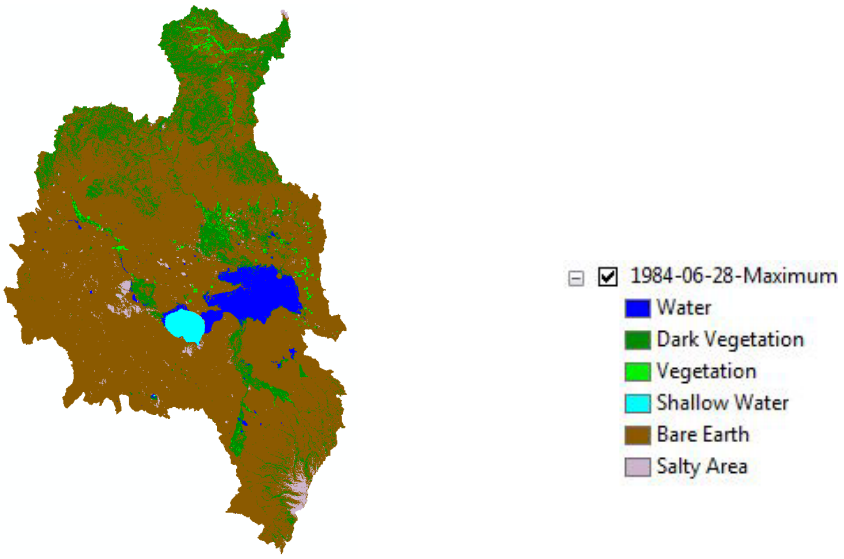

Figure 2-14: Maximum Likelihood Classification of the Watersheds that Contribute to the Malheur Lake Area for Midsummer 1984

3 RESULTS AND DISCUSSION

3.1 Supervised Classification Trends

In this section, I look at each of the supervised classifications and determine which of the algorithms are best for defining land cover. Also, I present the trends over time for the different land cover classes with respect to the different supervised classification algorithms. Figures 3-1 through 3-6 show the total watershed area for the different supervised classification algorithms for each of the land cover classes. Graphs of each of the total and individual watersheds along with the individual land cover classes are shown in Appendix B and are not examined separately in this report.

One good way to determine which supervised classification should be used to define land cover is through an analysis of the area of each of the land cover classes. As can be seen from Figures 3-1 through 3-6, the classifications for Water and Bare Earth between the supervised classification algorithms have little variation between them. The other land cover classes do not have such uniformity. Part of this can be explained by the size of the various land cover types. For example a 150,000 acre change in Bare Earth classification among the methods is a minimal difference, while this change for the Vegetation class is larger than the total classified area. The total area for Salty Area is similar between the minimum distance and Mahalanobis distance classifications, but the maximum likelihood classification has a much larger area. The total watershed area for Dark Vegetation varies between the classifications. The total watershed area

for Vegetation and Shallow Water seem to be somewhat uniform except for in 1998 when the maximum likelihood classification spikes and 2004 when the Mahalanobis distance classification spikes respectfully. The classification that seems to be the most uniform throughout is the minimum distance classification.

Additionally, the land cover areas can be examined through Min-Max normalization. Min-Max normalization takes data measurements and changes them into a value between 0 and 1 by subtracting the minimum value and then dividing by the difference of the maximum and minimum data measurements. Equation 3-1 was used to normalize the land cover areas to a range of 0-1:

$$MM\left(X_{ij}\right)=\frac{X_{ij}-X_{\min}}{X_{\max}-X_{\min}} \tag{3-1}$$

where $MM\left(X_{ij}\right)$ is the data point normalized between 0 and 1, X_{ij} is each data point, $X_{\min}$ is the minimum among the data points, and $X_{\max}$ is the maximum among the data points. This process will create a minimum value of 0 and a maximum value of 1 for each data set. Using the Min-Max normalization technique is a great way to compare values that are on different scales or different units (Mohamad, 2013).

Figures 3-7 through 3-12 display the normalized values for each land cover class. These figures seem to follow the trend of the total watershed area graphs from Figures 3-1 through 3-6, only on a more inflated scale. The Water class seems to be mostly uniform. Originally, the Bare Earth class seemed to have uniformity as shown in Figure 3-3, but now has more variation between the classes as shown in Figure 3-8. This is because the scale was drastically reduced, thus exposing the variations in the land cover classes. The Salty Area and Vegetation class have

some similarities between the minimum distance and Mahalanobis distance classifications, but the maximum likelihood classification is more variant. There seems to continue to be variation in the Dark Vegetation class. The Shallow Water class has some variation with the maximum likelihood classification, but the minimum distance and Mahalanobis distance seem to be mostly uniform except in 2004 when the Mahalanobis distance classification spikes. From the Min-Max normalization technique, the minimum distance classification seems to be the most uniform.

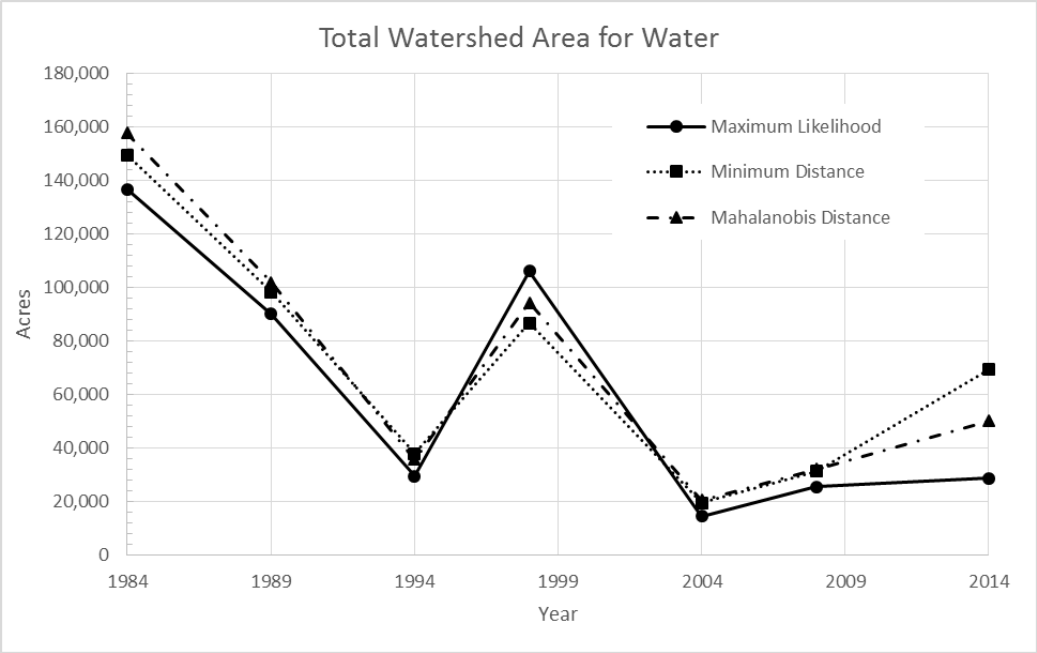

Figure 3-1: Total Watershed Area for Water Classification

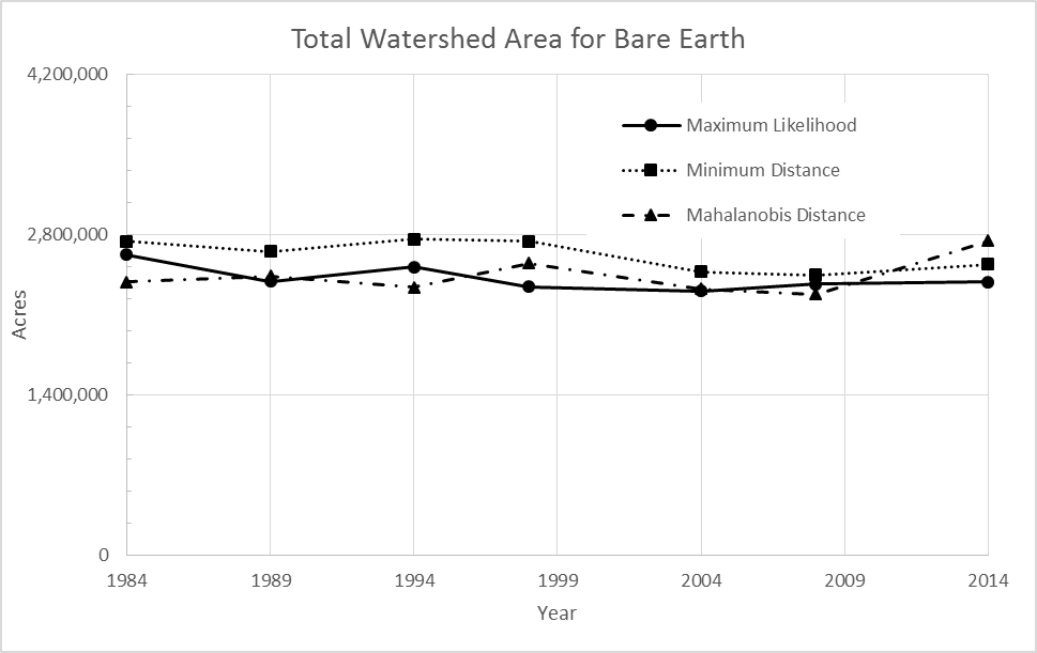

Figure 3-2: Total Watershed Area for Bare Earth Classification

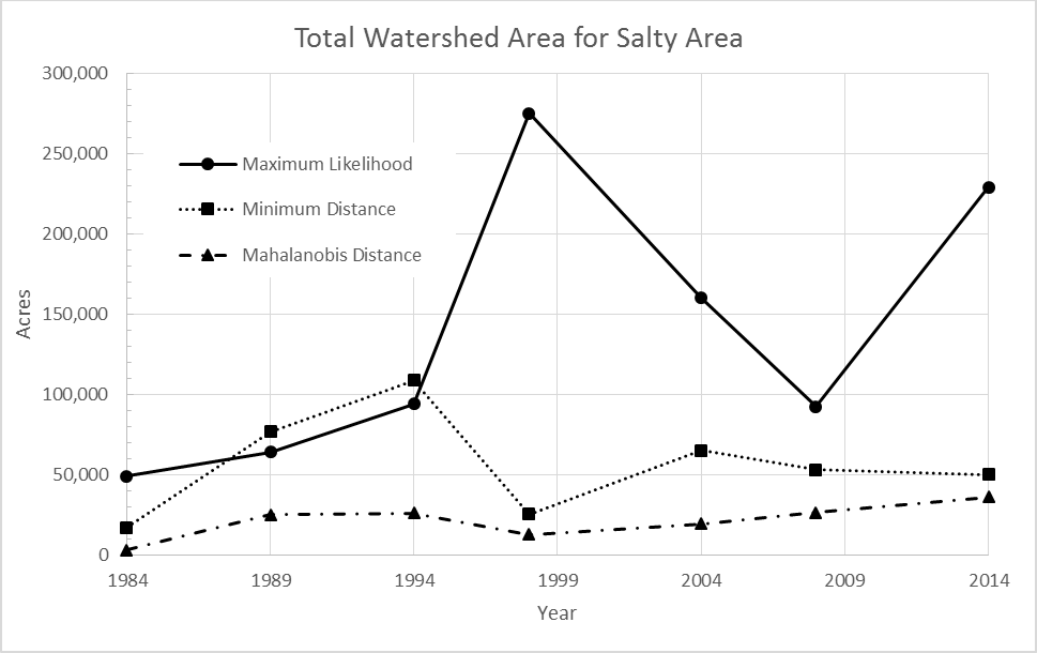

Figure 3-3: Total Watershed Area for Salty Area Classification

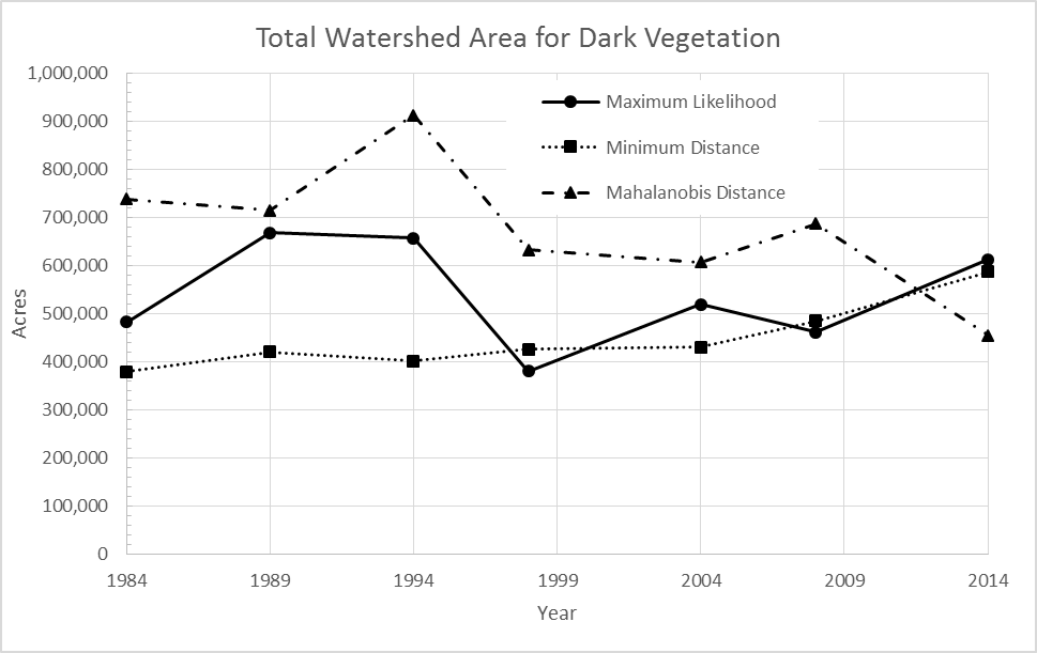

Figure 3-4: Total Watershed Area for Dark Vegetation Classification

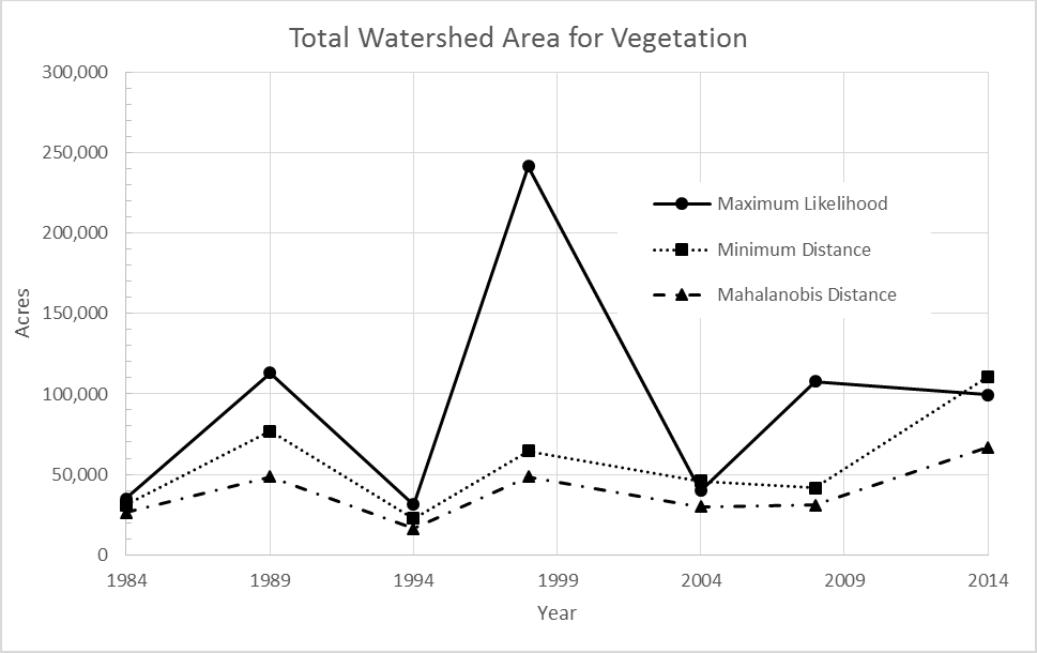

Figure 3-5: Total Watershed Area for Vegetation Classification

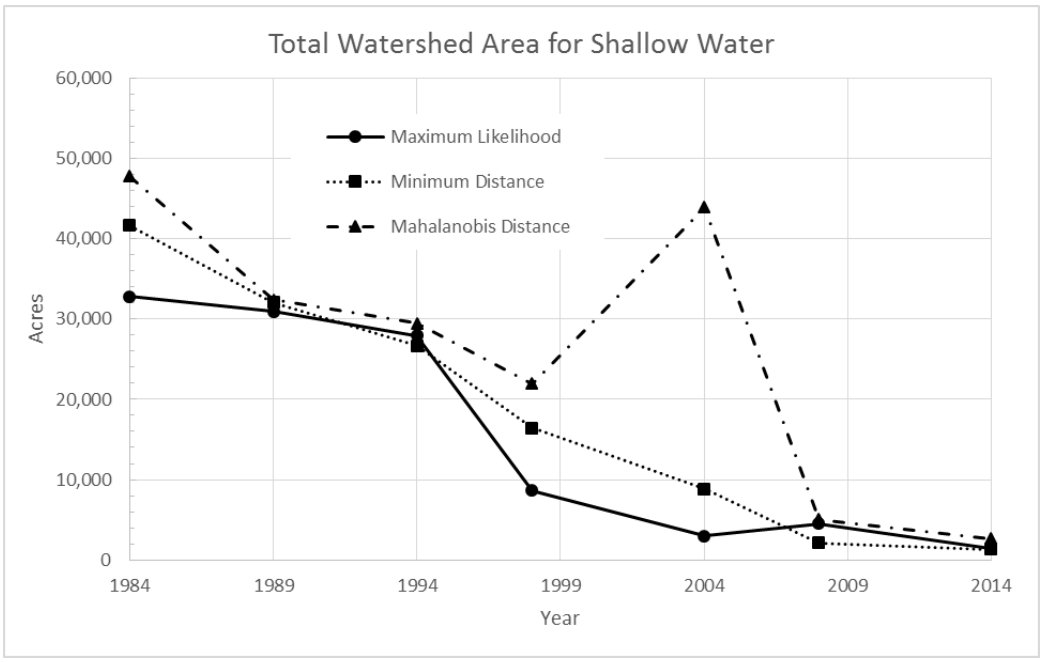

Figure 3-6: Total Watershed Area for Shallow Water Classifications

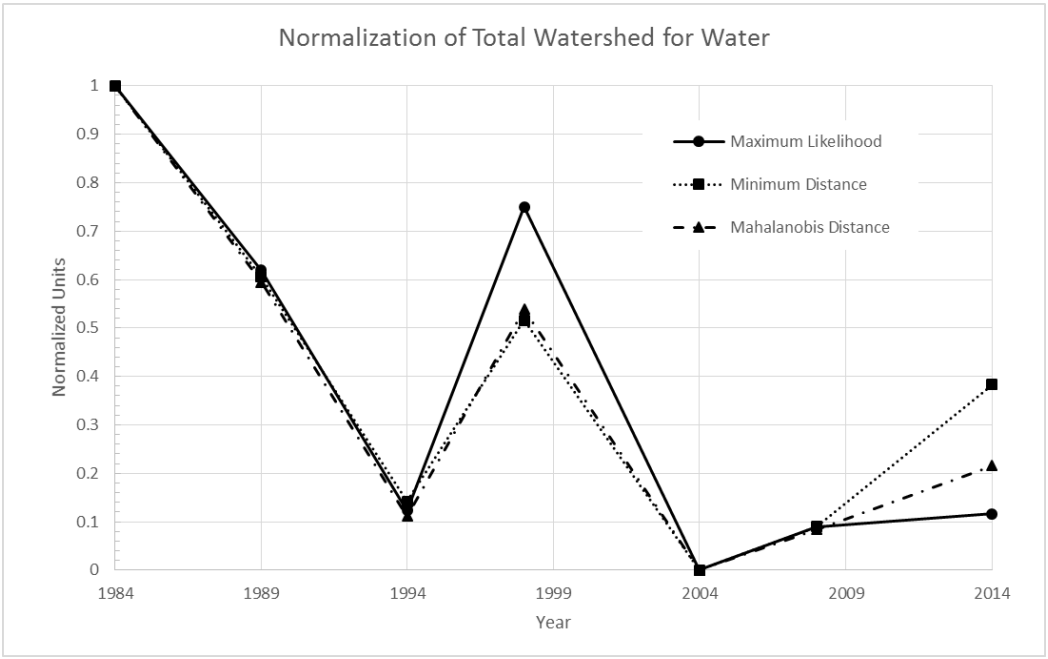

Figure 3-7: Normalization of the Total Watershed for Water Classification

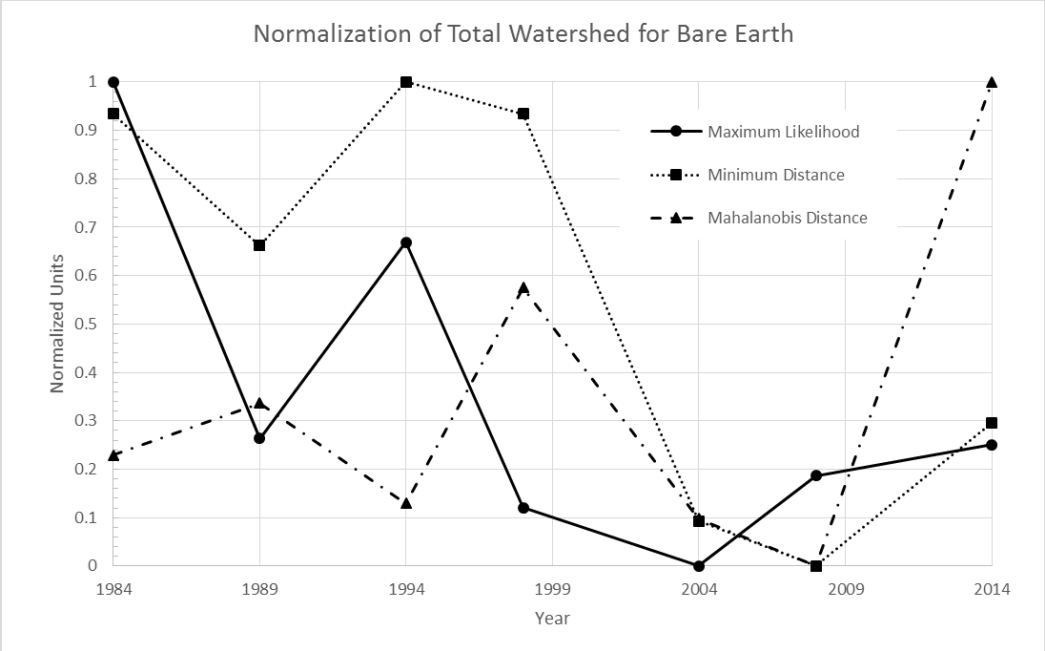

Figure 3-8: Normalization of the Total Watershed for Bare Earth Classification

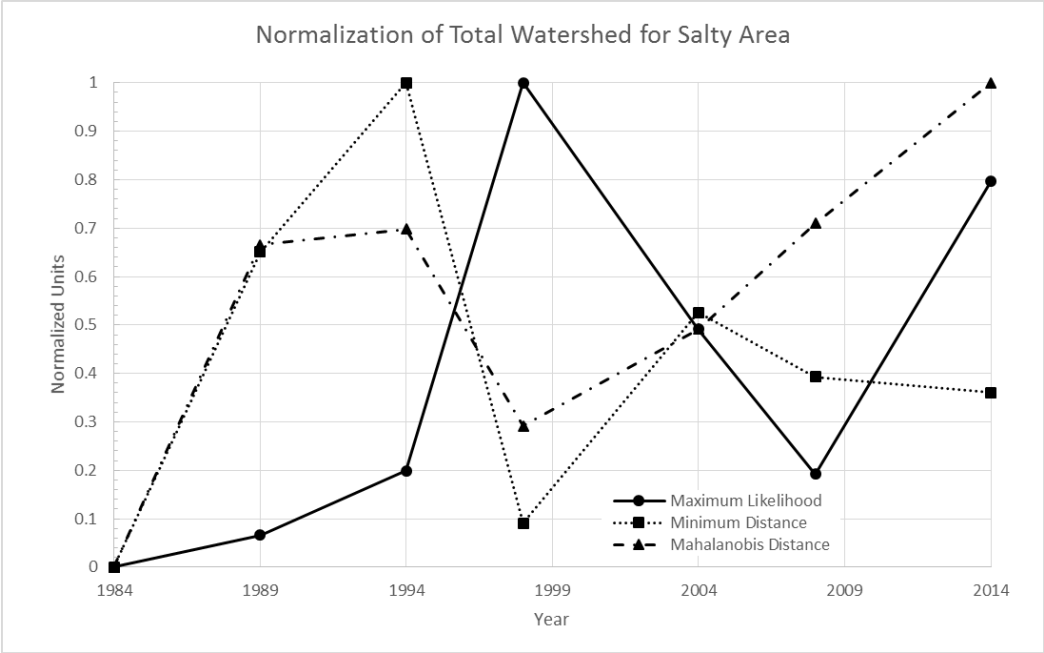

Figure 3-9: Normalization of the Total Watershed for Salty Area Classification

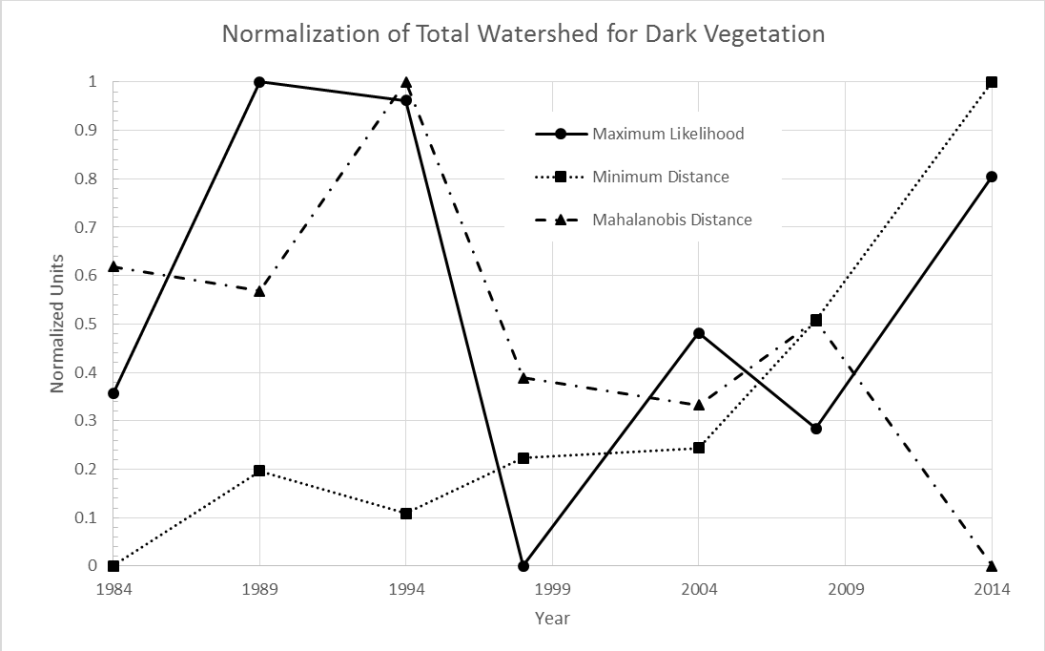

Figure 3-10: Normalization of the Total Watershed for Dark Vegetation Classification

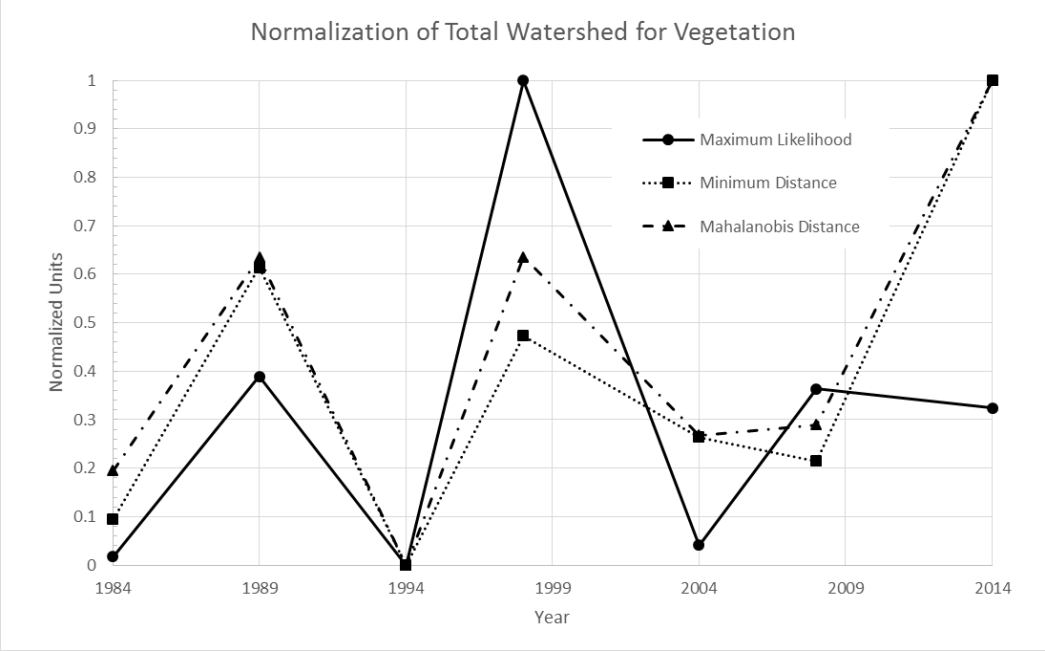

Figure 3-11: Normalization of the Total Watershed for Vegetation Classification

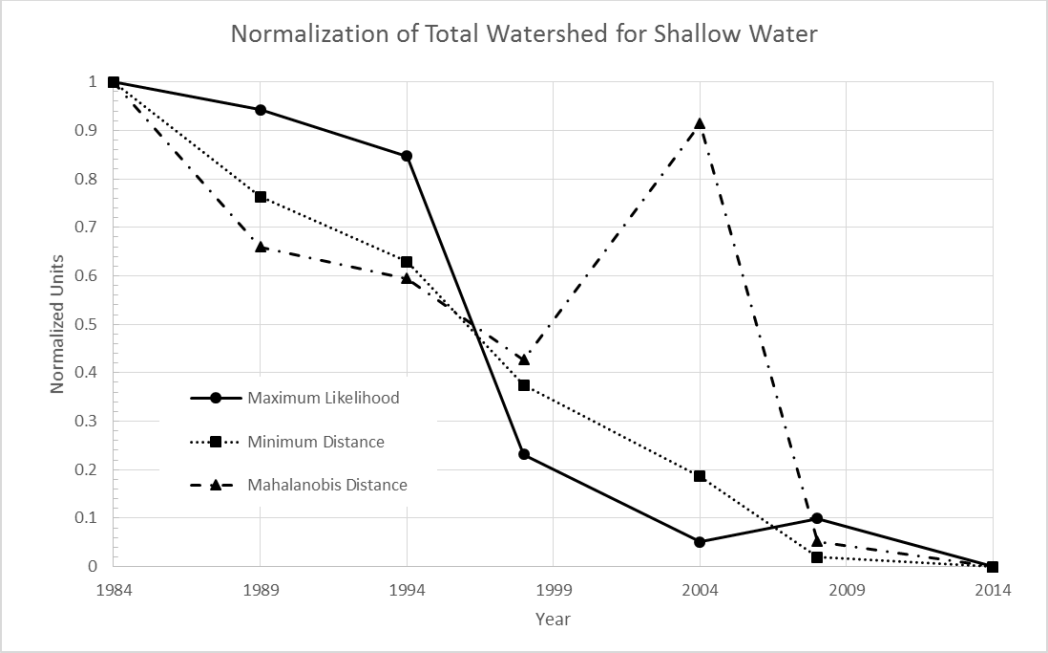

Figure 3-12: Normalization of the Total Watershed for Shallow Water Classification

Another qualitative way to determine which supervised classification to use is through visual inspection of the classified images. Figures 3-13 through 3-15 show the combined images for midsummer, 1989. The maximum likelihood classification has an area in the upper part of the image that appears to have more Salty Areas which does not seem to match with the rest of the image. This happened to be the case for all of the classifications except for midsummer 1984. The minimum distance classification has more Bare Earth classifications. The Mahalanobis distance classification seems to have a lot of different areas with water that are actually not water. Judging from the imagery and the uniformity in the graphs, I recommend the minimum distance classification be used for image processing in this study. One of the reasons that the minimum distance classification algorithm gave good results may be because the ISODATA classification also used minimum distance techniques.

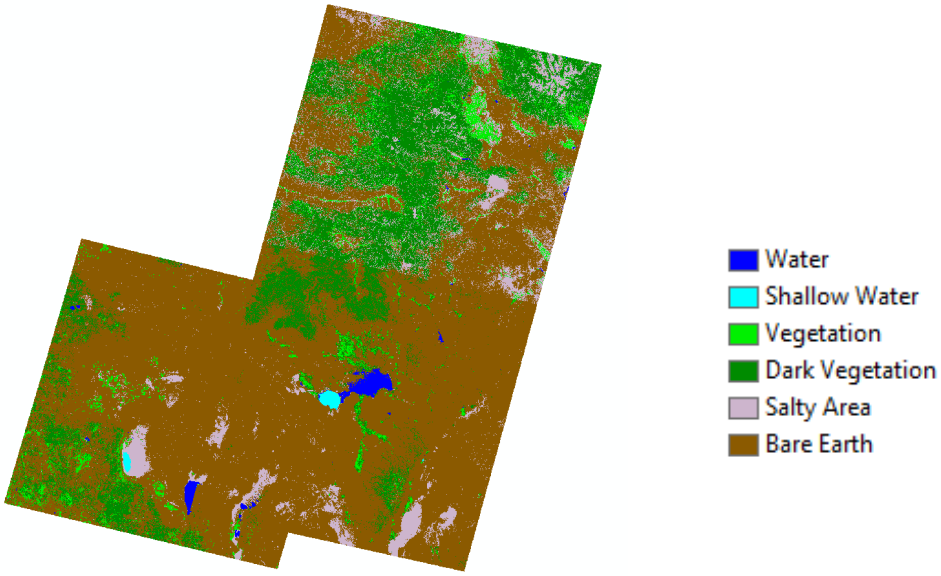

Figure 3-13: Maximum Likelihood Classification of Malheur Lake Combined Image for Midsummer 1989

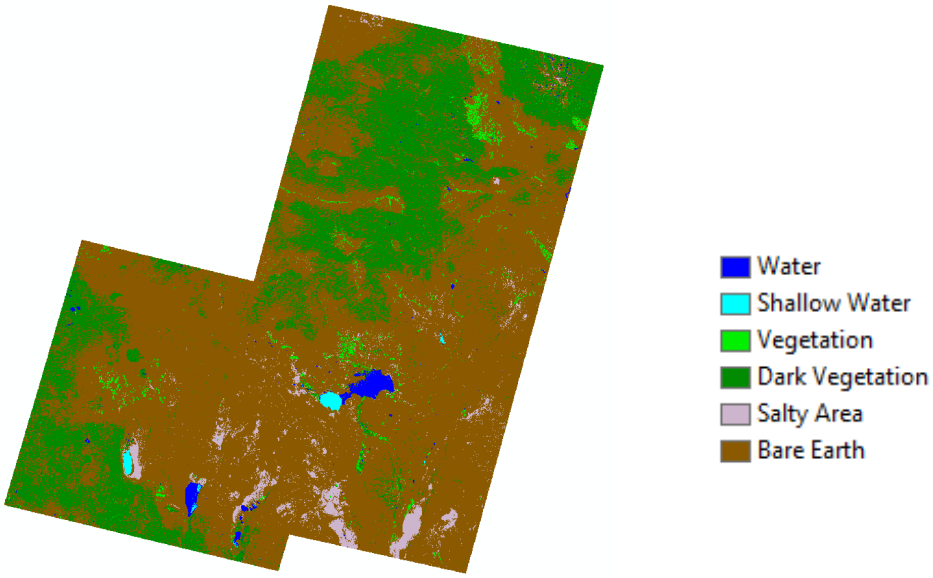

Figure 3-14: Minimum Distance Classification of Malheur Lake Combined Image for Midsummer 1989

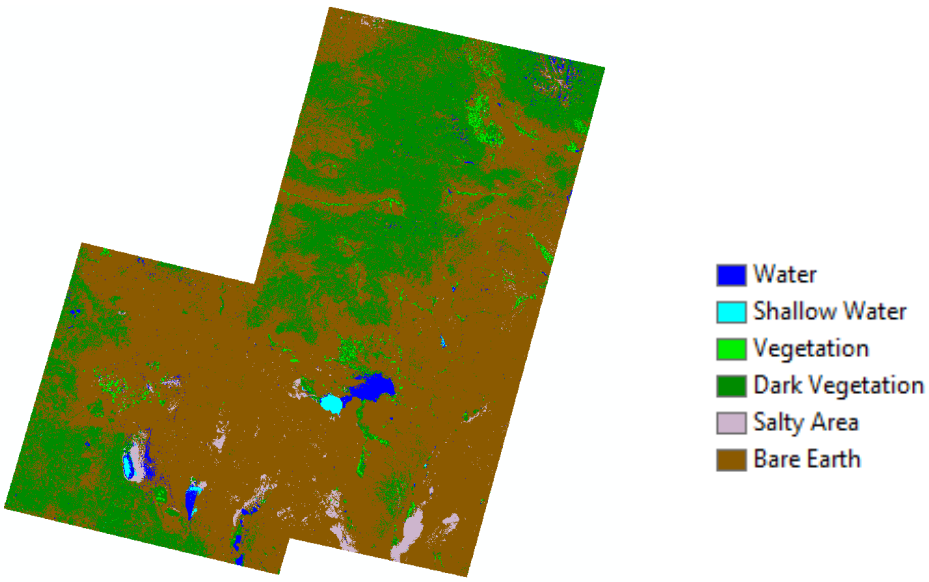

Figure 3-15: Mahalanobis Distance Classification of Malheur Lake Combined Image for Midsummer 1989

Figures 3-16 through 3-18 gives a sense of how the classifications and land cover types changed compared to each other over time. Table 3-1 shows the values for the total area of the watersheds for each classification and land cover class. Tables with a breakdown of the individual watersheds for each classification and land cover class are displayed in Appendix C and are not discussed in the body of this report. For the majority of the time from Table 3-1, the maximum likelihood classification had the largest area for Vegetation and Salty Area classes, the minimum distance classification had the largest area for the Bare Earth class, and the Mahalanobis distance classification had the largest area for Water, Shallow Water, and Dark Vegetation classes. One of the advantages of these graphs and tables is that a user can look at any year, in the extents, and determine what the amount of each area is for each class in the midsummer. However, since the images for the years 2004 and 2008 had scan lines, those areas were not included in the totals thus producing smaller areas during those years. Therefore,

interpreting between 1998 and 2014 may give lower areas than what is actually there because of the scan lines.

Figure 3-19 shows the statistics for the correlation of the logarithmic transform of the land cover variables against the year. This shows that all land cover variables were statistically significant with a 99% Confidence Interval except Dark Vegetation and Bare Earth. This may be because Bare Earth does not change much and Dark Vegetation is more of a forested area, which usually does not change much. This correlation indicates a general trend in the data.

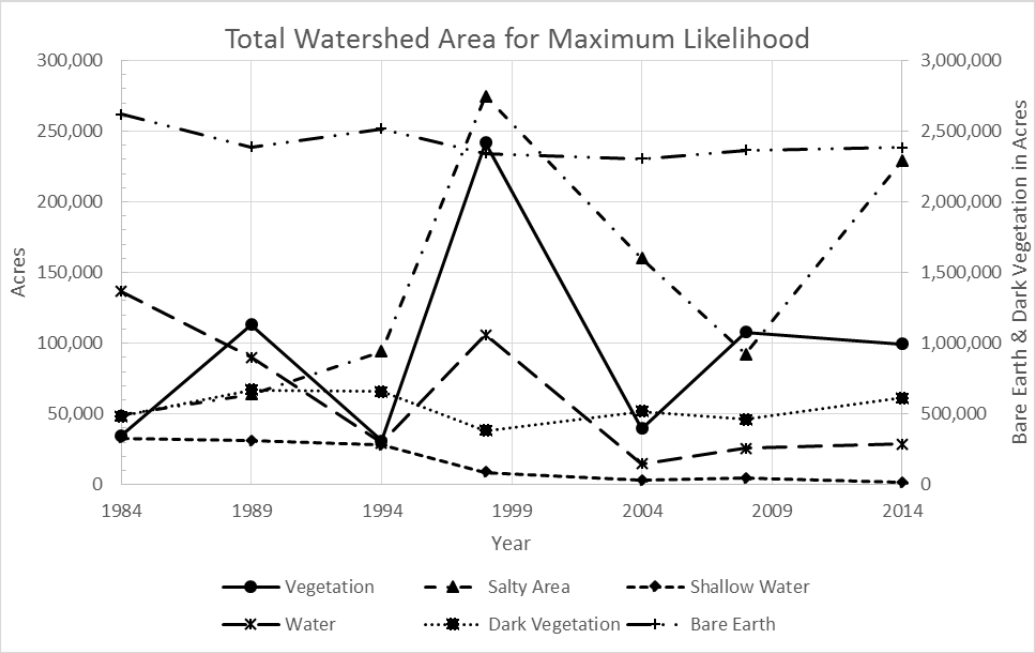

Figure 3-16: Total Watershed Area for Maximum Likelihood Classification with Land Cover Classes

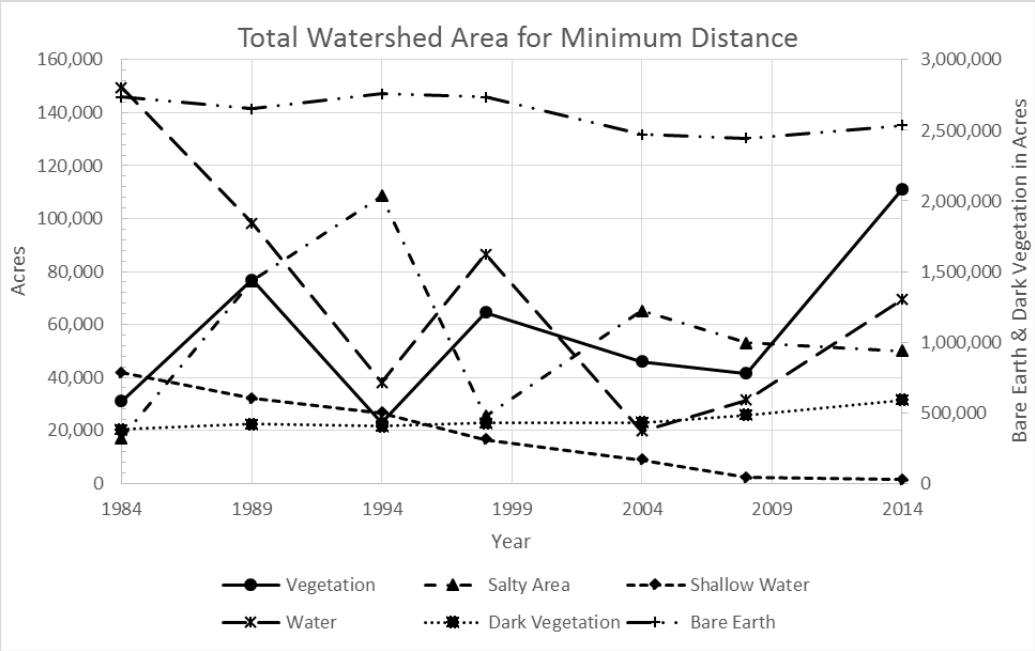

Figure 3-17: Total Watershed Area for Minimum Distance Classification with Land Cover Classes

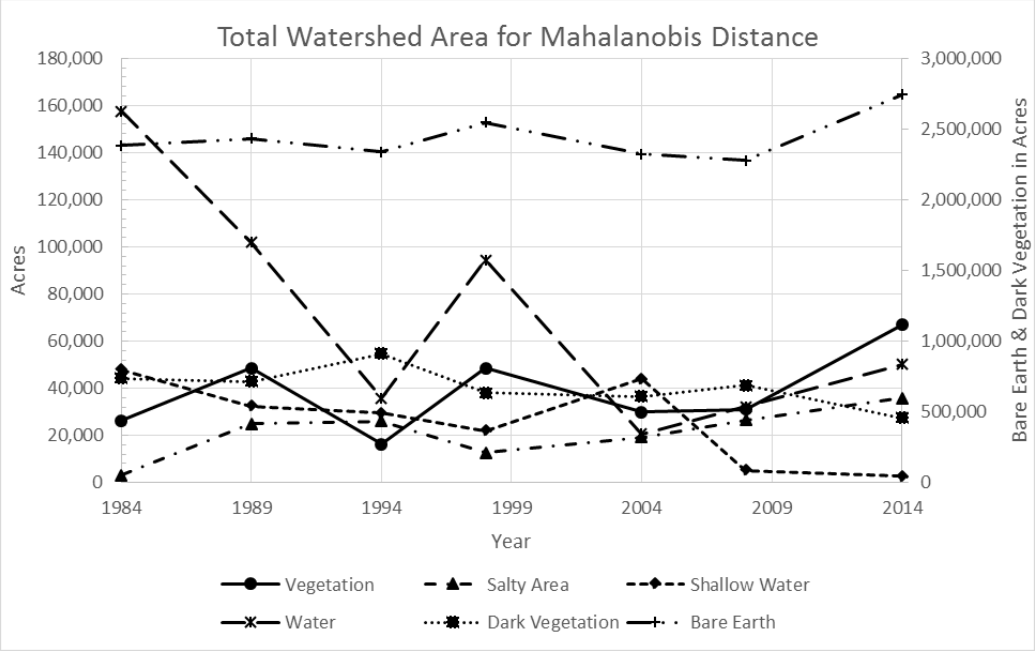

Figure 3-18: Total Watershed Area for Mahalanobis Distance Classification with Land Cover Classes

Table 3-1: Total Watershed Area with Classes and Classifications Specified

		Classes (Acres)					
Year	Classification	Water	Shallow Water	Vegetation	Dark Vegetation	Salty Area	Bare Earth
1984	Maximum	136,629	32,791	34,798	483,070	49,129	2,619,817
	Minimum	149,519	41,666	30,961	379,582	17,007	2,737,497
	Mahalanobis	157,588	47,823	26,150	738,028	3,157	2,383,487
1989	Maximum	90,188	30,986	113,150	668,533	64,040	2,389,337
	Minimum	98,294	32,108	76,903	420,491	76,564	2,651,871
	Mahalanobis	101,999	32,449	48,422	714,939	24,937	2,433,487
1994	Maximum	29,653	27,971	31,073	657,412	94,096	2,516,029
	Minimum	38,052	26,691	22,674	402,280	108,520	2,758,014
	Mahalanobis	35,862	29,504	16,284	912,109	26,002	2,336,472
1998	Maximum	106,119	8,666	241,757	380,448	274,791	2,344,434
	Minimum	86,643	16,444	64,469	426,019	25,355	2,737,286
	Mahalanobis	94,409	21,951	48,507	633,126	12,696	2,545,526
2004	Maximum	14,551	2,980	39,691	519,206	160,010	2,306,664
	Minimum	19,647	8,835	46,003	430,407	65,153	2,473,056
	Mahalanobis	20,574	43,941	29,848	607,579	19,259	2,321,902
2008	Maximum	25,520	4,508	107,670	462,249	92,503	2,364,998
	Minimum	31,369	2,099	41,612	485,370	53,012	2,443,986
	Mahalanobis	32,124	5,019	30,953	687,201	26,385	2,275,765
2014	Maximum	28,817	1,387	99,328	612,382	229,052	2,385,267
	Minimum	69,401	1,310	110,941	587,647	49,978	2,536,954
	Mahalanobis	50,147	2,657	66,950	455,546	35,903	2,745,029

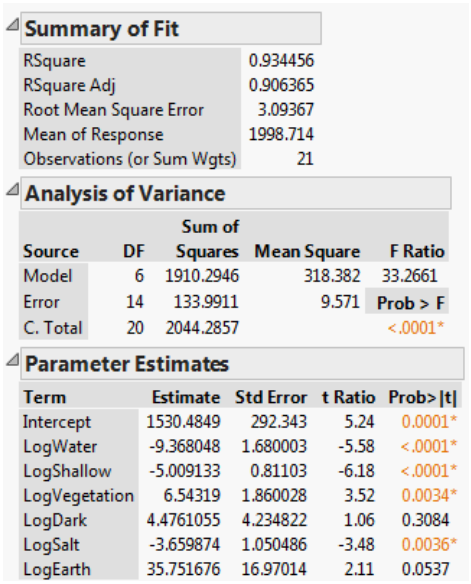

Summary of Fit

RSquare	0.934456
RSquare Adj	0.906365
Root Mean Square Error	3.09367
Mean of Response	1998.714
Observations (or Sum Wgts)	21

Analysis of Variance

Source	DF	Sum of Squares	Mean Square	F Ratio
Model	6	1910.2946	318.382	33.2661
Error	14	133.9911	9.571	Prob > F
C. Total	20	2044.2857		<.0001*

Parameter Estimates

Term	Estimate	Std Error	t Ratio	Prob>|t|
Intercept	1530.4849	292.343	5.24	0.0001*
LogWater	-9.368048	1.680003	-5.58	<.0001*
LogShallow	-5.009133	0.81103	-6.18	<.0001*
LogVegetation	6.54319	1.860028	3.52	0.0034*
LogDark	4.4761055	4.234822	1.06	0.3084
LogSalt	-3.659874	1.050486	-3.48	0.0036*
LogEarth	35.751676	16.97014	2.11	0.0537

Figure 3-19: Statistical Significance of Logarithmic Transform of Land Cover

3.2 Correlation of Watersheds with Climate Conditions

In this section, I present how the land cover types correlate with various measures of climate conditions over time. Figures 3-20 through 3-23 display the Palmer Drought Severity Index (PDSI) for the month of the main images used in the study until the year 2000. PDSI was created in 1965 by Wayne Palmer to determine the complete moisture status of an area and is calculated using temperature, precipitation, and soil moisture (NOAA, 2015). The PDSI does not take into account snow melt, frozen ground, or runoff, therefore making the index not a comprehensive view of a drought (NDMC, 2015a). Palmer states that his index does not look at all of the causes of drought (Palmer, 1965). Figures 3-24 through 3-26 give a good sense of the types of classifications I analyzed and their correlation with the land cover types; namely, water, vegetation, and earth classifications which are the combinations of Water and Shallow Water, Dark Vegetation and Vegetation, and Bare Earth and Salty Area land cover classes respectfully.

Looking at Figure 3-20 and Figure 2-2 for the year 1984, the area appears to be moist. Figure 3-24 confirms this with the highest amount of visible water in this study. Figure 3-26 has the highest amount of visible earth which may mean that the area is receiving much needed moisture. For July 1989, I noticed in Figure 3-21 that the area had a PDSI in the normal range. This seemed strange because Figure 3-24 had a drastically smaller amount of water visible. After some research, I found out that, from 1987 to 1989, the area suffered through the North American Drought. Figure 3-27 shows the height of the drought for the Malheur Lake area in 1988. Because the drought proceeded the 1989 image, the water levels drastically decreased, though the year itself was wet. Figure 3-28 shows that the level of discharge for the Donner und Blitzen and Silvies Rivers drastically decreased during this time frame. The data for this figure were downloaded from the USGS National Water Information System with the assistance of the

HydroDesktop program (Ames, 2012; USGS, 2015b). Figure 3-29 shows that the precipitation decreased by an average of 7 inches per year and the average high temperature in the summer decreased by about 7°F. The average precipitation was measured in tenths of millimeters per day and was converted to inches which were averaged for each year. The average high temperature in the summer was averaged from the high temperatures for the months of June, July, and August, if available. The average high temperature was interpolated for the year 2007 because the temperature was not available. Appendix D provides a table of the average precipitation, average summer high temperature, and average discharge. Figure 3-25 shows that the vegetation increased to the highest level recorded in this study. This may be because of many different factors. Some of these factors may include the farming activities in the area, the plant uptake of groundwater, a lower high temperature and possible error in the land cover classes.

For July 1994, Figure 3-22 indicates that the area had a PDSI in the severe drought range. The Governor of Oregon declared that the area was in a drought from 1991 to May 19, 1993 (Governor, 1991-2015). The discrepancy from the Governor of Oregon and the PDSI may be due to the amount of runoff and snow melt the area was receiving, which are not taken into account in the PDSI. The water level and the discharge decreased drastically as shown in Figures 3-24 and 3-28 respectively, which provide support that the area was in a drought before 2004 and had not yet fully recovered. The average precipitation and average summer high temperature had a gradual increase in these years, which means that the precipitation was most likely taken by evapotranspiration, infiltration, and percolation. The level of vegetation slightly decreased in Figure 3-25 but this is hard to judge from the graph. This is most likely due to the farming activities in the area and plant uptake of groundwater maintaining most of the vegetative area and possible error in the land cover classes.

For July 1998, Figure 3-23 indicates that the area had a PDSI in the extremely moist range. The area was not considered in a drought by the Governor of Oregon and there was not a drought since the last image of July 1994 (Governor, 1991-2015). Since the drought was over and the precipitation continued to increase, the level of water increased and the discharge in the Donner und Blitzen River increased. However, the Silvies River did not have any flow because of the previous drought and did not yet recover at this point in time. With the increase of the average summer temperature to over 78°F, the possible decline in farming activities, and potential error in the land cover classes may have decreased the level of vegetation.

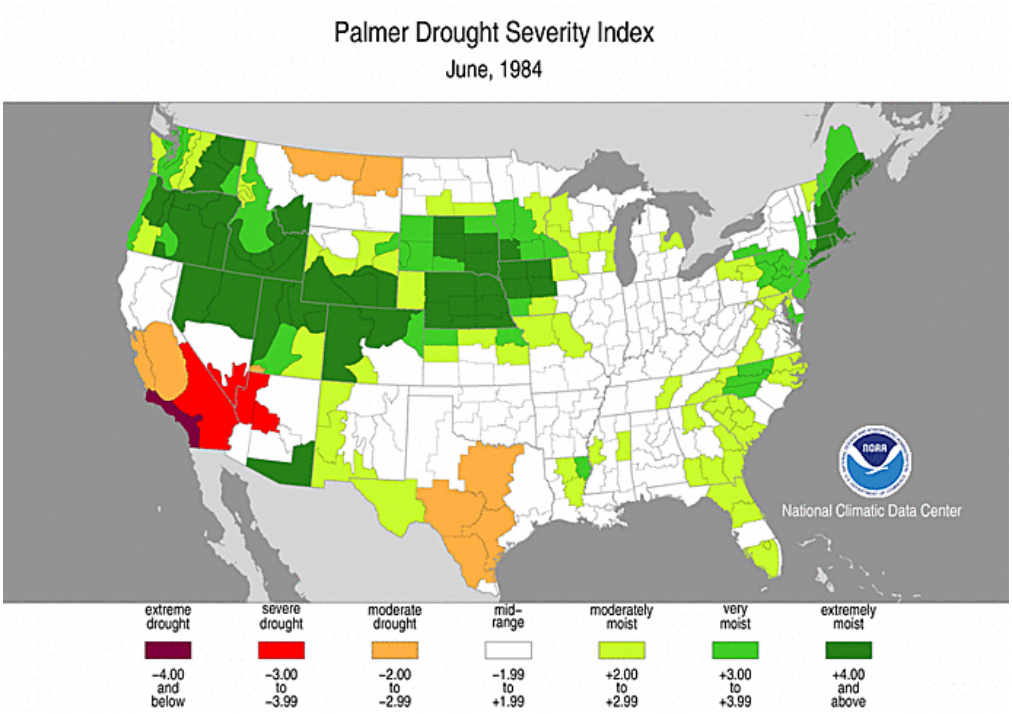

Figure 3-20: Palmer Drought Severity Index for June 1984 (NOAA, 2015)

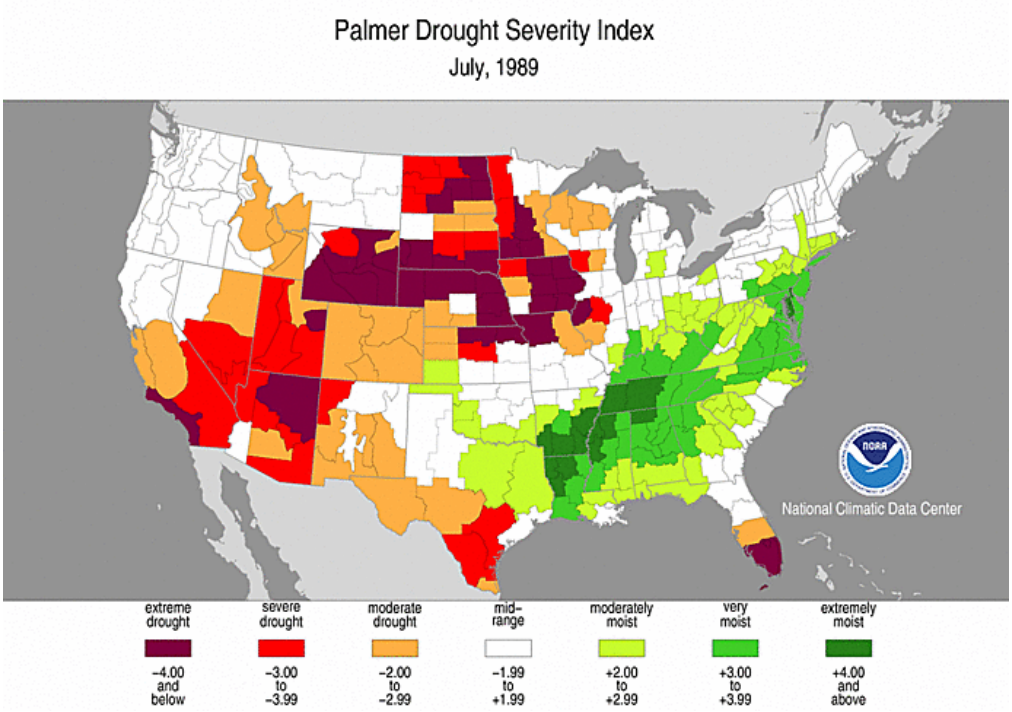

Figure 3-21: Palmer Drought Severity Index for July 1989 (NOAA, 2015)

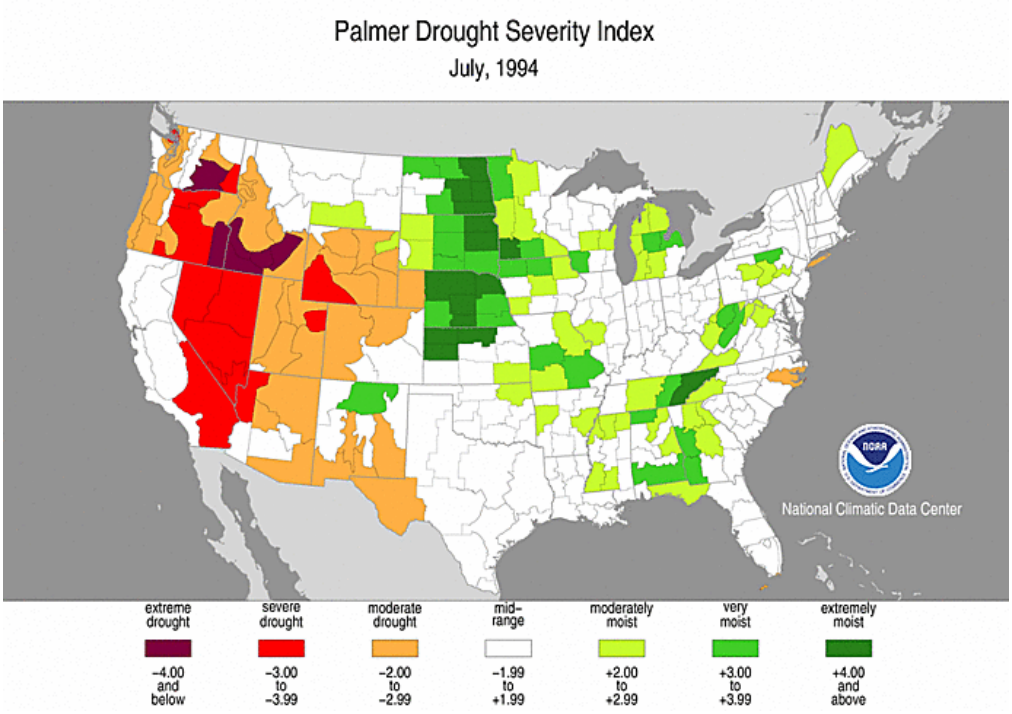

Figure 3-22: Palmer Drought Severity Index for July 1994 (NOAA, 2015)

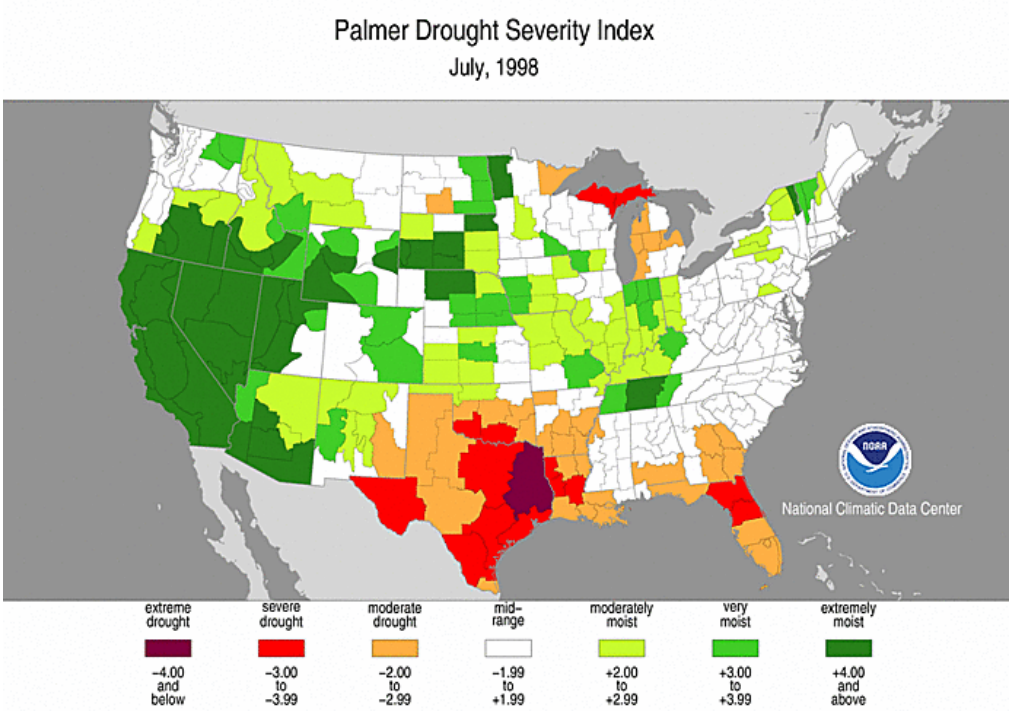

Figure 3-23: Palmer Drought Severity Index for July 1998 (NOAA, 2015)

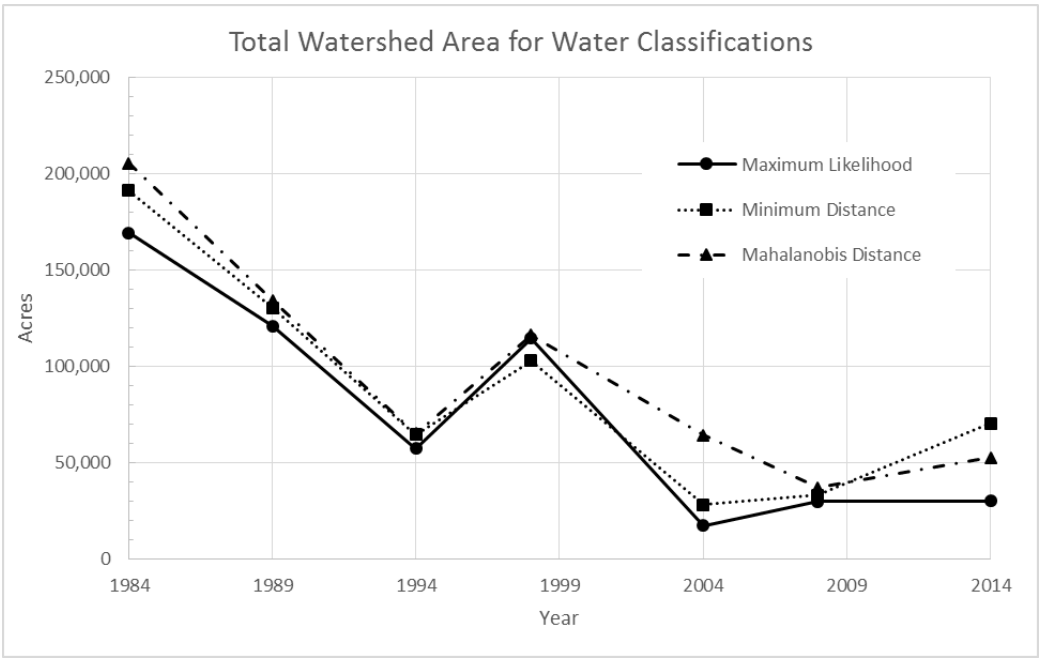

Figure 3-24: Total Watershed Area for Water and Shallow Water Classifications

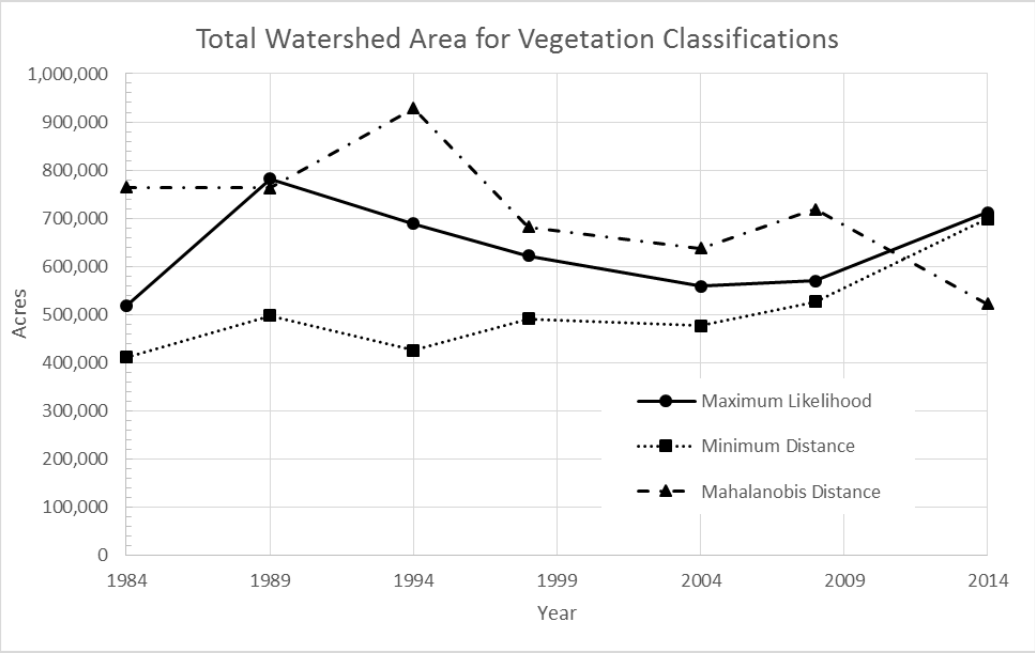

Figure 3-25: Total Watershed Area for Dark Vegetation and Vegetation Classifications

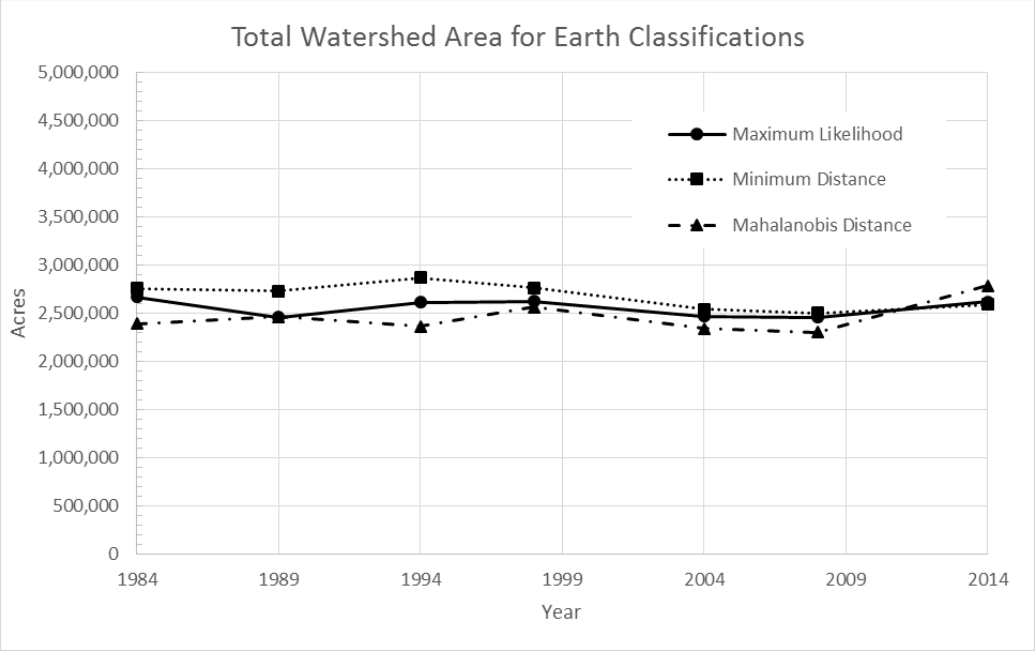

Figure 3-26: Total Watershed Area for Bare Earth and Salty Area Classifications

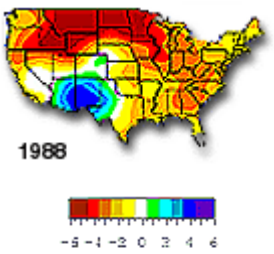

Figure 3-27: PDSI Reconstruction for the North American Drought in 1988 (NOAA, 2015)

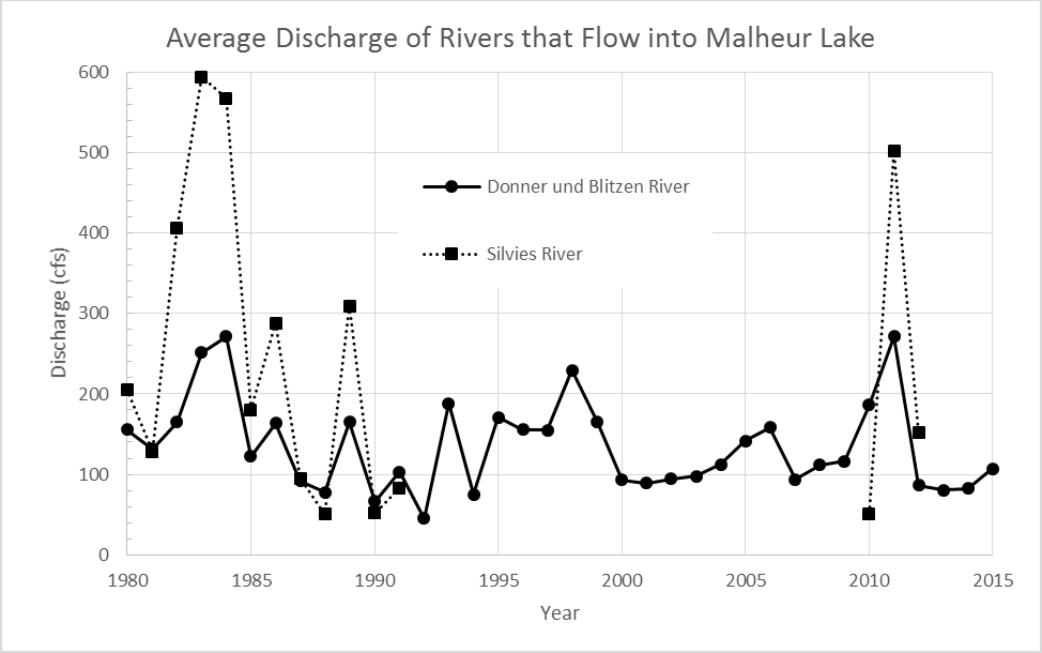

Figure 3-28: Average Discharge of Rivers that Flow into Malheur Lake (Ames, 2012; USGS, 2015b)

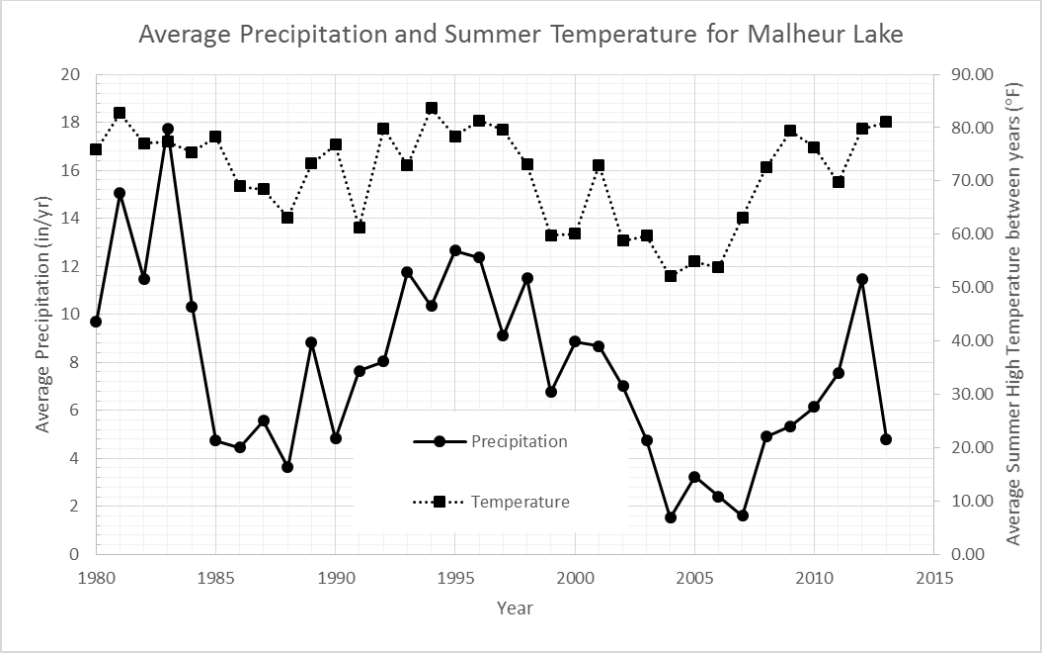

Figure 3-29: Average Precipitation and Summer High Temperature for Malheur Lake Note: There is Missing Temperature Data for 2007

Starting in the year 2000, the NDMC created a more effective rating system called the Drought Severity Classification that includes the PDSI, but also includes the Climate Prediction Center (CPC) Soil Moisture Model, USGS weekly streamflow, Standardized Precipitation Index (SPI), and objective drought indicator blends. This classification system can work on large and small areas, including an area as small as a HUC area. Using the HUC-8 shapefiles, I found that the area for July 13, 2004 was in a Moderate to Extreme Drought (NDMC, 2015b). The Moderate to Extreme Drought rating is shown in Table 3-2. However, I decided to include the PDSI maps, to have a comparison point to years that did not have the Drought Severity Classification, and the Drought Severity Classification table which are displayed in Appendix D. The Governor of Oregon declared that the area was in a drought from 2001 through 2003 (Governor, 1991-2015). The discrepancy from the Governor of Oregon and the Drought Severity Classification may be due to the fact that the area did not fully recover from the latest drought.

Because of the previous drought, the water level was even lower and the discharge decreased. During this time, the area noticed a drastic decrease in the average summer high temperature to about 60°F and a drastic decrease in precipitation of over 5 inches per year. The level of vegetation decreased most likely because of the drought.

For July 22, 2008, the area was rated as an Abnormally Dry period shown in Table 3-2. The Governor of Oregon declared that the area was in a drought for the year 2007 (Governor, 1991-2015). The drought rating of Abnormally Dry seems accurate since the area finished having a drought the previous year. The area decreased in precipitation by over 3 inches per year, the average discharge increased, and the average summer high temperature stayed about the same. Because of these factors, the level of vegetation increased and the level of water decreased.

For July 1, 2014, the area was rated as a Severe Drought shown in Table 3-2. The Governor of Oregon declared that the area was in a drought at this time and the drought continues until today (Governor, 1991-2015). Precipitation increased by over 4 inches per year and the average discharge in this period increased drastically (partly because the Silvies River had flow from 2010 to 2012), but the average summer high temperature increased drastically as well to an average of 77.26°F. Because of these factors, the level of water increased and the level of vegetation decreased. The level of vegetation most likely decreased because of the ensuing drought.

Table 3-2: Drought Level Averages for Watershed Area using Drought Severity Classification

		Drought Level						
Watershed	Week	None	Abnormally Dry	Moderate Drought	Severe Drought	Extreme Drought	Exceptional Drought	Intensity
Average	7/13/2004	0%	19.17%	34.12%	20.24%	26.46%	0%	Moderate to Extreme
Average	7/22/2008	0%	88.05%	11.87%	0.09%	0%	0%	Abnormally Dry
Average	7/1/2014	0%	0%	1.19%	98.80%	0.01%	0%	Severe

I compared the land cover variables with climate conditions using statistics. Figure 3-30 shows the statistics for the discharge, precipitation, and max summer high temperature. This shows that all of these variables were correlated at a statistically significant level with a 99% confidence interval. However, I could not compare the data, because the data had different time intervals. The precipitation, summer high temperature, and discharge have daily values and the land cover that I computed had values about once every 4 to 6 years. Therefore, I took the averages of precipitation, summer high temperature, and discharge about every 4 to 6 years to match up with the land cover years. After doing this, I noticed in Figure 3-31, which is the same as Figure 3-30 except the values are averaged, that the correlations of precipitation and max summer temperature were no longer statistically significant. This may change results. Figure 3-32 shows the logarithmic transform of the land cover variables and the average precipitation, summer high temperature, and discharge variables against the year. The same land cover classes were correlated at a statistically significant level with a 95% confidence interval, but the other variables were not statistically significant. The drought indicator was not included as there was not enough data to run the statistics.

Summary of Fit

RSquare	0.003909
RSquare Adj	0.003637
Root Mean Square Error	9.77882
Mean of Response	1995.732
Observations (or Sum Wgts)	11002

Analysis of Variance

Source	DF	Sum of Squares	Mean Square	F Ratio
Model	3	4126.9	1375.64	14.3857
Error	10998	1051687.3	95.63	Prob > F
C. Total	11001	1055814.2		<.0001*

Parameter Estimates

Term	Estimate	Std Error	t Ratio	Prob>|t|
Intercept	1996.5359	0.171087	11670	<.0001*
Discharge	-0.001424	0.000521	-2.73	0.0063*
Precipitation	-4.031357	1.010049	-3.99	<.0001*
MaxTemperature	-0.018907	0.004746	-3.98	<.0001*

Figure 3-30: Statistical Significance of Discharge, Precipitation, and Max Summer High Temperature

Summary of Fit

RSquare	0.472829
RSquare Adj	0.379799
Root Mean Square Error	7.961997
Mean of Response	1998.714
Observations (or Sum Wgts)	21

Analysis of Variance

Source	DF	Sum of Squares	Mean Square	F Ratio
Model	3	966.5980	322.199	5.0825
Error	17	1077.6877	63.393	Prob > F
C. Total	20	2044.2857		0.0108*

Lack Of Fit

Source	DF	Sum of Squares	Mean Square	F Ratio
Lack Of Fit	3	1077.6877	359.229	.
Pure Error	14	0.0000	0.000	Prob > F
Total Error	17	1077.6877		.
				Max RSq
				1.0000

Parameter Estimates

Term	Estimate	Std Error	t Ratio	Prob>|t|
Intercept	1989.3992	22.87425	86.97	<.0001*
AveragePrecipbetweenyears	-1.586501	0.917196	-1.73	0.1018
AverageSummerTemperaturebetweenyears	0.404879	0.387634	1.04	0.3109
Discharge	-0.03023	0.013901	-2.17	0.0441*

Figure 3-31: Statistical Significance of the Average of Discharge, Precipitation, and Max Summer High Temperature

Summary of Fit

RSquare	0.958543
RSquare Adj	0.924623
Root Mean Square Error	2.775715
Mean of Response	1998.714
Observations (or Sum Wgts)	21

Analysis of Variance

Source	DF	Sum of Squares	Mean Square	F Ratio
Model	9	1959.5352	217.726	28.2593
Error	11	84.7505	7.705	Prob > F
C. Total	20	2044.2857		<.0001*

Parameter Estimates

Term	Estimate	Std Error	t Ratio	Prob>|t|
Intercept	2404.0606	511.8714	4.70	0.0007*
LogWater	-9.732715	2.615768	-3.72	0.0034*
LogShallow	-4.586389	0.872295	-5.26	0.0003*
LogVegetation	4.5968627	1.96969	2.33	0.0396*
LogDark	-8.437153	7.760175	-1.09	0.3002
LogSalty	-5.093252	1.233503	-4.13	0.0017*
LogEarth	-12.12177	28.13534	-0.43	0.6749
AveragePrecipbetweenyears	-0.78251	0.612137	-1.28	0.2274
AverageSummerTemperaturebetweenyears	0.6510615	0.360833	1.80	0.0986
Discharge	-0.008791	0.007181	-1.22	0.2464

Figure 3-32: Statistical Significance of the Logarithmic Transform of Land Cover with Average of Discharge, Precipitation, and Max Summer High Temperature

3.3 Discussion

Figure 3-24 shows that the water goes through 3 wet-dry cycles but ends on a wet cycle. After running the analysis on the watersheds over a 30-year period, I determined that the area has gone through 3 wet-dry cycles and is currently in a dry cycle. Although the amount of water increased since 2008, because of increased precipitation and discharge, signs of a drought started in 2012. The Drought Severity Classification seems to be accurate for the three instances that I used the classification. However, more studies should be done to determine the actual effectiveness of the classification. The PDSI seemed to underestimate the severity of the drought when compared to the Drought Severity Classification. However, I did not observe how the PDSI did compared to the Drought Severity Classification during moist conditions. Therefore, I

cannot make any inferences when the area is wet. A more detailed study of vegetation patterns using remote sensing data could be undertaken to better correlate the effects of the drought on the local ecosystem and evaluate which index provides a better indication on drought impacts.

The watershed raster datasets provide good representations of the land cover in the Malheur Lake area. Each classification method has shortcomings. The minimum distance classification algorithm provided the best land cover classification out of the three studied. Thirty years of land cover data are useful in analyzing the trends that occur in the natural landscape and how these changes can affect the watershed. However, land cover does not tell the whole story about what is going on in the area. The use of other parameters including precipitation, discharge, temperature, drought, groundwater, along with land use help to show the bigger picture. Overall, the land cover classifications seem to follow the patterns established by the other parameters in how the water levels fluctuate and the onset of droughts effect the area. Also, the land cover classification correlations are statistically significant, except Dark Vegetation and Bare Earth, which is what would be expected of the land cover change.

Currently, creating land cover maps from Landsat imagery is not cost effective because of the amount of time needed to create the land cover maps for model analysis. This is because each time a user creates a land cover map for a new area or a new date in time, the user has to verify that the ROIs are accurate with the Landsat imagery and the ISODATA classification thus producing some error. A possible improvement would be producing an algorithm that can create an ROI type file that can capture the pixels of a land cover class, which can be loaded in many different types of images, and can run supervised classifications, thus making the supervised classifications more accurate and more like an unsupervised classification.

This research may prove useful in hydrological models. Generally, a user can download land cover shapefiles and run a watershed model. However, the shapefile that is usually downloaded is for one particular year and may not be good for the same year or years as the precipitation data. Users do not usually mind if the land cover data is not in sync with the precipitation or soil data unless there is a need to have a more accurate model. The user can download land use/land cover shapefiles online, but not back to 1982. Therefore, the methods of this study can be used to create the desired land cover maps to run more accurate models. To use the watershed raster datasets in a hydrological study, the user converts the watershed raster datasets into polygon shapefiles.

4 FUTURE WORK

4.1 Recommendations

This research evaluated the practicality of using Landsat imagery to create land cover maps in Malheur Lake, Oregon and used those data to analyze how the land cover changed over time. Remote sensing is a viable conduit for land cover mapping and is well established, using historical remote sensing data, especially Landsat images, to generate and analyze time series data. However, remote sensing is not as widely used. The use of the historical data to generate and analyze changes over time provides a demonstration of an important tool that is readily available to managers today.

As part of this research, I visually determined land cover classes using Landsat imagery, Google Earth imagery, and ISODATA classifications. I used these classes to create supervised classifications and clip out the watersheds for about 30 years of imagery. I used these watersheds to determine the area for each land cover class and noted how they changed over time. These results were then compared to time series data of precipitation, runoff, temperature, and drought indicators using statistics to determine if these changes were driven by environmental changes or other issues. The results indicate that the main drivers for land cover change in the Malheur lake watersheds are environmental, with changes tied most closely to precipitation and temperature patterns.

This work can be expanded in other aspects.

- Using ENVI, Landsat images can be made to have 72 bands to achieve more land cover classes making a better classification.
- Using the techniques of this study and applying them to other areas of the world that either have similar or different characteristics from Malheur Lake, Oregon to test the study's versatility. New land cover classes may need to be created in these new areas.
- Build a new algorithm that can create an ROI type file that can capture the pixels of a land cover class, which can be used in many different types of images. This algorithm could run the supervised classifications, thus making the supervised classifications perform more like an unsupervised classification producing more accurate results.

5 CONCLUSION

This research applied unsupervised classifications to calibrated Landsat images that contain the watersheds draining into Malheur Lake, Oregon to determine the land cover classes over time. After ROIs were created for the images, supervised classifications were applied to the calibrated Landsat images. The watersheds were then extracted from the supervised classifications using the ArcGIS software. I evaluated the Malheur Lake area about every 4 to 6 years over a 30-year period. Each Landsat image that contained Malheur Lake watersheds needed supporting images from the North and from the West to capture the totality of the watershed area as defined by the HUC-8 shapefiles. These methods provided mostly accurate watershed land cover maps of the area and should be able to provide such accuracy in other areas. Although the land cover classes are minimal, they are well correlated with environmental changes that would be expected to impact land cover types.

The results of the research show that the land cover generally correlates with climate conditions of precipitation, discharge, summer high temperature, and drought indicators. Also, most of the land cover classifications were statistically significant, except for the Bare Earth and Dark Vegetation classes which do not fluctuate as much since these are large areas.

This research can be expanded in a few areas. The methodology can be applied to other areas of the world with similar or different characteristics to Malheur Lake, Oregon. This will further test the validity of the method and possibly use other land cover classes. Using this

methodology, a new algorithm can be produced to create ROI type files to capture the pixels of a land cover class that can run the supervised classifications. In this way, the land cover classifications will be more accurate thus producing better watershed land cover maps that can be applied to models. ENVI's ability to create 72 bands per image with the Landsat imagery can be used to make a better land cover classification. I had up to 11 bands, but only had six available with the multispectral image. Wherefore, more bands gives the user the ability to classify more land cover classes.

In conclusion, this analysis showed how the land cover, for the watersheds that feed Malheur Lake, fluctuated every 4 to 6 years, which was used to better understand that the patterns of land cover change in this area were dependent on the climate conditions. Using these methods can provide land cover maps for the watersheds in hydrological studies for times that more closely match the time that the hydrological study is taking place.

REFERENCES

Adjei, Z. Y. A. (2015). *Using Remote Sensing to Explore the Time History of Emergent Vegetation at Malheur Lake, Oregon.* (Masters of Science), Brigham Young University, Brigham Young University.

Ames, D. P., Jeffrey S. Horsburgh, Yang Cao, Jiri Kadlec, Timothy Whiteaker, David Valentine. (2012). HydroDesktop: Web services-based software for hydrologic data discovery, download, visualization, and analysis. *Environmental Modelling & Software, 37*(November 2012), 146-156. doi:10.1016/j.envsoft.2012.03.013

Brown, D. G., Johnson, K. M., Loveland, T. R., & Theobald, D. M. (2005). RURAL LAND-USE TRENDS IN THE CONTERMINOUS UNITED STATES, 1950–2000. *Ecological Applications, 15*(6), 1851-1863. doi:10.1890/03-5220

Esri. (2015). ArcGIS Help 10.2, 10.2.1, and 10.2.2. Retrieved from http://resources.arcgis.com/en/help/main/10.2/

Excelis. (2015). Documentation Center. Retrieved from http://www.exelisvis.com/docs/home.html

Fry, J. A., Xian, G., Jin, S., Dewitz, J. A., Homer, C. G., Yang, L., . . . Wickham, J. D. (2011). Completion of the 2006 national land cover database for the conterminous united states. *Photogrammetric Engineering and Remote Sensing, 77*(9), 858-864.

Governor. (1991-2015). *Drought Declarations*. Retrieved from http://apps.wrd.state.or.us/apps/wr/wr_drought/declaration_status_report.aspx.

Hernandez, M., Scott N. Miller, David C. Goodrich, Bruce F. Goff, William G. Kepner, Curtis M. Edmonds, and K. Bruce Jones. (2000). MODELING RUNOFF RESPONSE TO LAND COVER AND RAINFALL SPATIAL VARIABILITY IN SEMI-ARID WATERSHEDS *ENVIRONMENTAL MONITORING AND ASSESSMENT, 64*, 285-298.

Huang, J., Victor Klemas. (2012). Using Remote Sensing of Land Cover Change in Coastal Watersheds to Predict Downstream Water Quality. *Journal of Coastal Research, 28*(4), 930-944.

Hubbard, L. L. (1975). *Hydrology of Malheur Lake, Harney County, southeastern Oregon* (75-21). Retrieved from http://pubs.er.usgs.gov/publication/wri7521

Javed, A., Khanday, M., & Rais, S. (2011). Watershed prioritization using morphometric and land use/land cover parameters: A remote sensing and GIS based approach. *Journal of the Geological Society of India, 78*(1), 63-75. doi:10.1007/s12594-011-0068-6

Johnson, D. M. (1985). *Atlas of Oregon lakes*. Corvallis, Oregon: Oregon State University Press.

Lu, D., Mateur Batistella, Emilio F. Moran, and Evaristo E. de Miranda. (2005). *A Comparative Study of Terra ASTER, Landsat TM, and SPOT HRG data*. Retrieved from Indiana University:

Mather, P. M., & Koch, M. (2011). Classification *Computer Processing of Remotely-Sensed Images* (pp. 229-284): John Wiley & Sons, Ltd.

Mohamad, I. B. a. D. U. (2013). Standardization and Its Effects on K-Means Clustering Algorithm. *Research Journal of Applied Sciences, Engineering and Technology, 6*(17), 3299-3303.

Mohd, O., Nanna Suryanna, Shahrin Sahib Sahibuddin, Mohd Faizal Abdollah, Siti Rahayu Selamat. (2012). Thresholding and Fuzzy Rule-Based Classification Approaches in Handling Mangrove Forest Mixed Pixel Problems Associated with in QuickBird Remote Sensing Image Analysis. *Agriculture and Forestry, 2*(6), 300-306. doi:10.5923

NDMC. (2015a). Comparison of Major Drought Indices: Palmer Drought Severity Index. Retrieved from http://drought.unl.edu/Planning/Monitoring/ComparisonofIndicesIntro/PDSI.aspx

NDMC. (2015b). U.S. Drought Monitor. Retrieved from http://droughtmonitor.unl.edu/Home.aspx

NOAA. (2015). Palmer Drought Severity Index. In PDSI (Ed.).

Palmer, W. C. (1965). *Meteorological Drought*. Retrieved from Washington, D. C.:

Treitz, P. M., Howarth, P. J., & Gong, P. (1992). Application of satellite and GIS technologies for land-cover and land-use mapping at the rural-urban fringe: a case study. *Photogrammetric Engineering and Remote Sensing, 58*(4), 439-448.

USDA. (2015). Geospatial Data Gateway. Retrieved from https://gdg.sc.egov.usda.gov/GDGOrder.aspx

USGS. (2011). Multi-Resolution Land Characteristics Consortium Retrieved from http://www.mrlc.gov/. Retrieved July 31, 2015 http://www.mrlc.gov/

USGS. (2015a). Land Cover Trends Project. *Overview/Summary.* Retrieved from http://landcovertrends.usgs.gov/main/sample.html

USGS. (2015b, September 18, 2015). National Water Information System (NWIS). Retrieved from http://hiscentral.cuahsi.org/pub_network.aspx?n=1

USGS. (2015c, Sept. 9, 2015). PRODUCT GUIDE. *LANDSAT 4-7 CLIMATE DATA RECORD (CDR) SURFACE REFLECTANCE.* Retrieved from http://landsat.usgs.gov/documents/cdr_sr_product_guide.pdf

Weng, Q. (2002). Land use change analysis in the Zhujiang Delta of China using satellite remote sensing, GIS and stochastic modelling. *Journal of Environmental Management, 64*(3), 273-284.

Xiao, J., Shen, Y., Ge, J., Tateishi, R., Tang, C., Liang, Y., & Huang, Z. (2006). Evaluating urban expansion and land use change in Shijiazhuang, China, by using GIS and remote sensing. *Landscape and Urban Planning, 75*(1–2), 69-80.

Zhou, L., X. Yang. (2008). Use of Neural Networks for Land Cover Classification from Remotely Sensed Imagery. *The International Archives of the Photogrammetry, Remote Sensing and Spatial Information Sciences, 37*(B7), 575.

APPENDIX A. WATERSHED RASTER DATASETS WITH LAND COVER

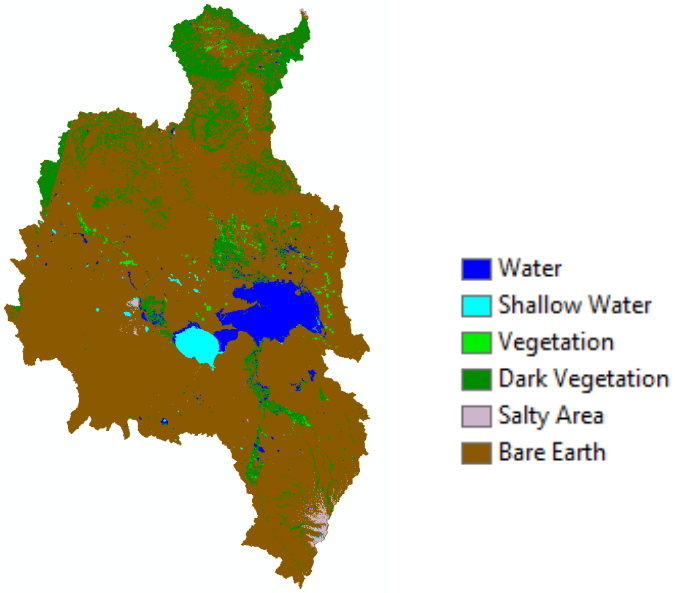

Figure A-1: Minimum Distance Classification of the Watersheds that Contribute to the Malheur Lake Area for Midsummer 1984

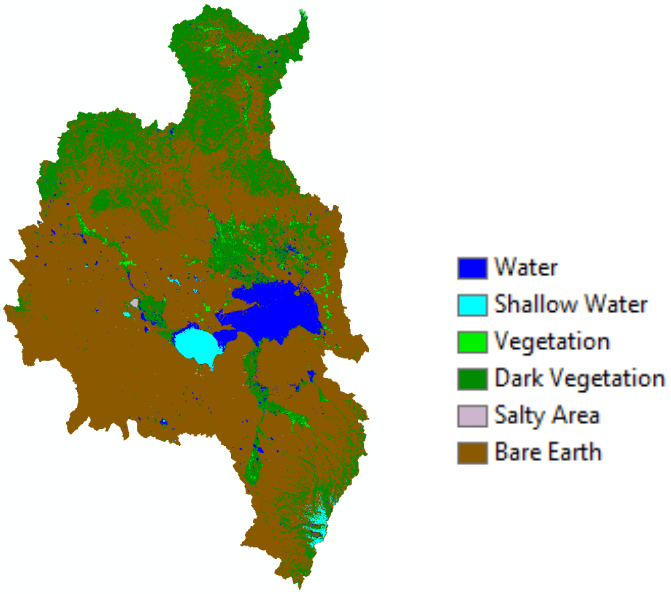

Figure A-2: Mahalanobis Distance Classification of the Watersheds that Contribute to the Malheur Lake Area for Midsummer 1984

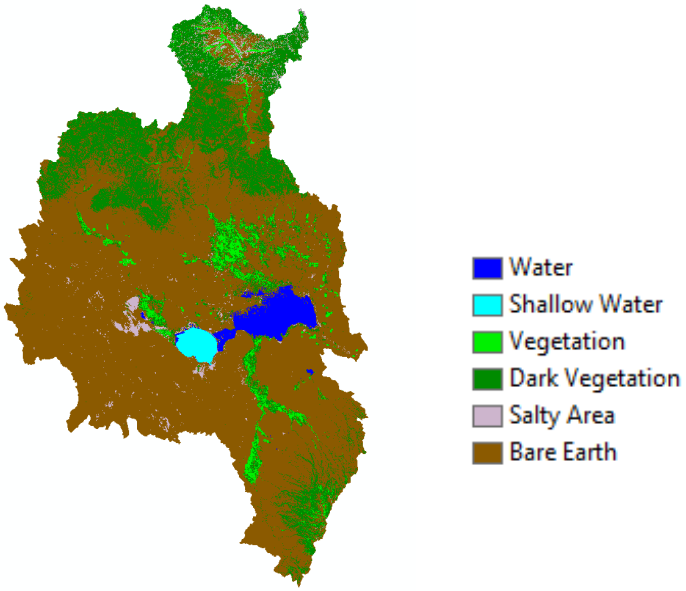

Figure A-3: Maximum Likelihood Classification of the Watersheds that Contribute to the Malheur Lake Area for Midsummer 1989

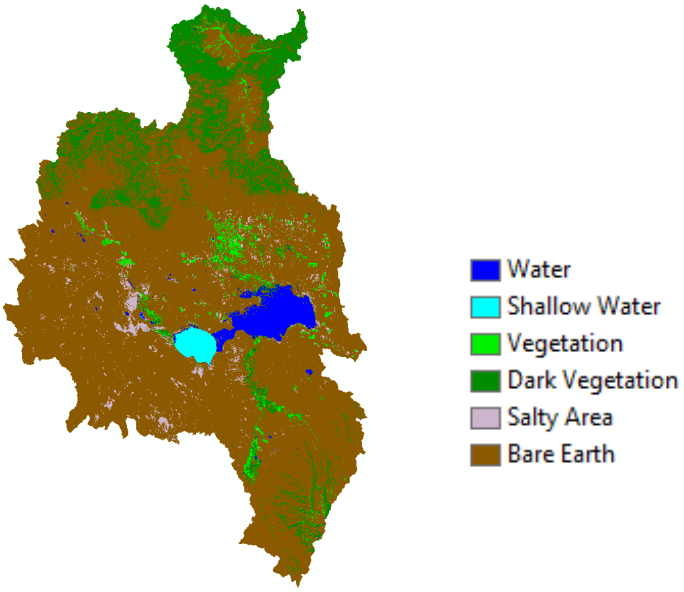

Figure A-4: Minimum Distance Classification of the Watersheds that Contribute to the Malheur Lake Area for Midsummer 1989

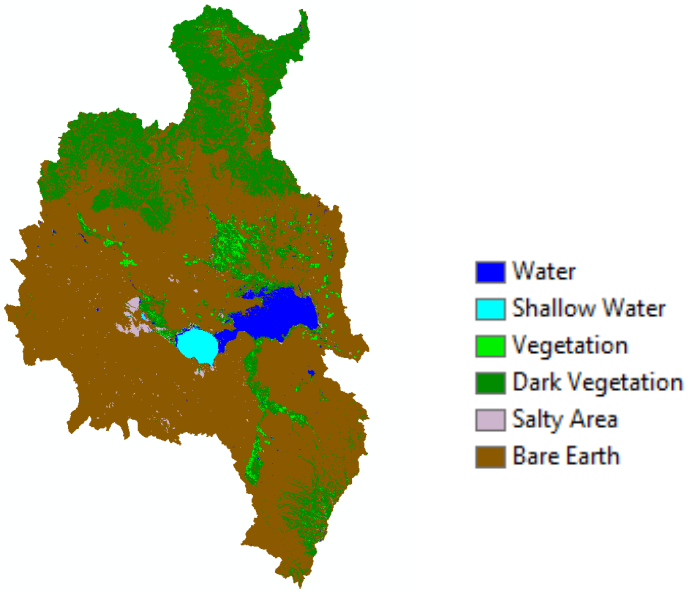

Figure A-5: Mahalanobis Distance Classification of the Watersheds that Contribute to the Malheur Lake Area for Midsummer 1989

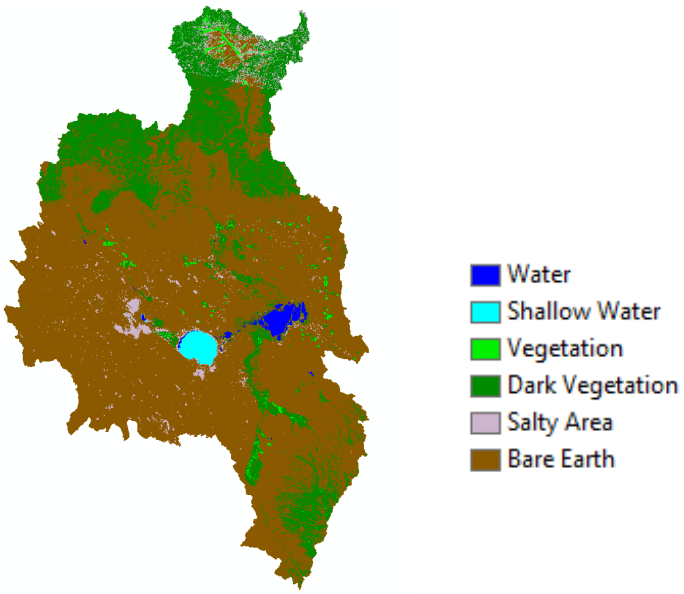

Figure A-6: Maximum Likelihood Classification of the Watersheds that Contribute to the Malheur Lake Area for Midsummer 1994

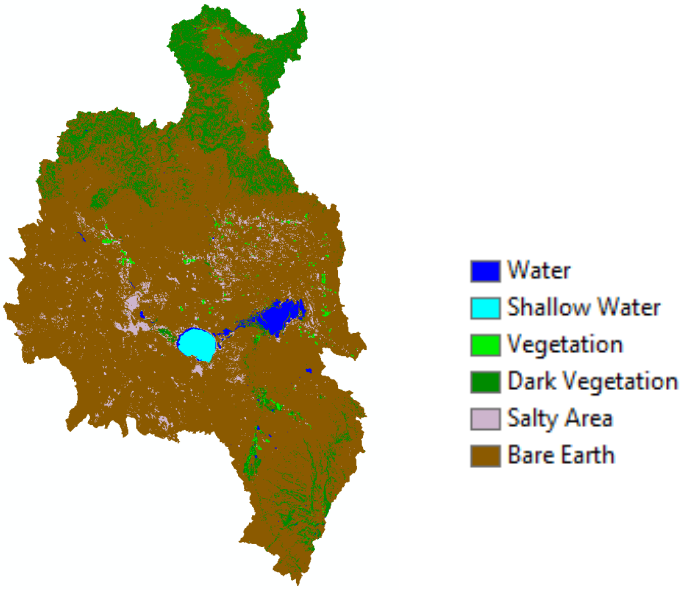

Figure A-7: Minimum Distance Classification of the Watersheds that Contribute to the Malheur Lake Area for Midsummer 1994

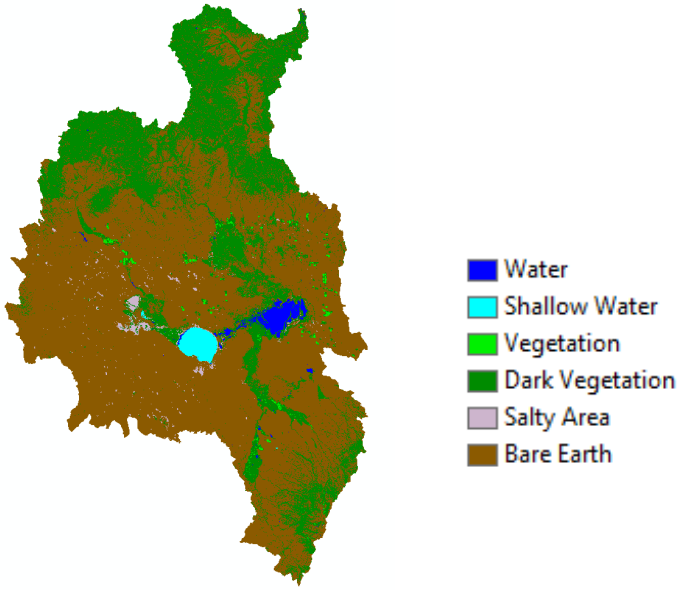

Figure A-8: Mahalanobis Distance Classification of the Watersheds that Contribute to the Malheur Lake Area for Midsummer 1994

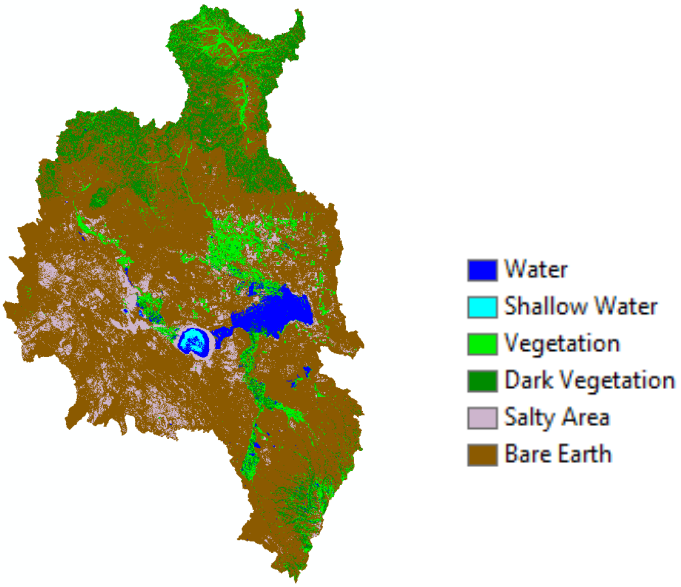

Figure A-9: Maximum Likelihood Classification of the Watersheds that Contribute to the Malheur Lake Area for Midsummer 1998

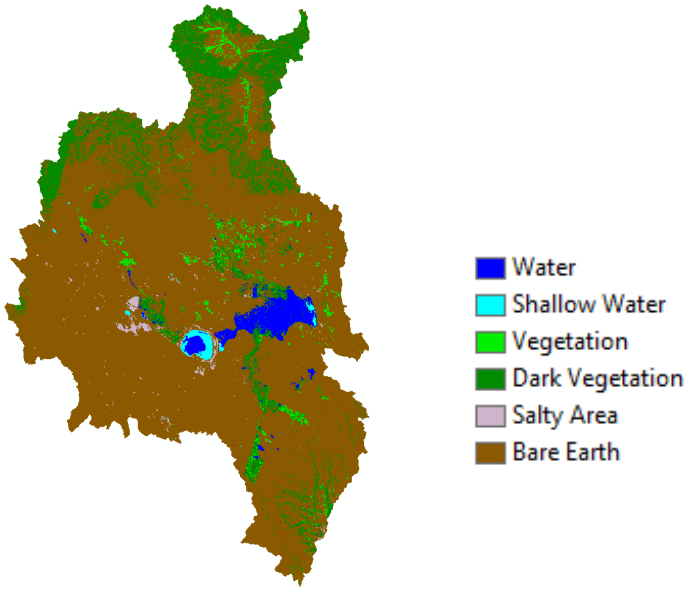

Figure A-10: Minimum Distance Classification of the Watersheds that Contribute to the Malheur Lake Area for Midsummer 1998

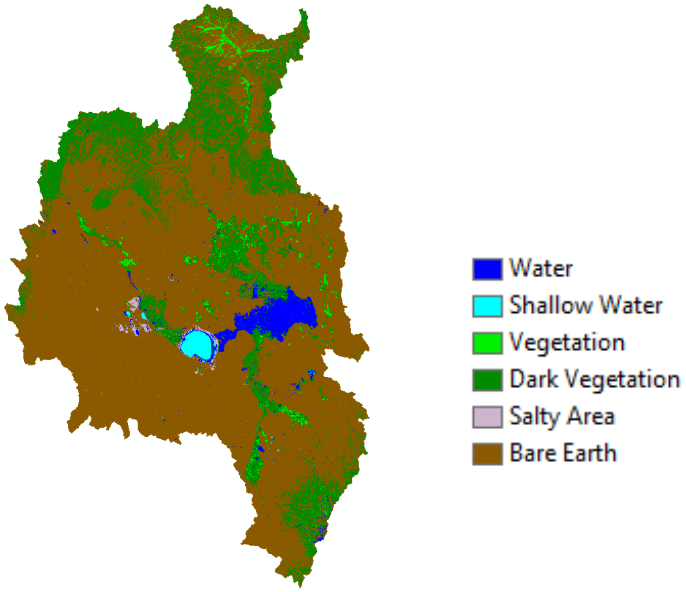

Figure A-11: Mahalanobis Distance Classification of the Watersheds that Contribute to the Malheur Lake Area for Midsummer 1998

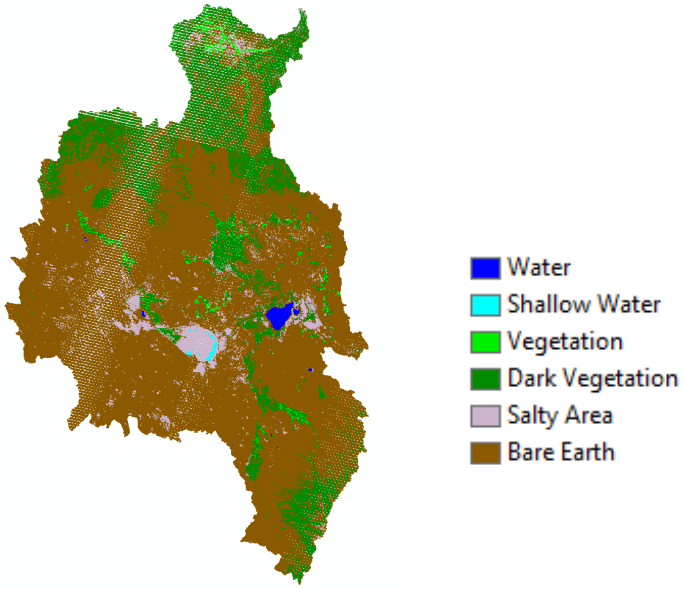

Figure A-12: Maximum Likelihood Classification of the Watersheds that Contribute to the Malheur Lake Area for Midsummer 2004

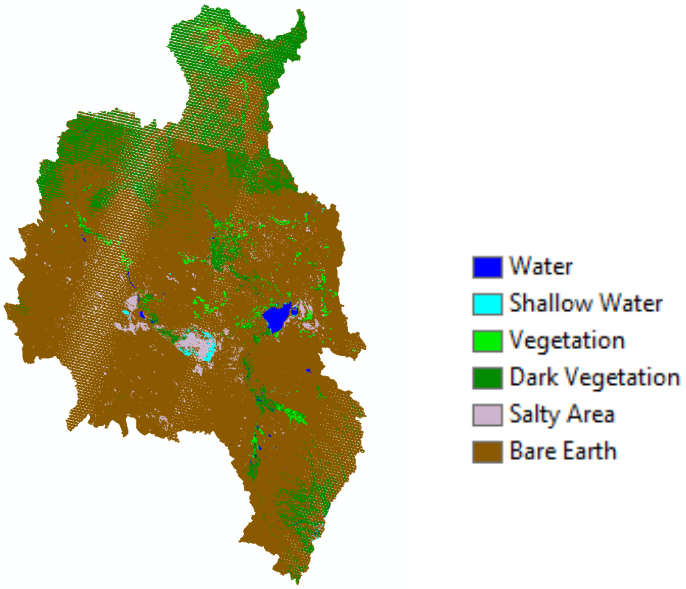

Figure A-13: Minimum Distance Classification of the Watersheds that Contribute to the Malheur Lake Area for Midsummer 2004

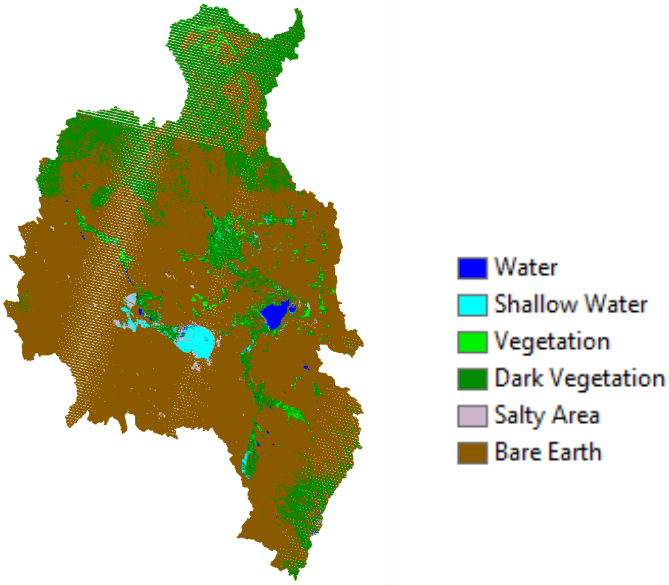

Figure A-14: Mahalanobis Distance Classification of the Watersheds that Contribute to the Malheur Lake Area for Midsummer 2004

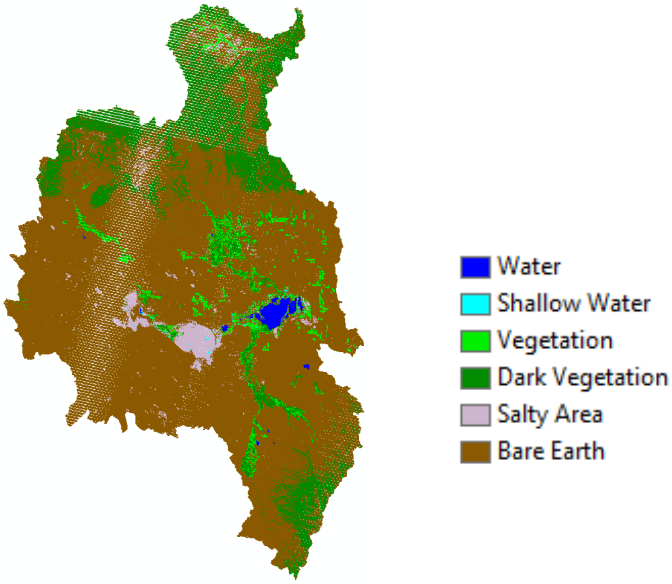

Figure A-15: Maximum Likelihood Classification of the Watersheds that Contribute to the Malheur Lake Area for Midsummer 2008

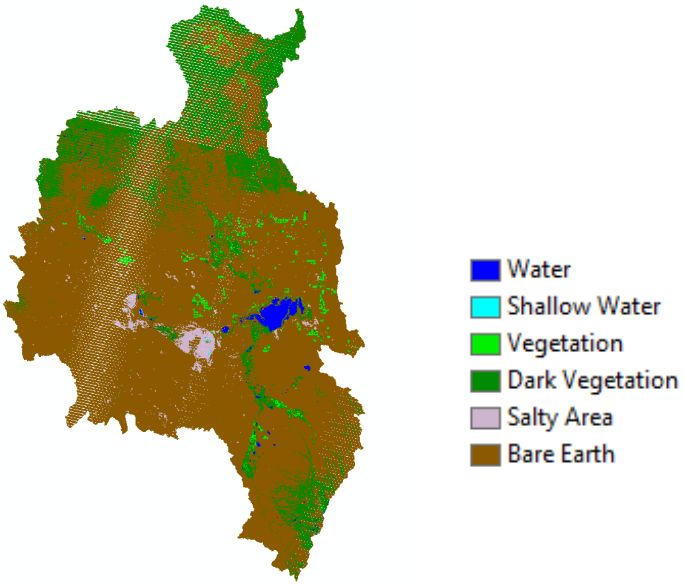

Figure A-16: Minimum Distance Classification of the Watersheds that Contribute to the Malheur Lake Area for Midsummer 2008

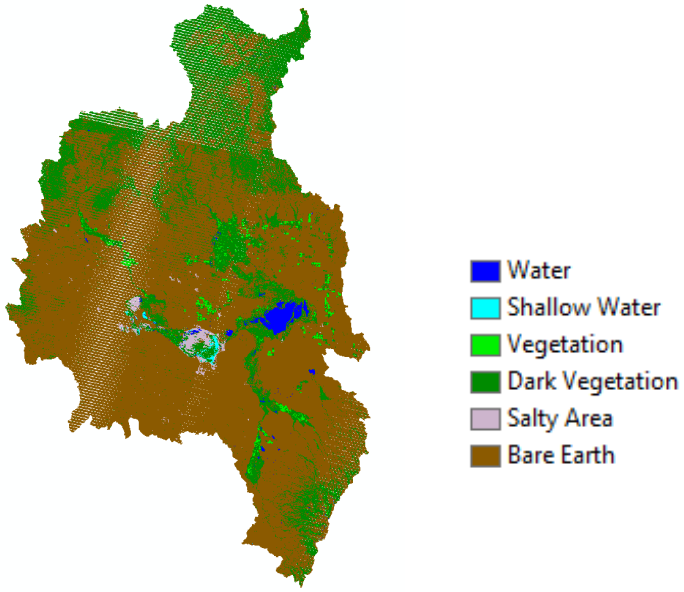

Figure A-17: Mahalanobis Distance Classification of the Watersheds that Contribute to the Malheur Lake Area for Midsummer 2008

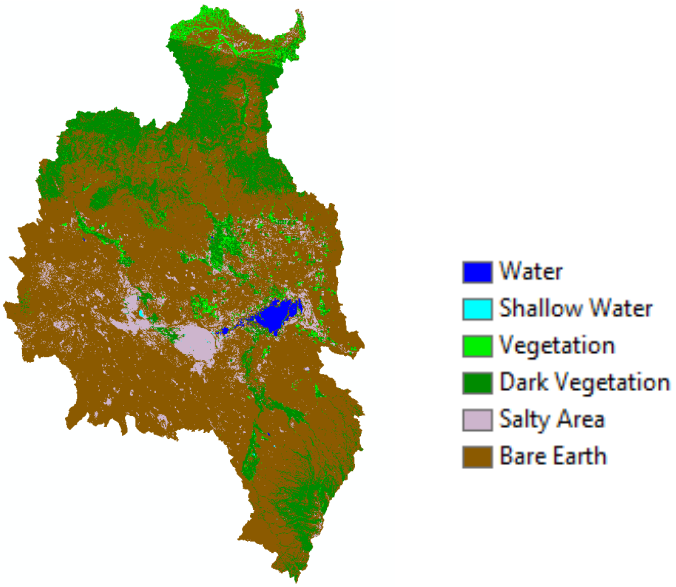

Figure A-18: Maximum Likelihood Classification of the Watersheds that Contribute to the Malheur Lake Area for Midsummer 2014

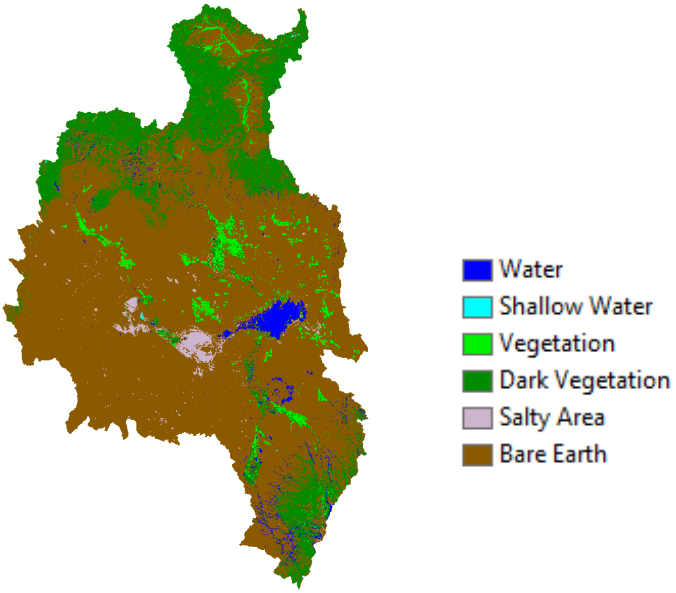

Figure A-19: Minimum Distance Classification of the Watersheds that Contribute to the Malheur Lake Area for Midsummer 2014

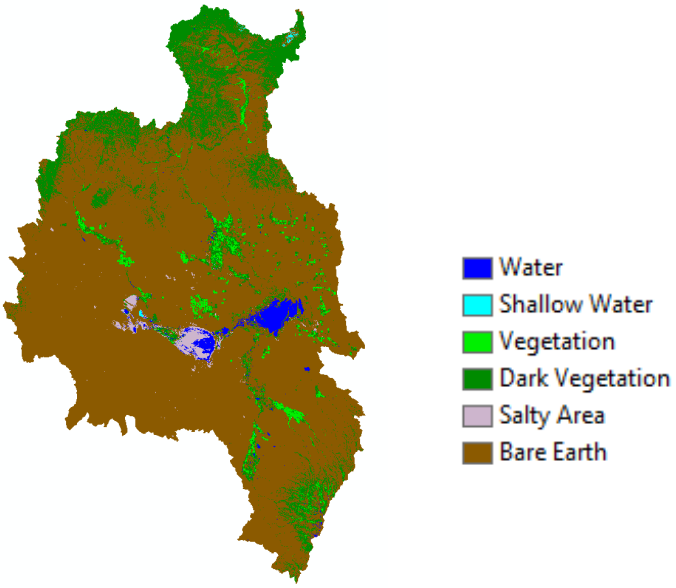

Figure A-20: Mahalanobis Distance Classification of the Watersheds that Contribute to the Malheur Lake Area for Midsummer 2014

APPENDIX B. GRAPHS OF THE DIFFERENT LAND COVER CLASSES

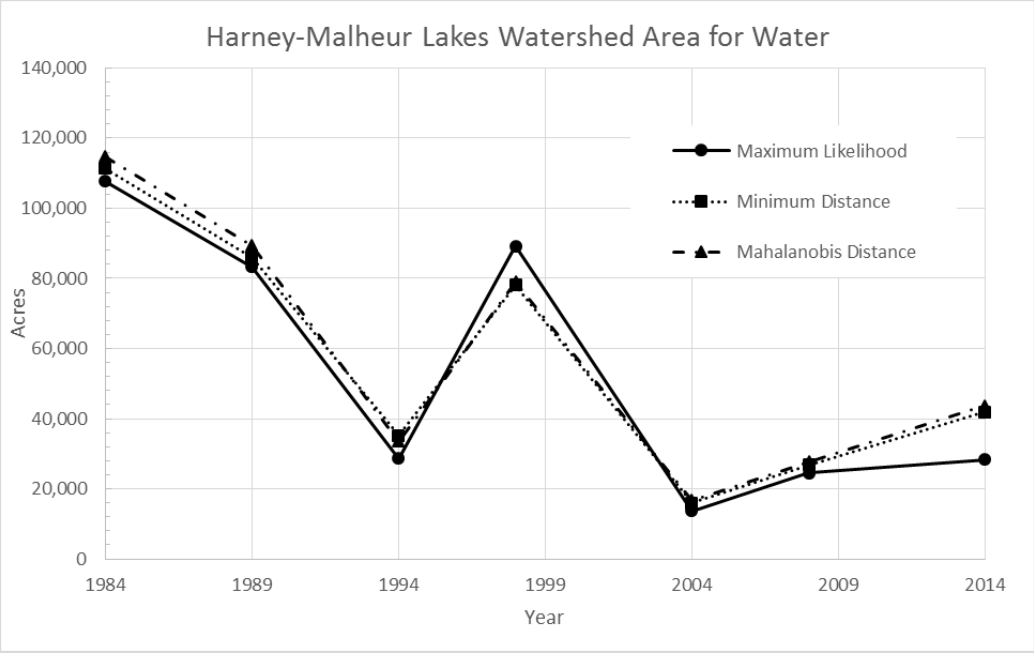

Figure B-1: Total Harney-Malheur Lakes Watershed Area for Water Classification

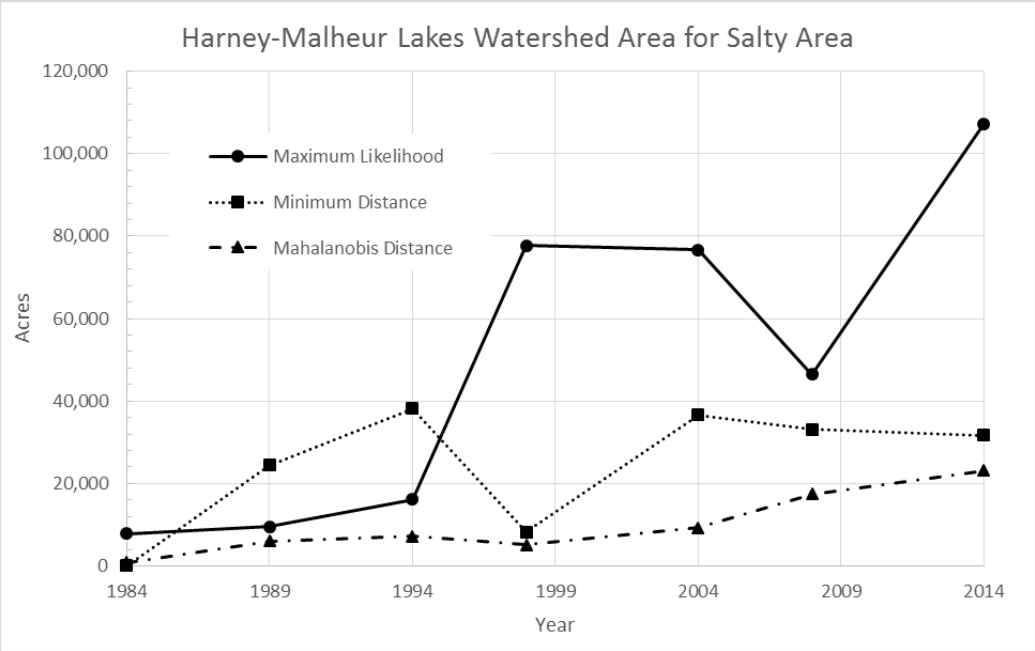

Figure B-2: Total Harney-Malheur Lakes Watershed Area for Salty Area Classification

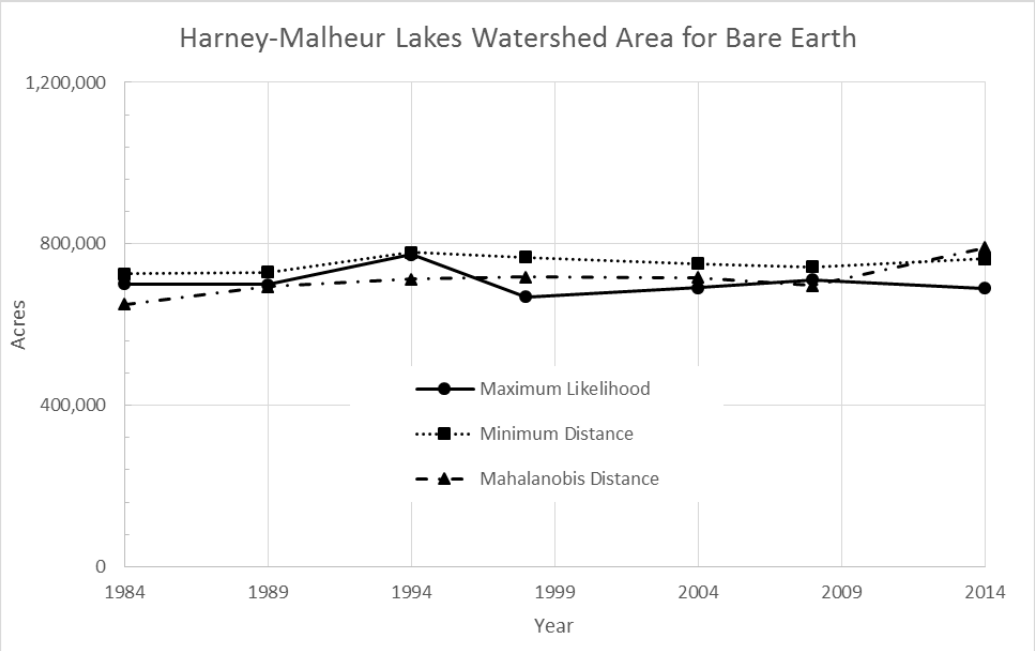

Figure B-3: Total Harney-Malheur Lakes Watershed Area for Bare Earth Classification

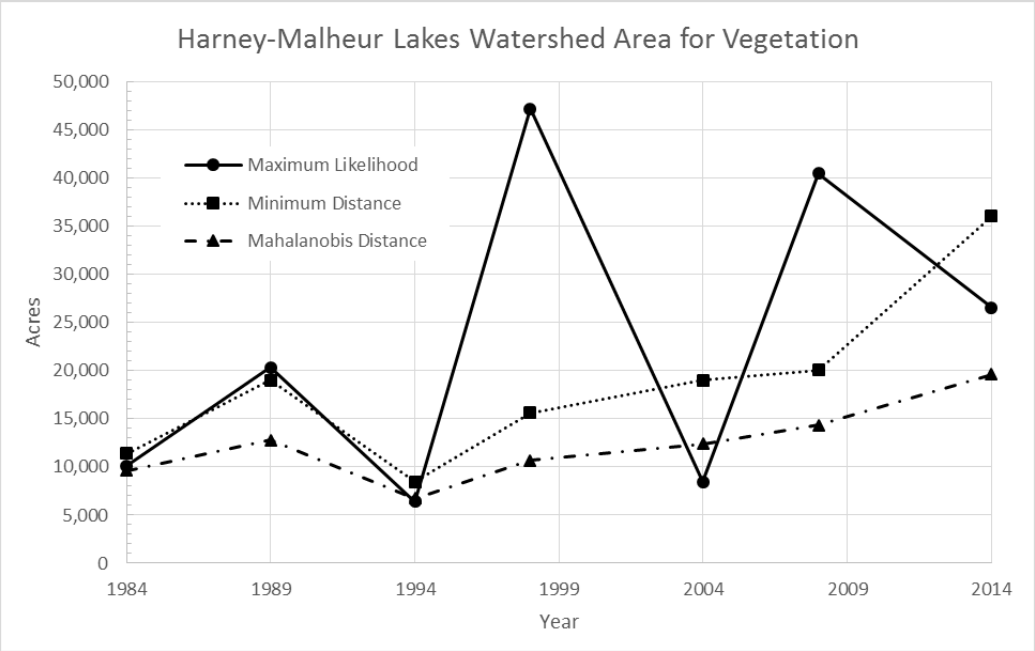

Figure B-4: Total Harney-Malheur Lakes Watershed Area for Vegetation Classification

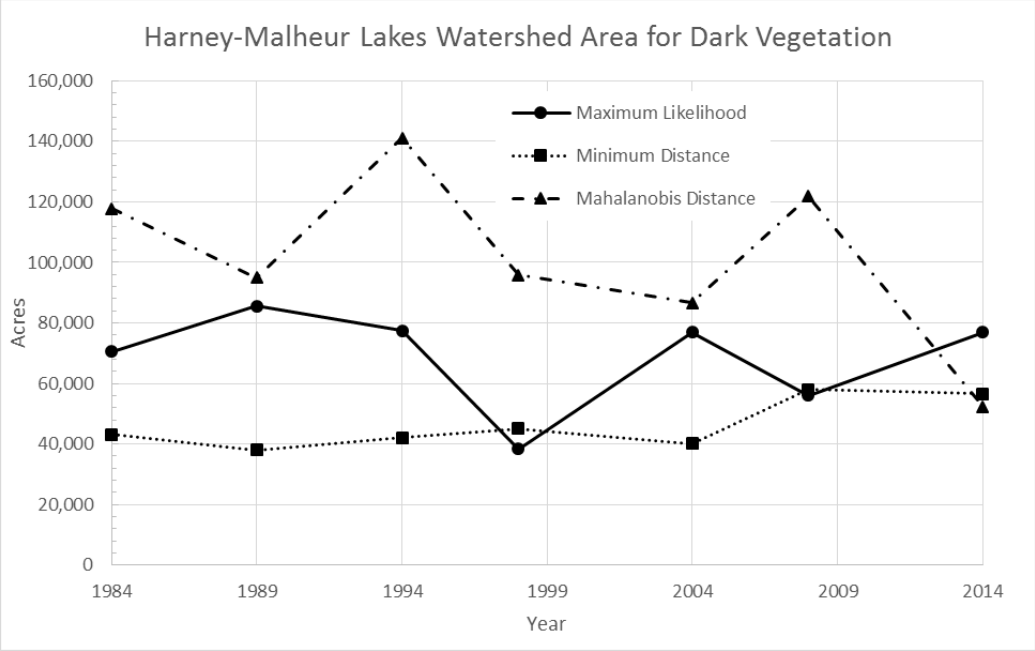

Figure B-5: Total Harney-Malheur Lakes Watershed Area for Dark Vegetation Classification

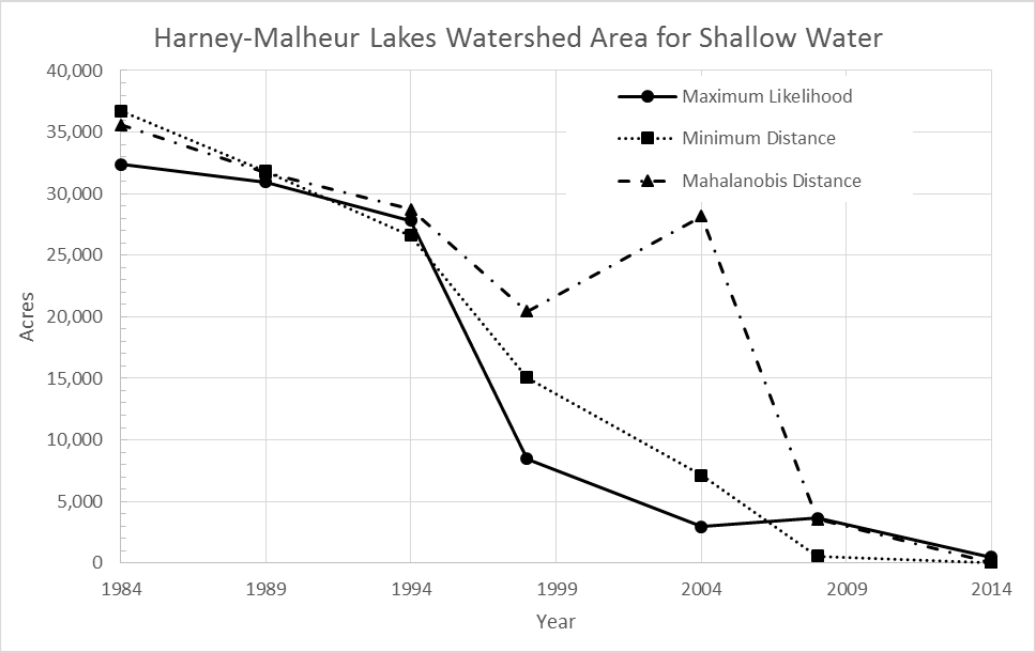

Figure B-6: Total Harney-Malheur Lakes Watershed Area for Shallow Water Classification

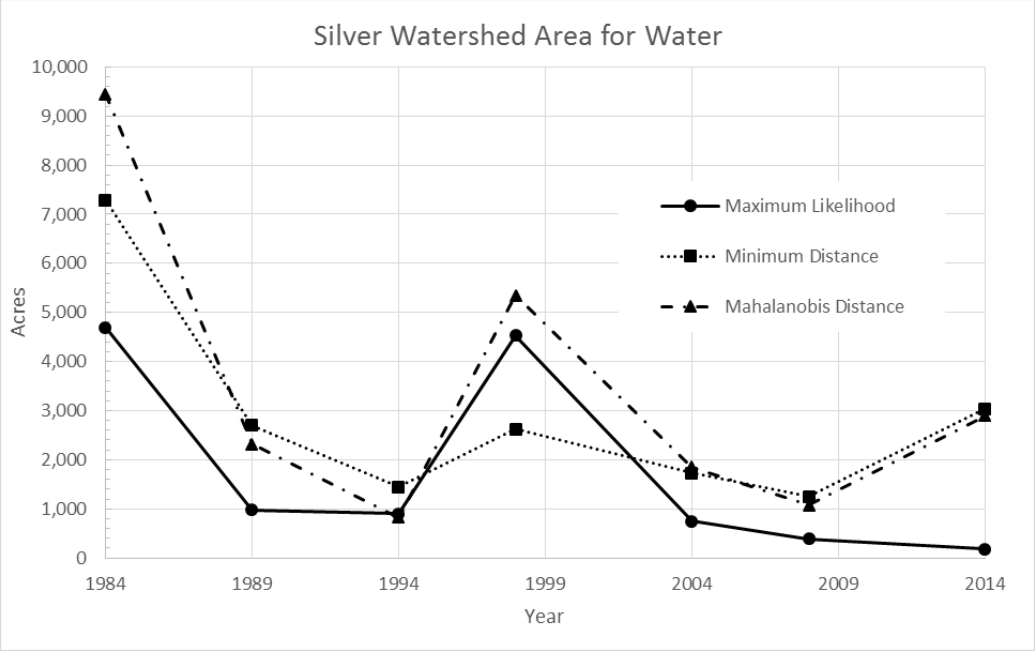

Figure B-7: Total Silver Watershed Area for Water Classification

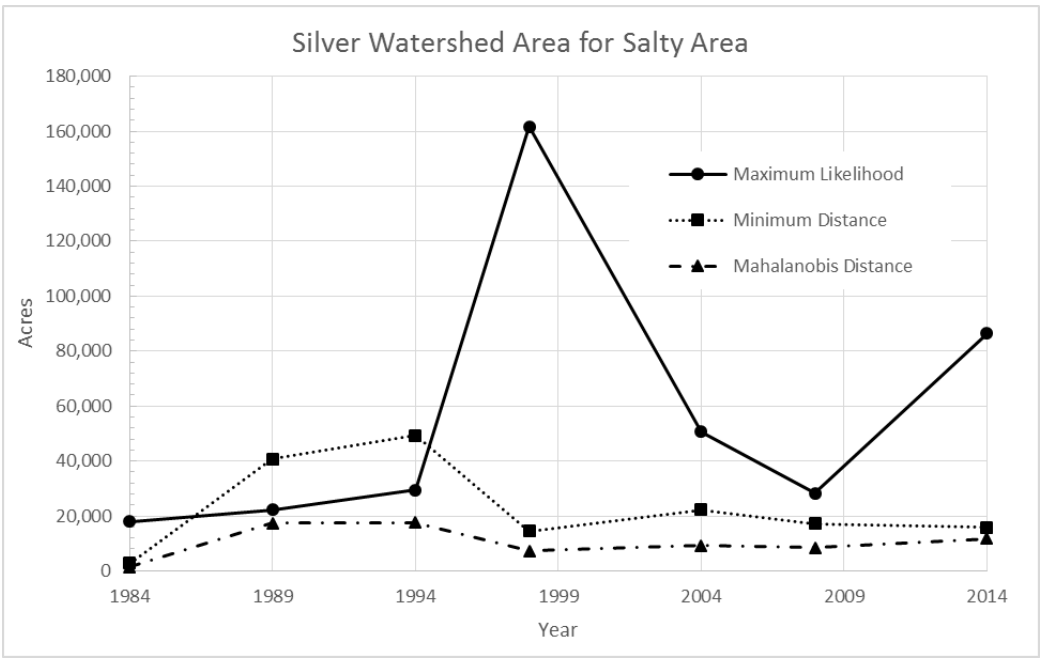

Figure B-8: Total Silver Watershed Area for Salty Area Classification

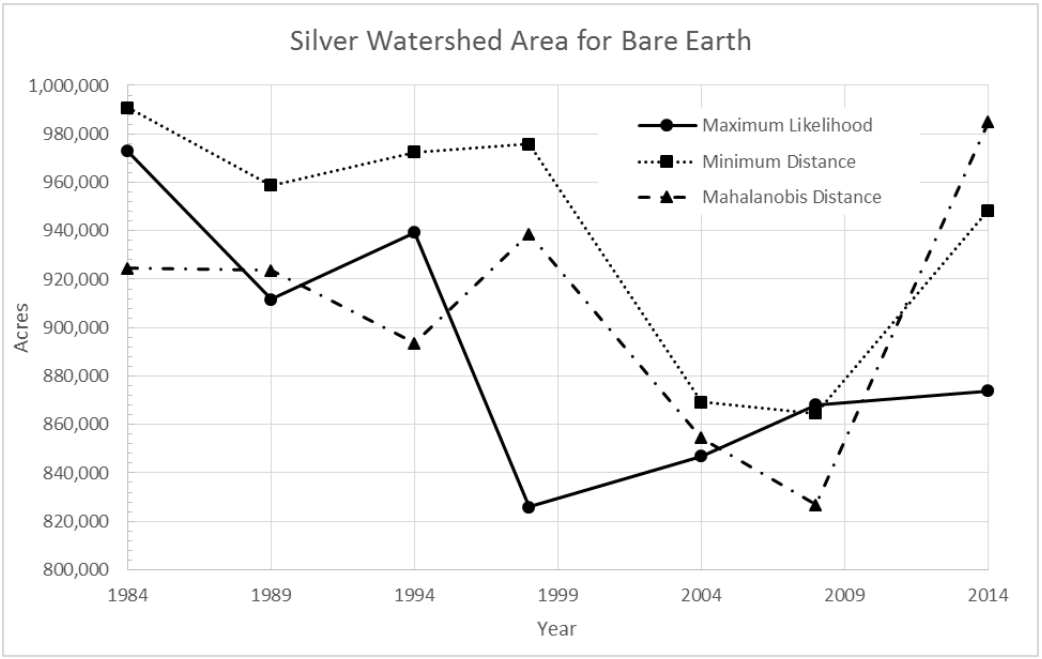

Figure B-9: Total Silver Watershed Area for Bare Earth Classification

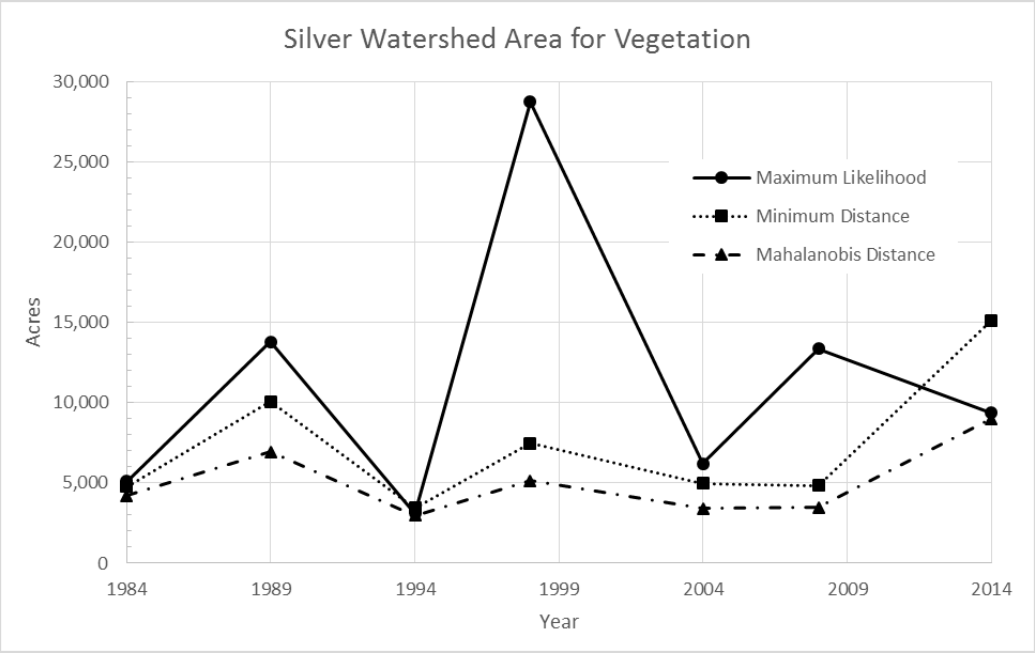

Figure B-10: Total Silver Watershed Area for Vegetation Classification

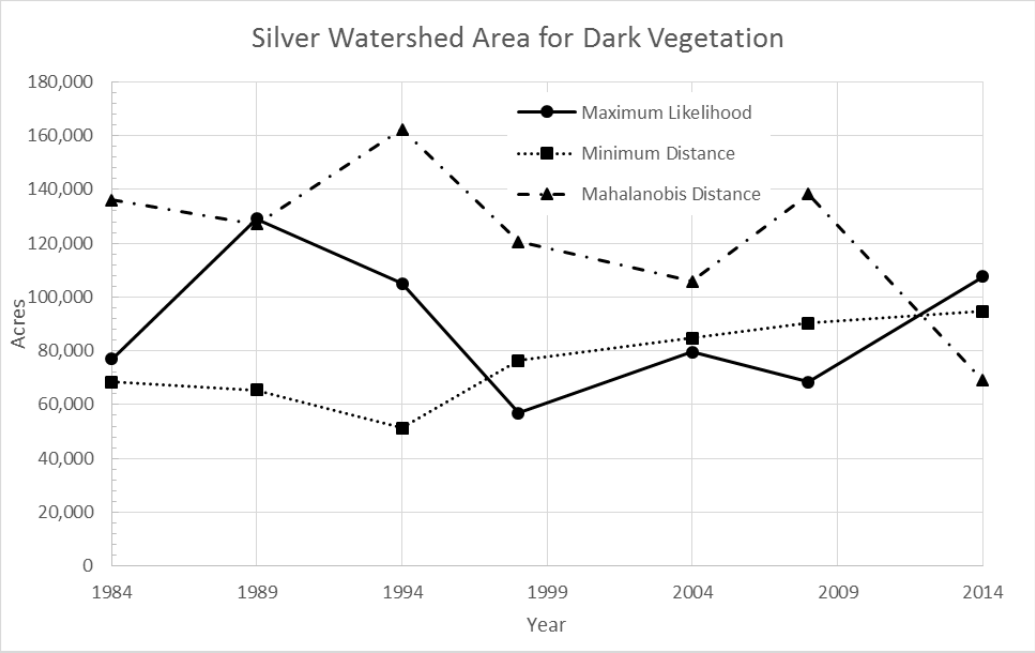

Figure B-11: Total Silver Watershed Area for Dark Vegetation Classification

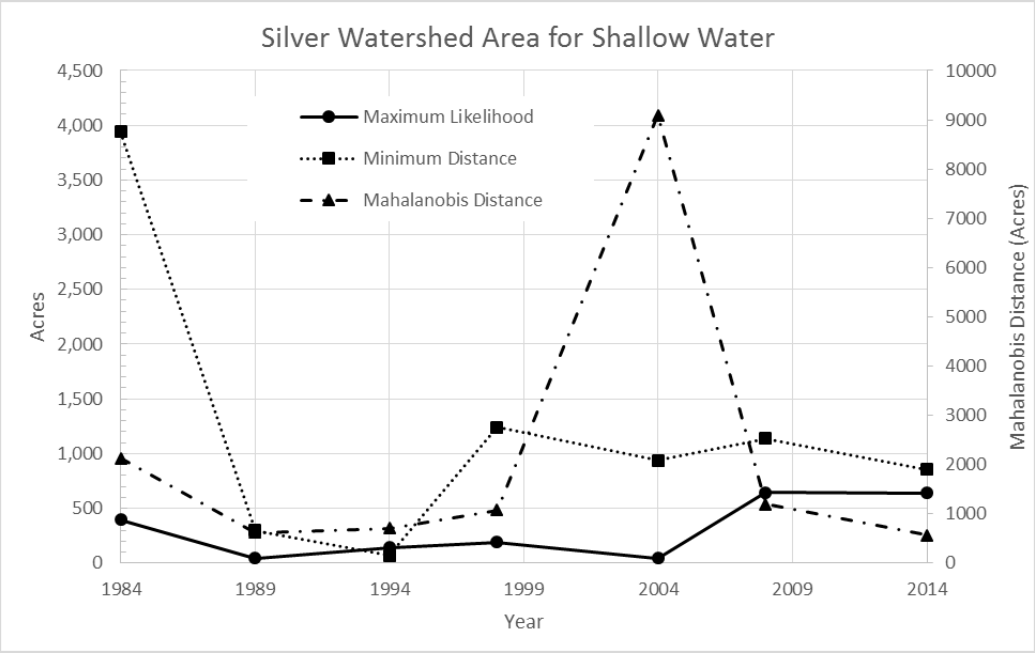

Figure B-12: Total Silver Watershed Area for Shallow Water Classification

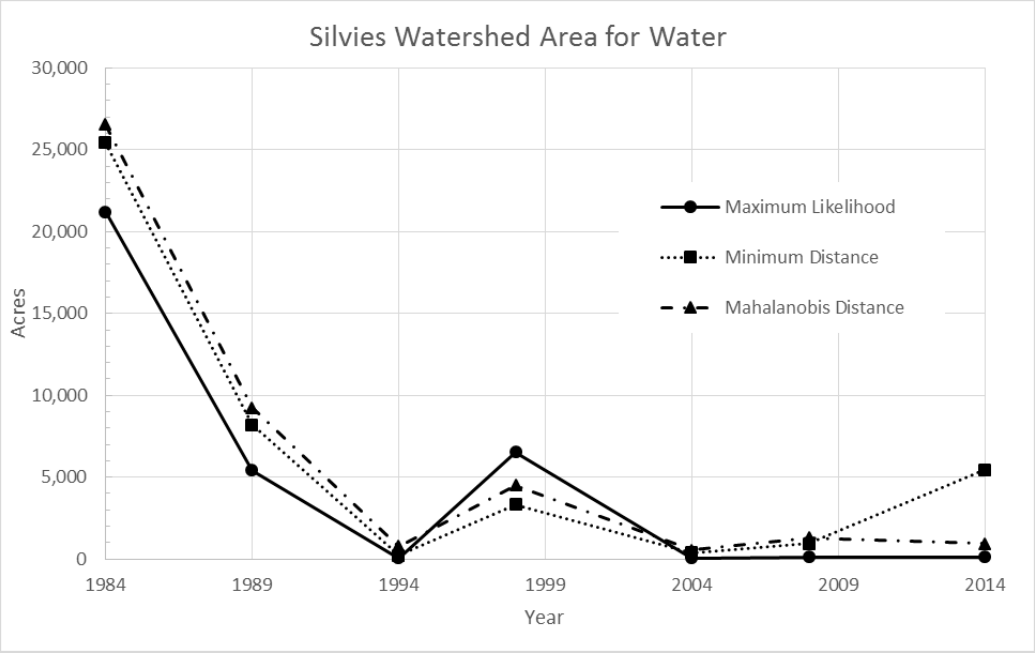

Figure B-13: Total Silvies Watershed Area for Water Classification

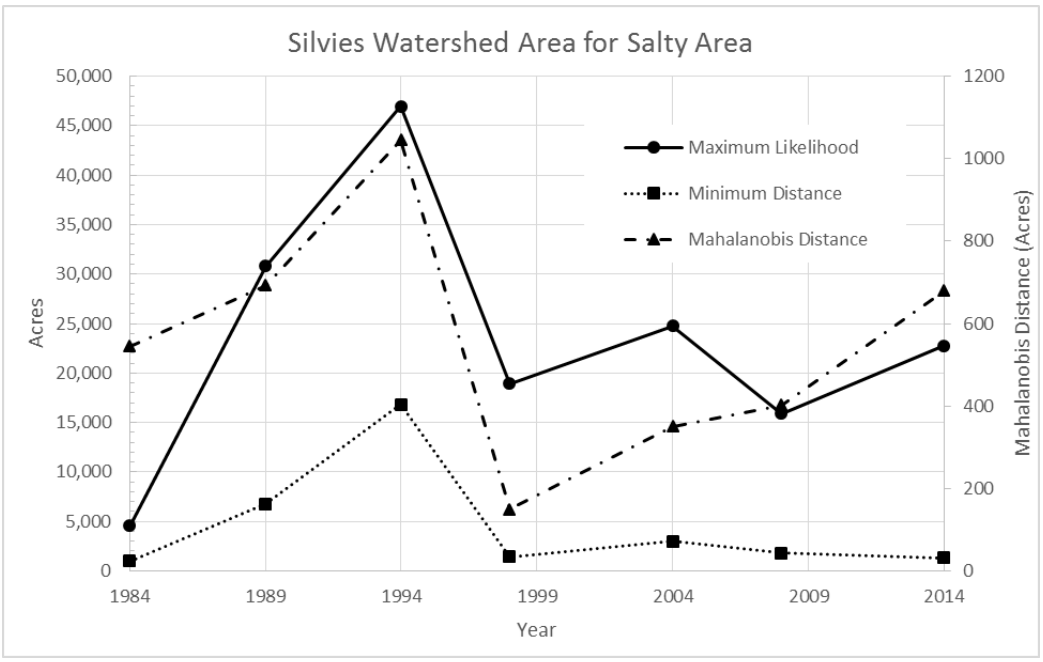

Figure B-14: Total Silvies Watershed Area for Salty Area Classification

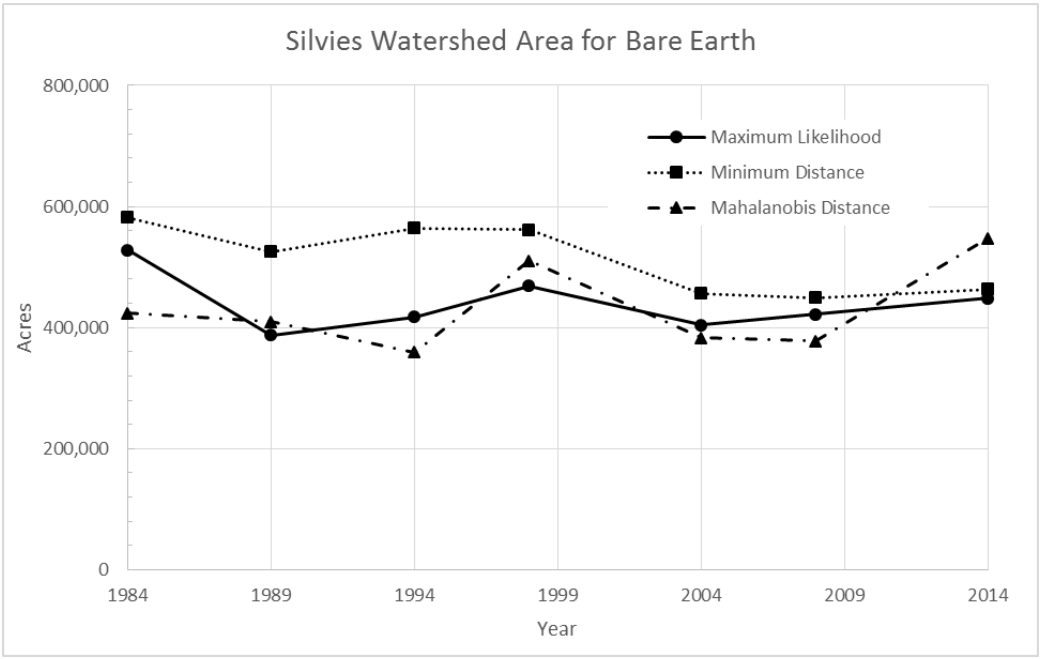

Figure B-15: Total Silvies Watershed Area for Bare Earth Classification

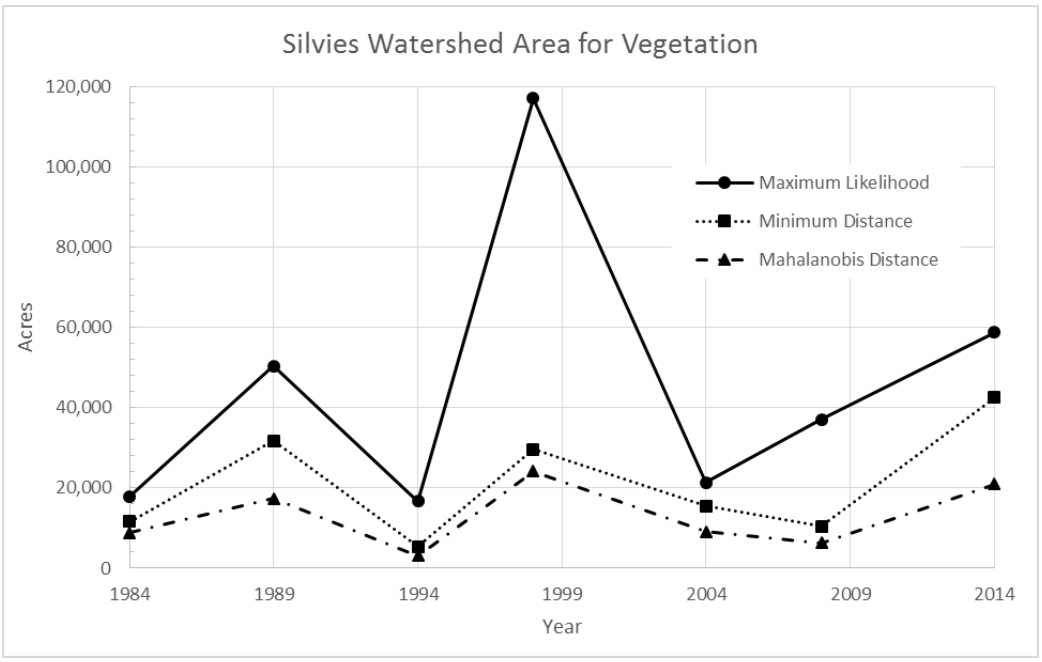

Figure B-16: Total Silvies Watershed Area for Vegetation Classification

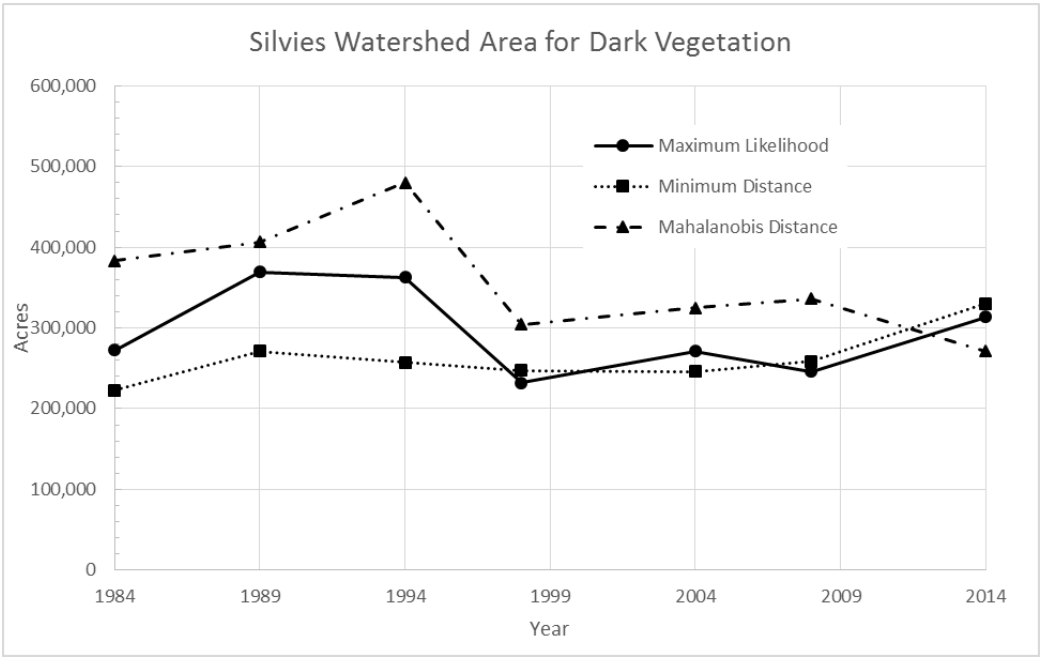

Figure B-17: Total Silvies Watershed Area for Dark Vegetation Classification

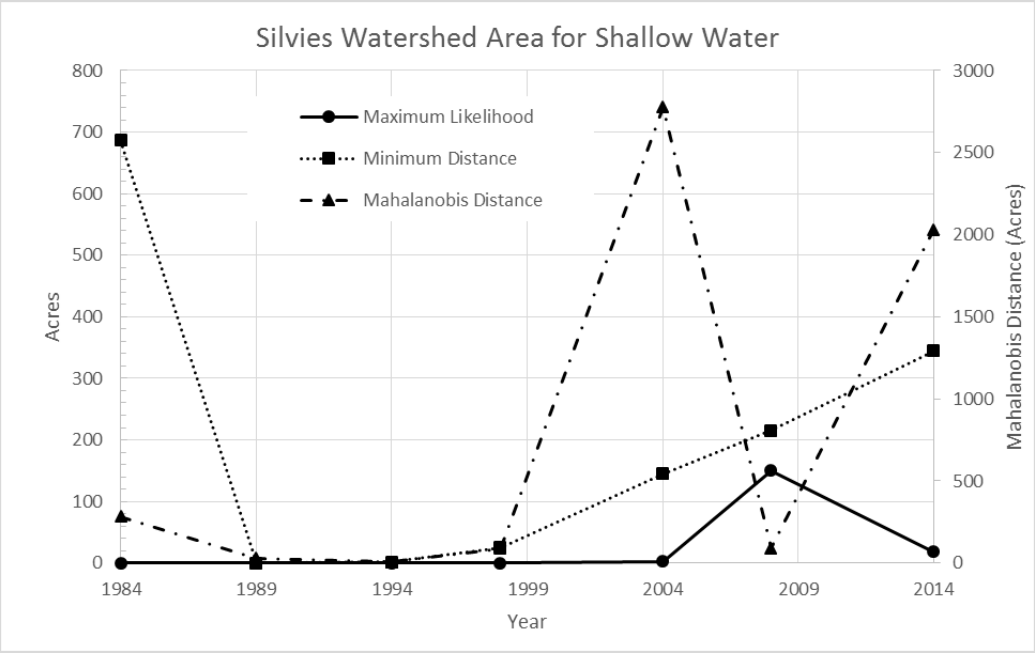

Figure B-18: Total Silvies Watershed Area for Shallow Water Classification

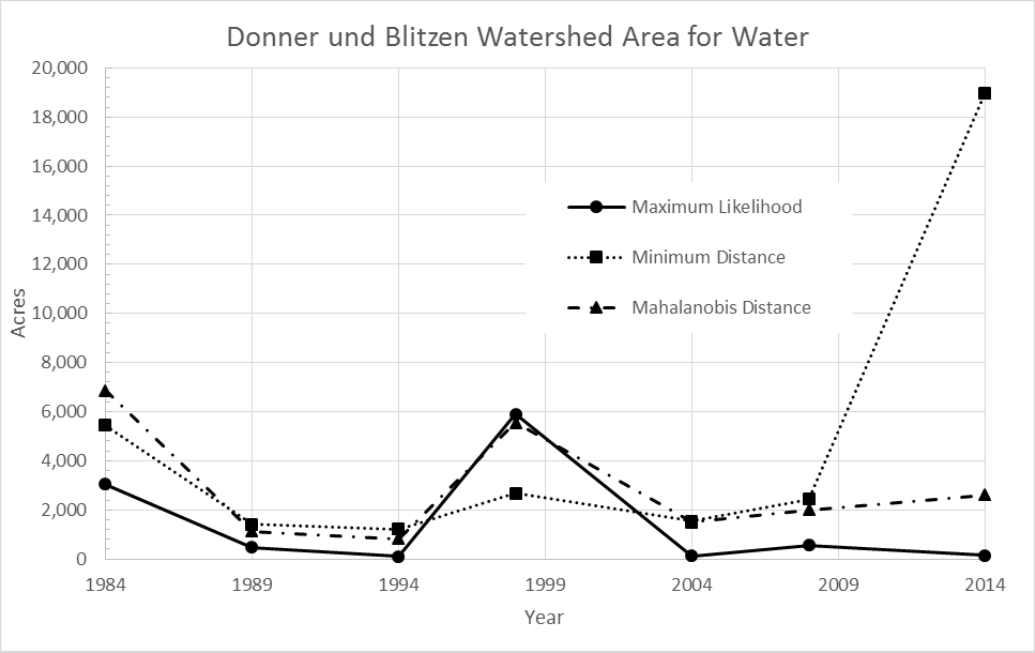

Figure B-19: Total Donner und Blitzen Watershed Area for Water Classification

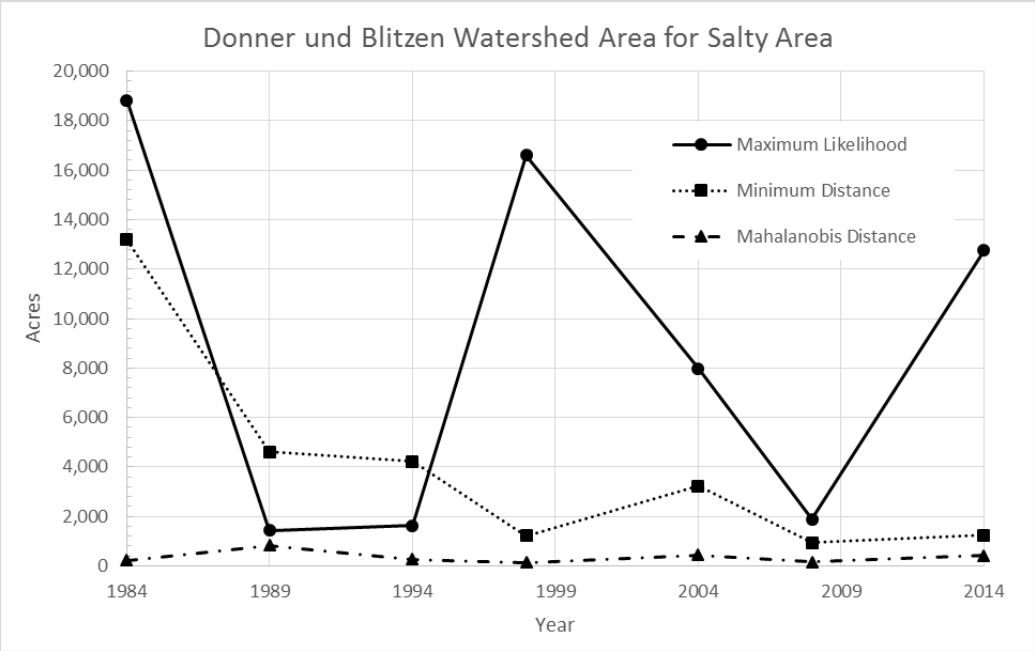

Figure B-20: Total Donner und Blitzen Watershed Area for Salty Area Classification

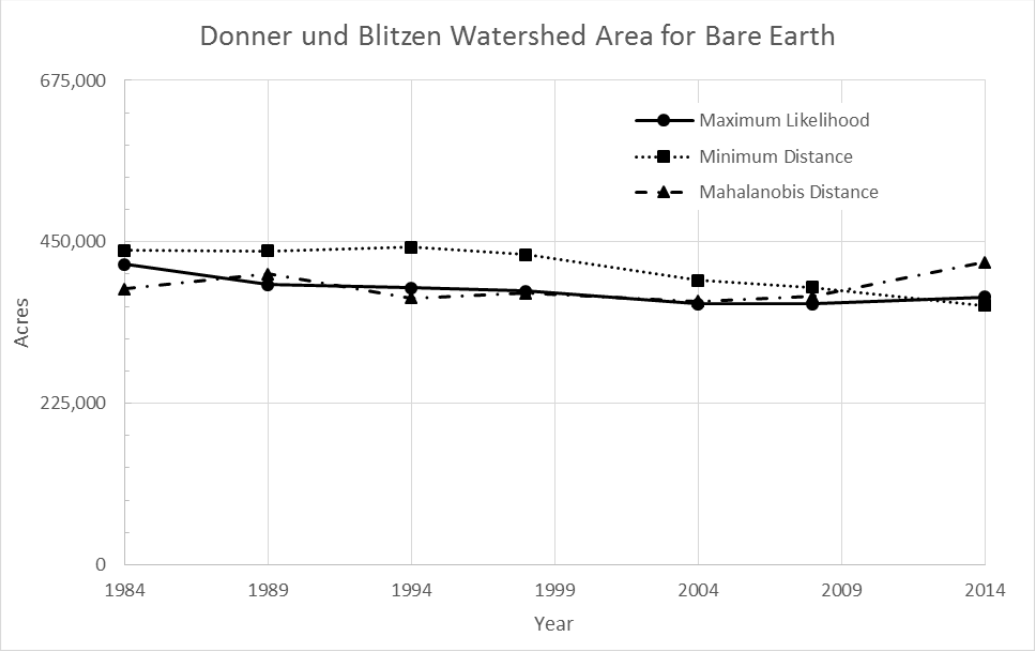

Figure B-21: Total Donner und Blitzen Watershed Area for Bare Earth Classification

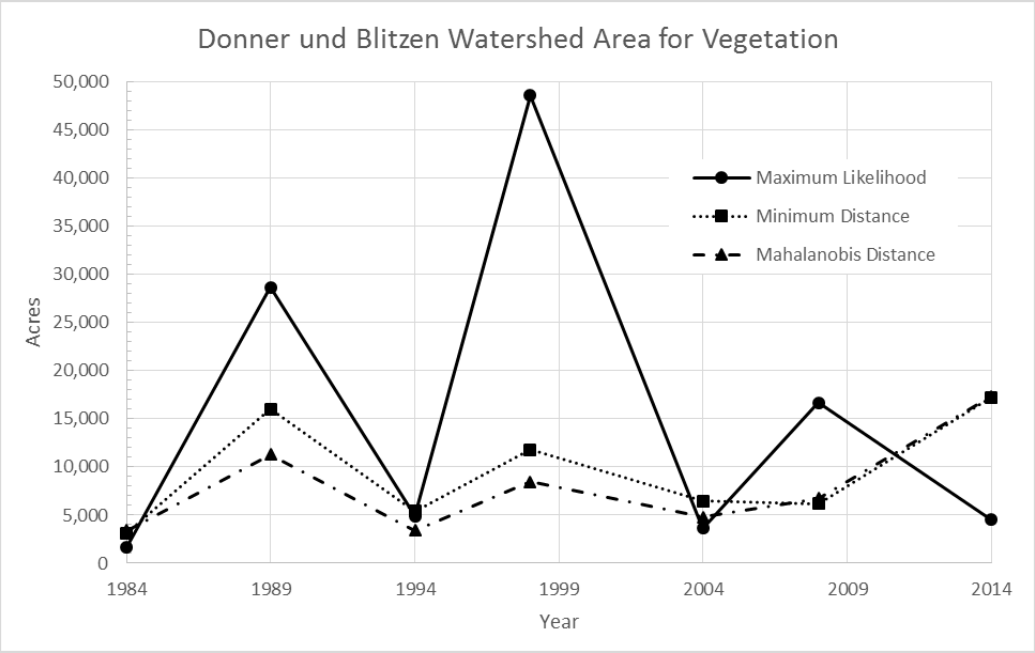

Figure B-22: Total Donner und Blitzen Watershed Area for Vegetation Classification

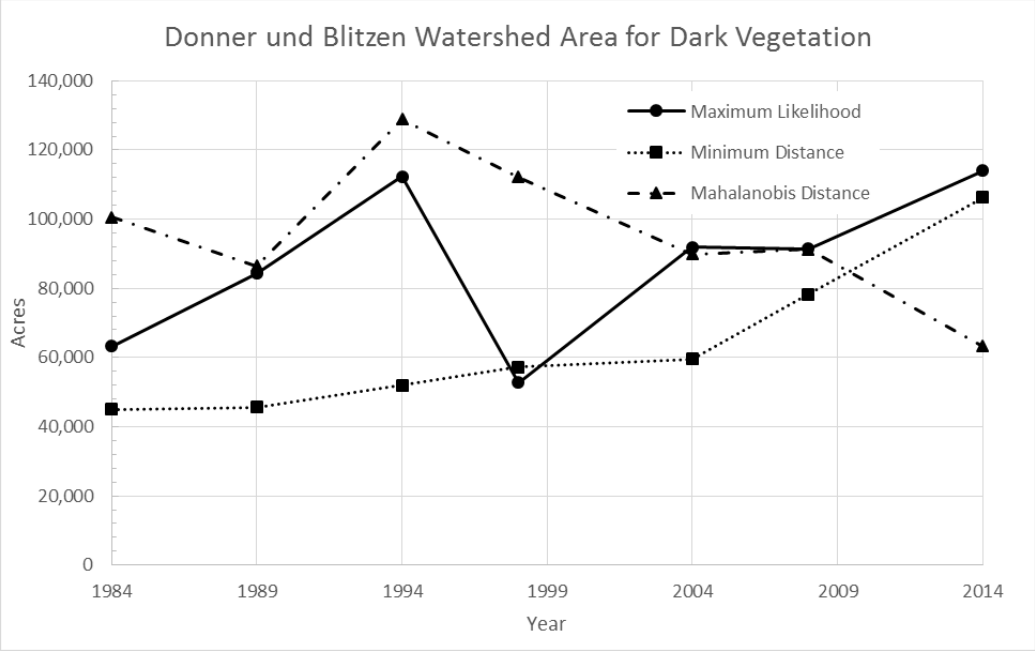

Figure B-23: Total Donner und Blitzen Watershed Area for Dark Vegetation Classification

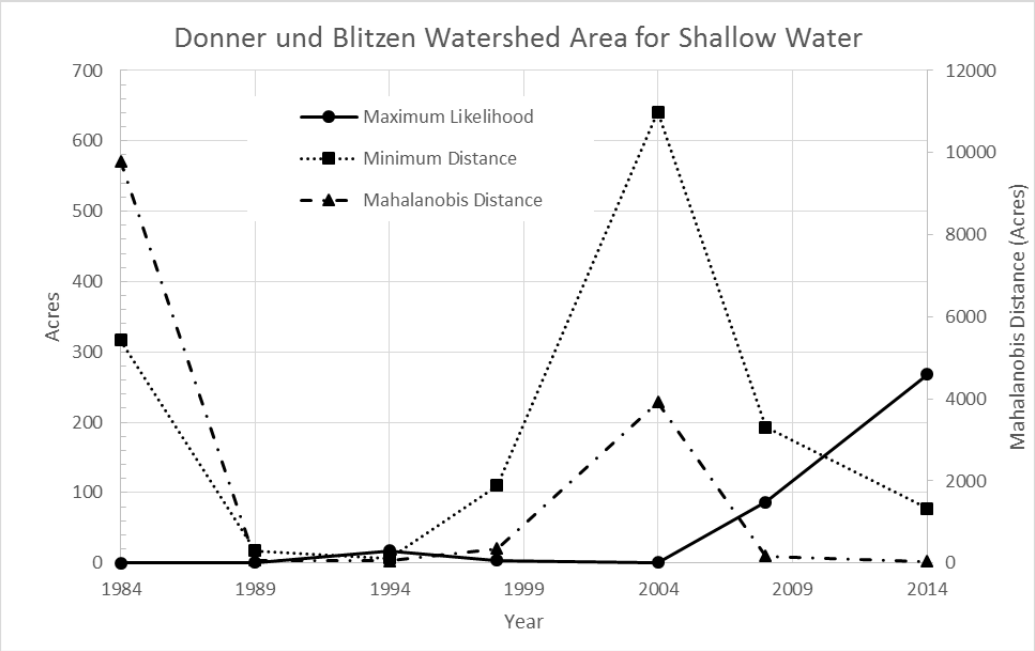

Figure B-24: Total Donner und Blitzen Watershed Area for Shallow Water Classification

APPENDIX C. TABLES OF THE DIFFERENT LAND COVER CLASSES

Table C-1: Harney-Malheur Lakes Watershed with Classes and Classifications Specified

		Classes (Acres)					
Year	Classification	Water	Shallow Water	Vegetation	Dark Vegetation	Salty Area	Bare Earth
1984	Maximum	107,682	32,394	10,110	70,570	7,792	700,816
	Minimum	111,382	36,721	11,408	43,213	109	726,532
	Mahalanobis	114,723	35,611	9,613	117,767	869	650,780
1989	Maximum	83,317	30,941	20,331	85,511	9,550	699,714
	Minimum	86,009	31,794	19,009	38,099	24,458	729,994
	Mahalanobis	89,321	31,736	12,821	94,991	6,061	694,434
1994	Maximum	28,584	27,810	6,394	77,387	16,081	773,108
	Minimum	35,183	26,614	8,473	42,118	38,131	778,844
	Mahalanobis	33,448	28,740	6,771	141,048	7,121	712,236
1998	Maximum	89,181	8,474	47,216	38,398	77,659	668,437
	Minimum	78,036	15,066	15,620	45,018	8,243	767,381
	Mahalanobis	79,026	20,429	10,704	95,901	5,168	718,135
2004	Maximum	13,626	2,934	8,463	76,908	76,715	691,743
	Minimum	15,984	7,113	19,005	40,152	36,659	751,476
	Mahalanobis	16,675	28,158	12,416	86,709	9,282	717,148
2008	Maximum	24,460	3,625	40,501	56,105	46,451	711,082
	Minimum	26,755	555	20,078	57,965	33,079	743,792
	Mahalanobis	27,750	3,570	14,373	121,779	17,478	697,276
2014	Maximum	28,380	459	26,588	77,003	107,207	689,726
	Minimum	41,934	34	36,070	56,546	31,617	763,162
	Mahalanobis	43,711	24	19,650	52,280	23,162	790,536

Table C-2: Silver Watershed with Classes and Classifications Specified

		Classes (Acres)					
Year	Classification	Water	Shallow Water	Vegetation	Dark Vegetation	Salty Area	Bare Earth
1984	Maximum	4,696	396	5,109	76,953	17,925	972,877
	Minimum	7,283	3,942	4,779	68,468	2,730	990,753
	Mahalanobis	9,450	2,131	4,223	136,118	1,523	924,510
1989	Maximum	978	44	13,799	129,175	22,219	911,740
	Minimum	2,696	297	10,061	65,423	40,750	958,729
	Mahalanobis	2,315	618	6,960	127,061	17,361	923,641
1994	Maximum	901	143	3,111	104,961	29,420	939,419
	Minimum	1,446	69	3,449	51,234	49,342	972,417
	Mahalanobis	823	709	2,966	162,353	17,570	893,536
1998	Maximum	4,530	189	28,754	56,906	161,616	825,943
	Minimum	2,619	1,243	7,480	76,400	14,447	975,748
	Mahalanobis	5,353	1,078	5,162	120,522	7,250	938,573
2004	Maximum	750	42	6,223	79,525	50,537	846,856
	Minimum	1,727	937	4,971	84,741	22,281	869,276
	Mahalanobis	1,850	9,092	3,429	105,891	9,178	854,493
2008	Maximum	394	647	13,363	68,430	28,247	868,159
	Minimum	1,245	1,137	4,835	90,330	17,178	864,515
	Mahalanobis	1,073	1,191	3,465	138,290	8,338	826,883
2014	Maximum	176	642	9,365	107,614	86,362	873,797
	Minimum	3,032	854	15,145	94,681	15,819	948,424
	Mahalanobis	2,894	568	9,017	68,982	11,650	984,844

Table C-3: Silvies Watershed with Classes and Classifications Specified

		Classes (Acres)					
Year	Classification	Water	Shallow Water	Vegetation	Dark Vegetation	Salty Area	Bare Earth
1984	Maximum	21,213	0	17,875	272,231	4,584	527,713
	Minimum	25,419	686	11,639	222,838	975	582,059
	Mahalanobis	26,556	282	8,886	383,529	545	423,817
1989	Maximum	5,418	0	50,360	369,582	30,833	387,422
	Minimum	8,181	0	31,823	271,328	6,747	525,536
	Mahalanobis	9,239	31	17,350	406,442	693	409,860
1994	Maximum	66	0	16,683	362,677	46,966	417,225
	Minimum	218	2	5,363	256,958	16,817	564,258
	Mahalanobis	771	5	3,112	479,821	1,045	358,861
1998	Maximum	6,518	0	117,192	232,327	18,923	468,655
	Minimum	3,317	26	29,577	247,297	1,446	561,953
	Mahalanobis	4,486	88	24,153	304,606	150	510,132
2004	Maximum	61	2	21,381	270,868	24,771	404,163
	Minimum	388	145	15,559	245,882	2,987	456,284
	Mahalanobis	546	2,778	9,190	325,156	350	383,225
2008	Maximum	109	150	37,104	246,272	15,918	422,006
	Minimum	947	215	10,510	258,799	1,809	449,279
	Mahalanobis	1,300	92	6,356	335,914	402	377,494
2014	Maximum	108	18	58,833	313,719	22,735	448,202
	Minimum	5,454	344	42,511	330,199	1,296	463,812
	Mahalanobis	938	2,032	20,950	271,023	680	547,992

Table C-4: Donner und Blitzen Watershed with Classes and Classifications Specified

		Classes (Acres)					
Year	Classification	Water	Shallow Water	Vegetation	Dark Vegetation	Salty Area	Bare Earth
1984	Maximum	3,038	0	1,705	63,316	18,828	418,411
	Minimum	5,436	317	3,135	45,064	13,193	438,153
	Mahalanobis	6,859	9,798	3,428	100,614	219	384,379
1989	Maximum	475	0	28,659	84,265	1,438	390,461
	Minimum	1,408	17	16,010	45,641	4,608	437,613
	Mahalanobis	1,124	64	11,292	86,445	822	405,551
1994	Maximum	102	17	4,885	112,387	1,629	386,277
	Minimum	1,205	7	5,388	51,971	4,230	442,496
	Mahalanobis	820	50	3,435	128,887	267	371,839
1998	Maximum	5,891	4	48,595	52,816	16,593	381,399
	Minimum	2,671	110	11,791	57,303	1,219	432,205
	Mahalanobis	5,543	356	8,488	112,097	127	378,686
2004	Maximum	114	1	3,626	91,905	7,987	363,902
	Minimum	1,549	641	6,468	59,631	3,226	396,020
	Mahalanobis	1,503	3,913	4,813	89,822	448	367,036
2008	Maximum	557	87	16,703	91,443	1,887	363,750
	Minimum	2,423	193	6,189	78,276	945	386,400
	Mahalanobis	2,002	167	6,759	91,218	168	374,112
2014	Maximum	152	268	4,542	114,046	12,748	373,542
	Minimum	18,982	78	17,215	106,221	1,246	361,556
	Mahalanobis	2,604	33	17,333	63,260	411	421,657

APPENDIX D. INDEX OF WEATHER TABLES AND FIGURES

Table D-1: Average Precipitation And Average Summer High Temperature for Malheur Lake

Year	Average Precip (in/yr)	Average Summer High Temp (F)
1980	9.69	75.90
1981	15.05	82.73
1982	11.48	77.06
1983	17.74	77.33
1984	10.32	75.36
1985	4.75	78.28
1986	4.45	68.96
1987	5.58	68.46
1988	3.63	63.20
1989	8.83	73.23
1990	4.83	76.81
1991	7.64	61.31
1992	8.04	79.87
1993	11.76	72.94
1994	10.34	83.61
1995	12.66	78.40
1996	12.37	81.31
1997	9.11	79.54
1998	11.51	73.13
1999	6.75	59.82
2000	8.86	60.08
2001	8.67	73.01
2002	7.01	58.80
2003	4.75	59.72
2004	1.54	52.16
2005	3.23	54.88
2006	2.41	53.78
2007	1.62	63.16
2008	4.91	72.55
2009	5.33	79.43
2010	6.14	76.30
2011	7.54	69.78
2012	11.46	79.75
2013	4.80	81.04

Table D-2: Average Discharge of Rivers that Flow into Malheur Lake

Date	Donner und Blitzen River Average Discharge (cfs)	Silvies River Average Discharge (cfs)
1980	156	206
1981	132	128
1982	165	407
1983	251	595
1984	271	568
1985	123	181
1986	163	288
1987	92	95
1988	78	51
1989	165	310
1990	66	52
1991	103	83
1992	45	
1993	188	
1994	75	
1995	171	
1996	156	
1997	155	
1998	230	
1999	165	
2000	93	
2001	89	
2002	94	
2003	98	
2004	113	
2005	142	
2006	158	
2007	94	
2008	112	
2009	116	
2010	186	51
2011	272	502
2012	86	151
2013	80	
2014	82	
2015	107	

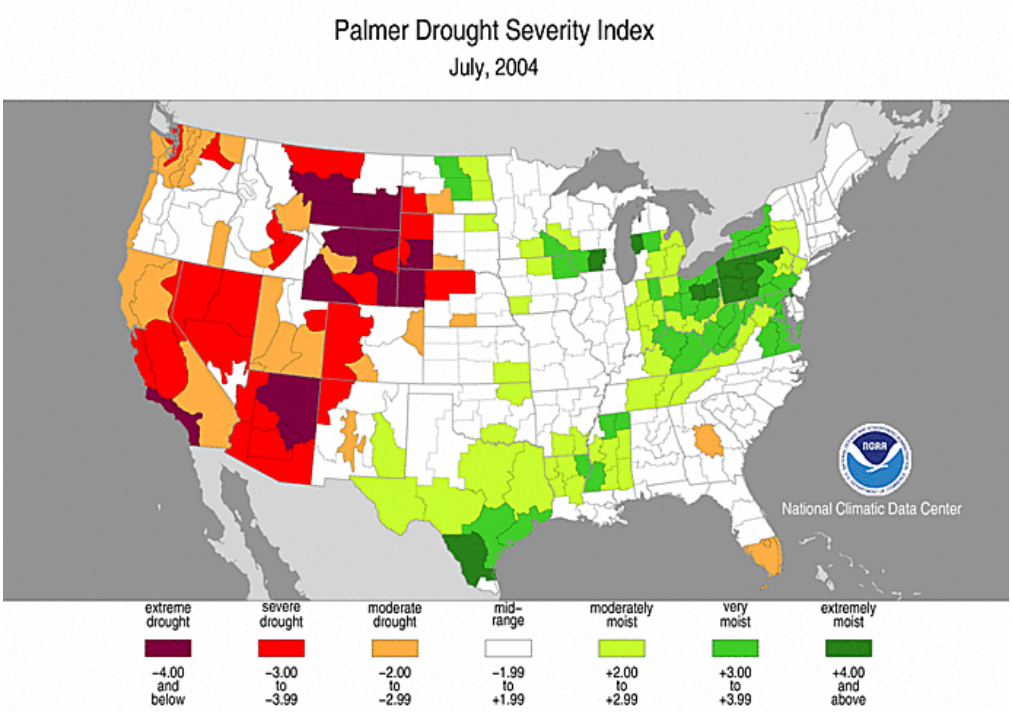

Figure D-1: Palmer Drought Severity Index for July 2004 (NOAA, 2015)

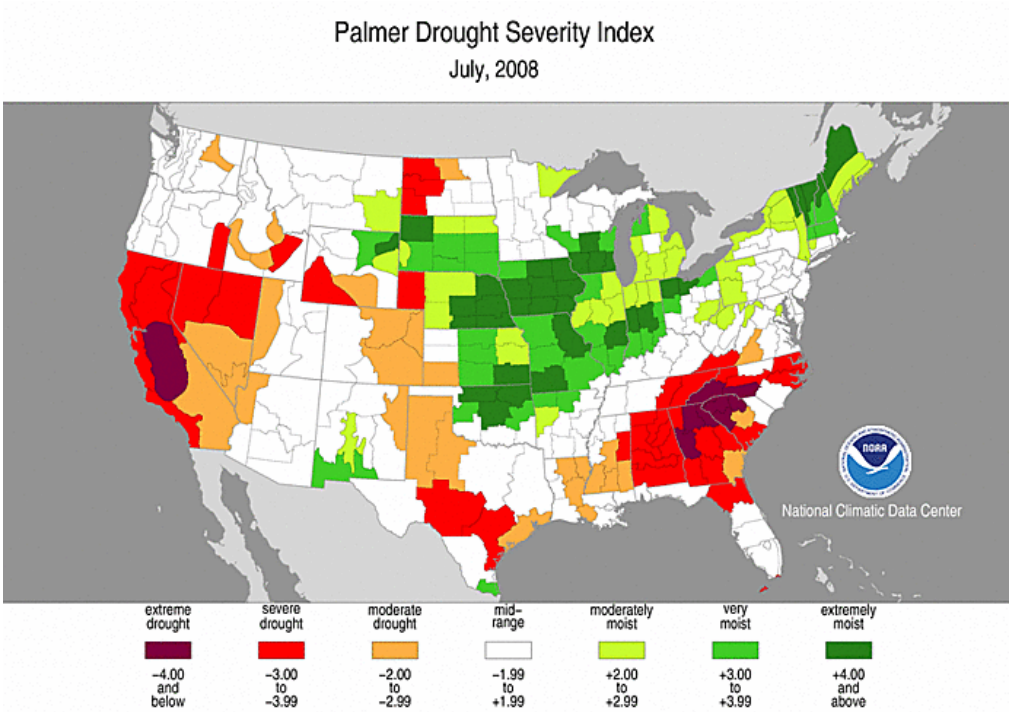

Figure D-2: Palmer Drought Severity Index for July 2008 (NOAA, 2015)

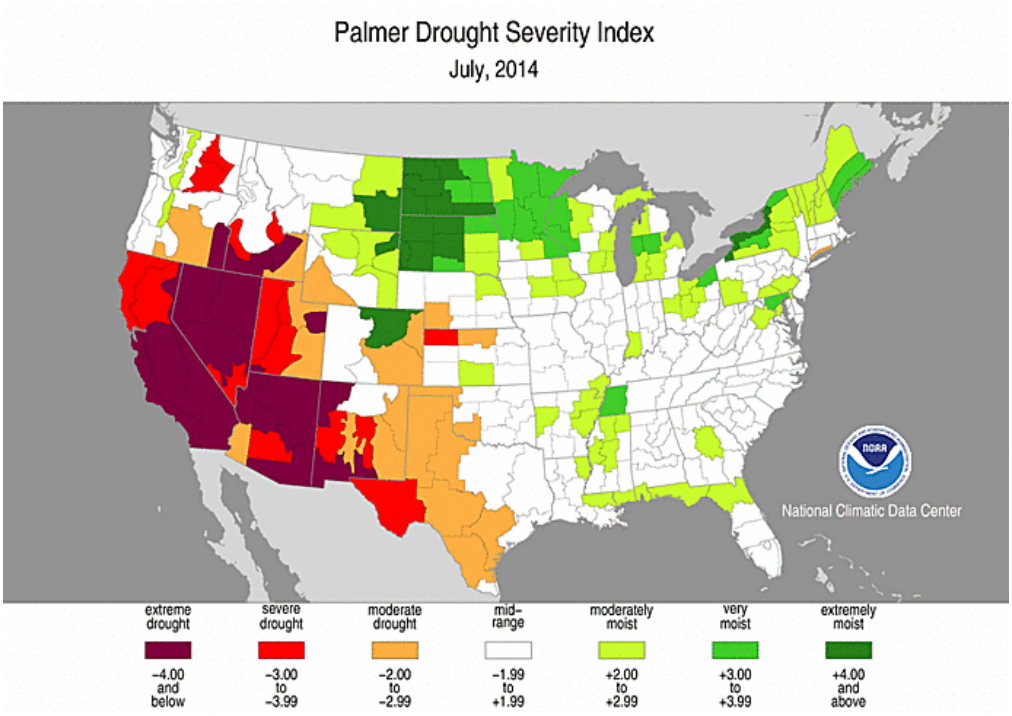

Figure D-3: Palmer Drought Severity Index for July 2014 (NOAA, 2015)

Table D-3: Drought Severity Classification (NDMC, 2015a)

			Ranges			
Category	Description	Possible Impacts	Palmer Drought Severity Index (PDSI)	CPC Soil Moisture Model (Percentiles)	USGS Weekly Streamflow (Percentiles)	Standardized Precipitation Index (SPI)
D0	Abnormally Dry	Going into drought: short-term dryness slowing planting, growth of crops or pastures Coming out of drought: some lingering water deficits pastures or crops not fully recovered	-1.0 to -1.9	21 to 30	21 to 30	-0.5 to -0.7
D1	Moderate Drought	Some damage to crops, pastures Streams, reservoirs, or wells low, some water shortages developing or imminent Voluntary water-use restrictions requested	-2.0 to -2.9	11 to 20	11 to 20	-0.8 to -1.2
D2	Severe Drought	Crops or pasture losses likely Water shortages common Water restrictions imposed	-3.0 to -3.9	6 to 10	6 to 10	-1.3 to -1.5
D3	Extreme Drought	Major crop/pasture losses Widespread water shortages or restrictions	-4.0 to -4.9	3 to 5	3 to 5	-1.6 to -1.9
D4	Exceptional Drought	Exceptional and widespread crop/pasture losses Shortages of water in reservoirs, streams, and wells creating water emergencies	-5.0 or less	0 to 2	0 to 2	-2.0 or less

Table D-4: Drought Level for Watershed Area using Drought Severity Classification for the Years 2004, 2008 and 2014

		Drought Level						
Watershed	Week	None	Abnormally Dry	Moderate Drought	Severe Drought	Extreme Drought	Exceptional Drought	Intensity
Donner und Blitzen	7/13/2004	0%	0%	0%	23.97%	76.03%	0%	Extreme
Silvies	7/13/2004	0%	63.34%	36.66%	0%	0%	0%	Abnormally Dry
Silver	7/13/2004	0%	8.47%	55.62%	24.95%	10.95%	0%	Moderate
Harney-Malheur Lakes	38181	0%	4.88%	44.20%	32.05%	18.87%	0%	Moderate to Severe
Donner und Blitzen	7/22/2008	0%	67.59%	32.41%	0%	0%	0%	Abnormally Dry
Silvies	7/22/2008	0%	100%	0%	0%	0%	0%	Abnormally Dry
Silver	7/22/2008	0%	84.61%	15.05%	0.34%	0%	0%	Abnormally Dry
Harney-Malheur Lakes	7/22/2008	0%	100%	0%	0%	0%	0%	Abnormally Dry
Donner und Blitzen	7/1/2014	0%	0%	0%	100%	0%	0%	Severe
Silvies	7/1/2014	0%	0%	4.77%	95.23%	0%	0%	Severe
Silver	7/1/2014	0%	0%	0%	100%	0%	0%	Severe
Harney-Malheur Lakes	7/1/2014	0%	0%	0%	99.96%	0.04%	0%	Severe